Fuel efficiency and fouling control coatings in maritime transport

Lindholdt, Asger; Dam-Johansen, Kim; Yebra, Diego Meseguer; Kiil, Søren; Weinell, Claus Erik; Olsen, Stefan Møller

Publication date:
2015

Document Version
Peer reviewed version

Fuel efficiency and fouling control coatings in maritime transport

Asger Lindholdt

Ph.D. Thesis

June 2015

Department of Chemical and Biochemical Engineering
CHEC Research group
Technical University of Denmark
DK-2800 Kgs. Lyngby
Denmark

Preface

This dissertation is the outcome of three years of research, conducted partly at the CHEC research group under the department of Chemical and Biochemical Engineering at the Technical University of Denmark (DTU) and partly at Hempel A/S. The work has been supervised by Associate Professor Søren Kiil; Professor Kim Dam-Johansen; Stefan M. Olsen, PhD; and Diego M. Yebra, PhD. This research was financially supported by the Hempel Foundation and the Technical University of Denmark (DTU).

I would like to thank all those who contributed to this PhD dissertation. Whether it was through a time-consuming, in-depth analysis of the work or just a friendly chat at the coffee machine, these were contributions I am grateful for. Firstly, I would like to thank my supervisor, Søren Kiil, for his very thorough dedication to improving the scientific level of this work. I am pleased that Kim Dam-Johansen gave me the chance to join the CHEC group and work in the field of coatings, which I know has a special place in his heart within the scientific world. Diego M. Yebra has been an inspiration due to his hard work, constant desire for improvements, and in-depth feedback. Stefan M. Olsen has been a tremendous support in the scientific work, but he has also supported me on a personal level, especially when the project was not going well, which is when support is most needed. I have been extremely fortunate to have worked with two very skilled technicians at DTU: Rasmus L. Christensen and Nikolaj V. Nissen. Their work has undoubtedly been crucial to the successful raft design and construction. Furthermore, it was a pleasure to work with them, as they always had a positive approach. The workshop at the institute of Chemical and Biochemical Engineering has provided vast support with the concept and practical implementation, all the way from the placement of nuts and bolts for the raft design, to the rotors on the raft, cylinder design, and much more. The particular people who were involved, for whom I am truly grateful, are Ivan H. Pedersen, Søren V. Madsen, Jens H. Poulsen, and Danni J. Axelsen. I greatly enjoyed our inspiring talks, which ranged from simple solutions to almost unimaginable underwater constructions to testing marine coatings—and to life outside DTU. The CHEC group at RISØ (DTU), especially Freddy Christensen, Kristian Estrup, and Ulrik B. Henriksen, deserve a sincere thank you for always helping me. I was very quickly welcomed as “one of your own,”

and I enjoyed every moment of my time at Risø. At the CHEC group, I truly appreciated the collaboration, support, and friendly environment amongst the PhD students. In particular, I would like to thank my office mates, Jeppe Hjort and Hao Wu; my fellow PhD students working within the field of coatings, Kristian P. Nørgaard and Shizhong Zhang; and my friend, Seyednezamaddin Azizaddini. Thank you for helping with my project and making every day at the CHEC group more fun. I have also been fortunate to collaborate with many brilliant people from Hempel, who have been an enormous help to me. In the antifouling department in Spain, I would like to thank, in particular, Antonio Sanchez and Eduardo Andres. I spent most of my time in the Fouling Release department at Hempel A/S in Lundtofte. I enjoyed my time at this department very much, due to the excellent work carried out there, but also, and more importantly, due to the friendly and supportive environment. Every single time I asked for help, it was given to me; this has truly been a great experience. The people whom I worked with are Ciarán Dunbar, Peter Thorlaksen, Christina Kjær, Kim F. Sørensen, Anders Bloom, Lena S. Nielsen, Dorthe Hillerup, Albert C. Noguer, Regina Bohm, Heidi Vedel, Annie O. Andersen, and Ulrik Bork. An additional thank you goes to Ciarán Dunbar for helping with the coating application and the positive mood at the shared office. Claus Weinell has also been an important help, as he readily answered questions related to his previous work with the laboratory rotor setup. I am grateful to him for sharing his knowledge and responding so quickly.

Finally, I would like to thank my mother Kirsten, my father Uwe, and my brother Malik, who I love very much, for their love and outstanding support. I would not have made it to high school without them, since I did not particularly fancy school or science, and I certainly did not believe I could master them. My wife, Marie, has provided tremendous support by letting me spend long hours at work when needed; she has been a constant source of happiness. I love you so much because you are you—I hope you know that. My daughter, Milla, came to this world at the end of the PhD project, and she has been an amazing treasure ever since. Milla and all other children are on my mind when I think of the main purpose of this project: to provide a better world through less pollution from ships. My wish, perhaps naïve, is that this project will contribute to a better and cleaner world, at least one tiny bit.

Summary

First, this thesis concerns the drag performance of fouling control coatings (FCCs) used to protect hulls on ships against biofouling and, therefore, minimize any drag therefrom. A systematic overview of the literature and description of the experimental methods used to quantify the drag of FCCs has been made. Also, the advantages and disadvantages of the reported methods are listed; these provide an assessment of the most efficient methods to quantify the drag performance of FCCs. In addition, the main parameters impacting FCCs and the main findings for the drag performance of the mostly used FCC technologies are outlined. It was found that the drag performance of FCCs varies, depending on whether the FCC has been newly applied, has experienced dynamic exposure, or has experienced static seawater exposure. The summarized data revealed that the most common drag performance method currently used consists of measuring drag when coatings are newly applied and after static exposure. It was found that the main limitation of this method primarily arises due to incorrect exposure conditions, when compared to larger commercial ships that mainly are moving with few and shorter idle periods. As a result, it was determined that other methods must be explored in order to accurately measure the long-term drag performance of FCCs in conditions that mimic those encountered by ships' hulls during actual voyages.

In an experimental study, five commercial FCC systems were applied to smooth disks with a radius of 11.45 cm. The drag performances in the newly applied coating condition and after one month of static immersion in natural seawater were measured using a friction disk machine (FDM). The four best performing coatings were re-examined for their drag performance after an additional 2.5 months of immersion. The five FCCs in the newly applied coating condition when applied on completely smooth substrates revealed a small difference and, in most cases, one that was less than the experimental uncertainty. After one month of static immersion, the hydrogel-based fouling release coating (FRC) with biocides had the lowest drag, while the fluorinated FRC had the highest drag. The hydrogel-based FRC without biocides and the two self-polishing copolymer (SPC) coatings showed intermediate performances. After 3.5 months of static immersion, the two hydrogel-based FRCs showed

superior drag performance, compared to the two SPC coatings. Furthermore, the drag performances of two different FCC systems with varying substrate roughness values (i.e., the roughness below the coating system) were measured in the newly applied condition.An increase in the substrate roughness led to increased drag for both FCC systems, but the FRC was impacted less by the higher substrate roughness than the SPC coating.

To overcome the limitations from investigating only the drag of newly applied coatings and coatings after static immersion, an experimental setup was designed and built to estimate the changes in the skin friction of four FCCs over an extended period of time in conditions simulating the vast majority of ship profiles (i.e., speed and activity) in the present market. The setup consisted of two separate parts; one part aged FCCs directly in seawater in a dynamic manner similar to that experienced by a ship's hull, and a second, laboratory part measured the torque (drag) of coated cylinders in a rotary setup. Four commercial FCCs were exposed for 53 weeks in Roskilde Fjord, Denmark, i.e., in relatively cold seawater (salinity of 1.2 wt%), from the spring of 2013 to the autumn of 2014. The in situ immersion conditions consisted of five-week cycles. Two weeks consisted of static immersion. This was followed by three weeks of dynamic immersion, in which the cylinders were rotated in natural seawater at a tangential velocity of 8.1 knots. It was found that the skin friction generally increased more during the static immersion, as opposed to the dynamic exposure, which revealed the need for exposure conditions that mimic those of larger commercial ships. Furthermore, with regard to the entire exposure period, it was found that the skin friction of the investigated FCCs decreased in the following order: fluorinated FRC (highest skin friction), hydrogel-based FRC without biocides, silylated acrylate SPC coating, and hydrogel-based FRC with biocides (lowest skin friction). However, the differences in skin friction between the latter three coatings were found to be small and often within the experimental uncertainty. After 25 weeks of immersion and mechanical cleaning, the differences in skin friction were, on average, less than 1%, i.e., within the experimental uncertainty, for velocities relevant for larger commercial ships. The roughness parameters, Rt(50) and R_z, were found to be poor indicators of the drag performance in the newly applied and mechanically cleaned coating condition.

Resumé (Summary in Danish)

Denne afhandling omhandler overfladefriktionsstudier for bundmalinger som bruges til at beskytte skibes skrog mod biologisk begroning og dermed minimere modstanden herfra. Der er lavet et gennemgående studie som samler overfladefriktionsstudier og deres test metoder for bundmalinger fra litteraturen. Heri gennemgås fordele og ulempe ved de nævnte metoder og ydermere præsenteres de mest effektive metoder til at bestemme overfladefriktionen for bundmalinger. Parametrene, der påvirker bundmalinger mest og hovedkonklusioner for de friktionsmæssige ydeevner, beskrives. Det konkluderes, at den friktionsmæssige ydeevne af bundmalinger afhænger af om malingen er nymalet tilstand, efter dynamisk eller statisk eksponering i havvand. De opsummerede data viser at mange metoder har forsøgt at kvantificere friktionen, hvor de mest almindelige er friktionstest i nymalet tilstand efterfulgt af friktionstest efter statisk eksponering. Det er dog fundet, at andre metoder må udforskes for at måle friktionen af bundmalinger der er repræsentativ for større kommercielle skibes sejlads ved at efterligne forholdene skibes skrog møder under reel sejlads.

I et eksperimentelt studie blev fem kommercielle bundmalinger påført en glat disk med en radius på 11,45 cm. Friktionen blev målt med en friktionsdiskmaskine (FDM) i både nymalet tilstand og efter én måneds statisk eksponering i havvand. De fire bedste bundmalinger (laveste friktion) blev genundersøgt for deres friktionsbidrag efter yderligere 2,5 måneder med statisk eksponering. En lille forskel og i de fleste tilfælde insignifikant forskel blev observeret for de fem nymalede malinger påført på en glat disk. Efter én måned med statisk eksponering viste en hydrogel baseret slipletmaling (eng. fouling release coating) med biocid den laveste friktion, mens den fluorinerede slipletmaling viste den højeste friktion. En hydrogel baseret slipletmaling uden biocid og to selvpolerende malinger (eng. self-polishing copolymer (SPC)) viste en friktion, der var højere en den hydrogel baserede slipletmaling, men lavere end den fluorinerede slipletmaling. Efter 3,5 måned med statisk eksponering afslørede friktionsmålinger, at de hydrogel baserede slipletmalinger havde en signifikant lavere friktion end de selvpolerende malinger. Ydermere blev friktionen målt for to forskellige malingssystemer med varierende substratruheder (den ruhed der er nedenunder

malingen) undersøgt i deres nymalede tilstand. En forøgelse af substratruheden førte til en forøgelse af friktionen for begge bundmalingssystemer, men slipletmalingen var mindre påvirket af den højere substratruhed end den selvpolerende maling.

For at overkomme begrænsningerne ved kun at måle friktion for bundmalinger i den nymalede tilstand og efter statisk eksponering blev der udviklet og bygget en opstilling til at måle bundmalingers friktion over tid under betingelser der efterligner de forhold størstedelen af de industrielle skibes skrog, møder når de sejler (hastighed og aktivitet) i det nuværende marked. Opstillingen bestod af to dele; én hvor bundmalinger blev ældet direkte i havvand og én hvor friktionen blev målt på malede cylindre i en rotoropstilling. Fire kommercielle bundmalinger var eksponeret ved molen på DTU Risø campus (relativt koldt havvand med saltindhold på 1.2 vægt procent) fra forår til efterår i årene 2013 og 2014 svarende til i alt 53 uger. Eksponeringen direkte i havvand bestod af cyklusser på fem uger bestående af to ugers statisk eksponering efterfulgt af tre ugers rotation med en tangentiel hastighed på 8.1 knob. Efter hver eksponeringsperiode blev friktionen målt. Det blev fundet, at friktionen typisk var højere efter de statiske perioder sammenlignet med perioderne med rotation. Desuden blev det fundet, at overfladefriktionen af de undersøgte bundmalinger mindskedes i følgende rækkefølge: Fluorineret slipletmaling (højeste overfladefriktion), hydrogel baseret slipletmaling uden biocid, silyleret akrylat selvpolerende maling og hydrogel baseret slipletmaling med biocid (laveste overfladefriktion). Bortset fra den fluorinede slipletmaling var forskellen i overfladefriktion mellem bundmalingerne lille. Efter 25 ugers eksponering og mekanisk rensning var forskellen i overfladefriktion mindre en 1 % hvilket var mindre end den eksperimentelle usikkerhed ved de undersøgte hastigheder, der er relevant for større kommercielle skibe. Ruhedsparametrene Rt(50) og R_z viste sig at være ringe parametre til at forudsige overfladefriktionen af nymalede og mekanisk rensede bundmalinger.

Introductory overview of the Ph.D. thesis

This Ph.D. thesis deals with determining the drag performance of fouling control coatings in the maritime transport sector, as indicated by the title: “Fuel efficiency and fouling control coatings in maritime transport.” The backbone of the thesis is comprised of three articles, provided in Chapters 1, 3, and 4, respectively:

- Effects of biofouling development on drag forces of hull coatings for ocean-going ships: a review
- Measurements of drag performance of statically exposed fouling control coatings using a spinning disk
- Estimation of long-term drag performance of fouling control coatings using an ocean-placed raft with multiple dynamic rotors

The review article (chapter 1) was, in essence, a literature study, based on already published articles in the scientific literature. The main purpose of the review article was to provide an overview for readers who are new to the topic of drag performance and FCCs and, furthermore, to identify state-of-the-art drag performance measurement methods of FCCs, along with potential improvements.

An experimental part of the study used a friction disk machine to measure the torque of disks with newly applied coatings and after they had been statically immersed (chapter 3). The disks were immersed at the raft facility of TNO, at the harbor of Den Helder, the Netherlands. The experimental part of this study was carried out in the summer of 2013 at TNO’s laboratory facilities.

The other experimental part consisted of measuring the drag development of coatings exposed in a manner similar to that of voyaging ships (chapter 4). This method was based on land- and in situ-based rotor setups. The development of the rotor setup was comprised of several stages. After a thorough evaluation of ideas inspired by the scientific literature, it was found that the land-based rotor setup developed by Weinell et al. (2003) would be useful to measure the drag performance of FCCs, while a dynamic, in situ-based rotor setup could simulate the exposure conditions that voyaging ships encounter. The land-based rotor setup was already available; therefore, only minor work had to be carried out to ensure the

applicability of this setup. The dynamic in situ rotor was developed at the department of Chemical and Biochemical Engineering at the Technical University of Denmark (DTU). The drawings and design were completed in February 2013. The majority of the construction work was then given to external companies, although some parts were built by Asger Lindholdt (author) and the department of Chemical and Biochemical Engineering at DTU. The raft with dynamic rotors was ready for use by the middle of May 2013. The experimental exposure periods for the rotor setup were from May 21, 2013 to November 13, 2013 (25 weeks) and from April 1, 2014 to October 22, 2014 (28 weeks). The exposure conditions applied to the cylinders with FCCs consisted of 2 weeks with static immersion, followed by 3 weeks with dynamic immersion. Drag measurements were carried out at the end each immersion period, i.e., every 2 or 3 weeks.

Besides the three articles, the following sections are also part of this Ph.D. thesis:

- Summary of the thesis
- Scientific hypotheses (hypotheses of interest to verify or reject)
- Comparison of the static immersion study with the FDM, and the dynamic and static immersion study with the rotor setups
- Conclusion for the entire work, including ideas for further work
- Appendix, containing a detailed manual explaining how to use the rotor setups (land-based and in situ), detailed descriptions of the main parts of the rotor setups, an explanation of how the roughness was measured, potential improvements of the rotor setups, and details of the coating application.

Table of contents

Contents

1. Chapter 1 – Literature review

The content of this chapter was accepted for publication in the Journal of Coatings Technology and Research (JCTR) December 2014 with the title "Effects of biofouling development on drag forces of hull coatings for ocean-going ships: a review". The authors are Asger Lindholdt, Kim Dam-Johansen, Stefan M. Olsen, Diego M. Yebra and Søren Kiil. There have been minor changes compared to the journal article in order to match the format of this thesis, but otherwise it remains as presented in the JCTR.

Abstract

This review presents a systematic overview of the literature and describes the experimental methods used to quantify the drag of fouling control coatings (FCCs). It also summarizes the findings of FCC's drag performance and identifies the main parameters impacting it. The advantages and disadvantages of the reported methods listed in this review provide an assessment of the most efficient methods to quantify the drag performance of FCCs. This review determines that drag performance of FCC technology varies depending on whether the coating condition is newly applied, after dynamic or static seawater exposure. The summarized data reveals that, while several methods have attempted to quantify drag performance of FCCs, other methods must be explored in order to accurately measure the long-term drag performance of FCCs in conditions mimicking those that ship hulls encounter during actual voyages.

Introduction

The fuel efficiency of ships is paramount, due to the high cost of fuel and the environmental concerns connected to fossil fuel consumption (e.g., emission of greenhouse gases, SO2, and NOx). Commercial ships typically experience dry-docking intervals of 3 to 5 years, although extended dry-docking of up to 7.5 years can be granted for certain larger ship classes (e.g., Germanischer Lloyd SE (2013)); during that time, substantial biofouling can occur. Biofouling is defined as the accumulation of micro- and macro-organisms, such as the settlement of bacteria, algae, slime, weed, or barnacles on man-made structures (Yebra et al., 2004).

Biofouling adversely affects ships through the loss of speed, decreased maneuverability, increased fuel consumption and thereby increased emissions of harmful gases, increased frequency of dry-dockings, and translocation of invasive species. Frictional resistance represents a considerable part of a ship's resistance. For example, frictional resistance causes 70 to 90% of the total resistance for slow trading ships (e.g., bulk carriers and tankers) and often less than 40% for faster trading ships (e.g., cruise liners and container ships) (MAN Diesel & Turbo, 2011). The remaining resistance can be attributed primarily to wave-making. Air resistance above the waterline only makes up a minor portion of the total resistance, that is, typically 2% or less for slow trading ships and 10% or less for fast trading ships (MAN Diesel & Turbo, 2011). The fouling control coating (FCC) has a high impact on the fuel consumption of ships. Milne (as cited in Townsin (2003)) reported, for instance, that the world fleet could save a potential $720 million USD (value in the year 1989) in fuel costs due to the reduced frictional resistance of ships with the introduction of so-called ablative FCCs. An additional $2289 million USD could be saved due to extended interdocking periods and, consequently, lower dry-dock costs. The introduction of a new, improved FCC (in this case, the ablative coating), can largely benefit the economy and environment. It is, therefore, essential to improve the drag assessment tools of FCCs in order to reduce fuel consumption. Despite the impact of FCCs on fuel efficiency, environmental issues, and climate change, this topic did not gain much attention until the early 1990s, when an increase in publications took place (Lejars et al., 2012). Researchers have used various experimental methods to attempt to predict an FCC's performance with regard to frictional resistance. Nevertheless, large uncertainties exist regarding the correct identification of the optimal coating and its impact on the frictional resistance of ships over time. This paper focuses on the topic of FCCs and their associated frictional resistance. Furthermore, it presents a summary of the most relevant experimental methods and research results regarding the frictional resistance of FCCs. The article also explores the impact FCCs have on fuel consumption, the main parameters that affect drag performance, the drag results for various types of FCCs, and the methods and correlations used to predict an FCC's drag impact on full-size ships. For more information introducing the topic of FCC mechanisms and their impact on drag forces, see Hellio and Yebra (2009).

Drag performance of fouling control coatings

The primary role of FCCs is to minimize the drag of the ship. Primarily, drag results from a combination of the coating's surface roughness, potential mechanical damage, and accumulation of biofouling (note that these parameters are interrelated). This section presents a short introduction to the most important FCCs and their mechanisms with respect to reduction of friction and biofouling. In this paper, the term FCC refers to any type of underwater top-coat that has an antifouling potential (i.e., both fouling release and conventional biocidal antifouling coatings). The terms fouling control coatings or antifouling coatings are also evidenced in the literature to describe the entire coating category used for biofouling prevention.

An unprotected ship hull will become biofouled after a relatively short immersion time (Barret, 1985). The development of biofouling drastically limits the speed and/or increases the fuel consumption. For this reason, mankind has tried to prevent or limit biofouling for centuries. Indeed, the oldest sources are dated to 700 B.C (Almeida et al., 2007). The two main FCC technologies commercially available today are conventional biocidal antifouling coatings and the so-called fouling release coatings. For a thorough review of the principles and mechanisms of biocidal antifouling coatings, see Yebra et al. (2004), Kiil et al. (2001) and Kiil et al. (2002). For fundamental principles and mechanisms of FCCs, see Lejars et al. (2012).

An optimal FCC must meet strict requirements (Chambers et al., 2006):

- Prevention (limitation) of biofouling, regardless of a ship's operating profile
- Environmental soundness
- Economic viability
- Longevity
- Strong adhesion with the underlying coating (tie-coat)
- Mechanical strength
- Long-term durability
- Low drag
- Specific target (i.e., targeted only for species that can attach to ship hulls)

Recent developments in the area of fouling release and biocidal hybrid antifouling coatings are excluded from the generic descriptions since they represent novel working mechanisms (e.g., Thomas et al. (2004) and Fathom Focus (2013)).

Principle of biocide-based antifouling coatings

The principle and mechanisms behind biocide-based antifouling coatings are fairly well characterized by the incorporation of active ingredients (biocides) into a film-forming organic matrix. Upon immersion, the active ingredients are released in a controlled manner to prevent or limit biofouling. Various kinds of biocide-based antifouling coating systems exist, such as control depletion polymers (CDP) and self-polishing copolymer (SPC) coatings, and they are often grouped according to the type of binder. This paper excludes older biocide-based antifouling coatings such as soluble- and insoluble matrix coating technologies, as they have little market share for larger commercial ships.

Self-polishing copolymer coatings

SPC coatings are characterized by several distinct properties (Yebra et al., 2004). They exhibit a controlled biocide release rate, which allows a fairly constant leaching rate over time at constant seawater conditions. Also, the polishing rate typically increases linearly, not exponentially with speed. As a result, at low or no speed, a slow polishing rate will occur, providing biofouling protection. The polishing rate of SPC coatings can be up to 15 µm per month, although they are often much lower at typical conditions for a traveling ship (e.g., Kiil et al. (2002) and Monfared et al. (2008)). Another property is a thin and stable leached layer thickness established between two distinct moving fronts: the dissolving pigment, or leaching front; and the eroding polymer front (Kiil et al., 2001). The leached layer thickness is fairly stable and low, with values typically ranging between 10 µm and 20 µm (Yebra et al., 2004).

The term self-polishing has, traditionally, been associated with a progressive thickness depletion confined at the outer surface of the SPC coating, which leads to a continuously renewed bioactive surface (Olsen & Yebra, 2013). The exact definition has, however, been an issue of intense debate over the years. Almeida et al. state that the efficiency of SPC coatings has allowed for dry-docking intervals of up to 5 years (Almeida et al., 2007). However, marine paint companies often claim efficiency up to 7.5 years for their best performing SPC coatings (Det Norske Veritas, 2010).

Control depletion polymers

CDPs, also known as ablative or erodible coatings, are similar to the traditional soluble matrix technologies. The difference stems from the fact that CDPs use synthetic organic resins in addition to rosin derivatives. Once in contact with seawater, the biocides dissolve together with the soluble binder, and the dissolution process-controlling ingredients are removed from the surface. A key difference between the CDP and SPC coatings is the fact that the binder dissolution mechanism is driven by hydration and dissolution, not hydrolysis. CDP technologies are effective for up to 36 months (Yebra et al., 2004).

Principle of fouling release coatings

The working mechanism of traditional FCCs relies on a dual mode of action, that is, non-stick properties and a biofouling (fouling) release behavior. The principle of FCCs is to use the exerting force of water against the hull of a traveling ship to remove or limit biofouling. Biofouling organisms have difficulty adhering to the smooth, low-energy surface; thus, either they move away to find a more favorable site for settlement or the seawater flowing over the hull removes them during the voyage (Kovach & Swain, 1998). FCCs are, therefore, particularly suited for ships that travel at sufficiently high velocities and remain in port for only brief periods of time. In contrast, these coatings are less likely to benefit ships, such as pleasure boats, traveling at low velocities and remaining in port for long periods of time.

Present FCCs are based on cross-linked poly-dimethylsiloxanes (PDMS), and they usually contain oil additives to enhance their slippery properties. Fluoropolymer FCCs can contain oils with fluorinated acrylate polymers, perfluoropolyether polymers, and poly (ethylene glycol) fluoropolymers (Lejars et al., 2012). Studies have shown that surface properties do not solely dictate the fouling release properties, however; coating thickness also plays an important role in bio-adhesion. For example, if FCCs are too thin (below ≈ 100 µm dry film thickness), barnacles can adhere to the underlying coatings, thereby establishing firm adhesion. A thin film does not have the ability to absorb the cutting force of the barnacles as they attach to the surface, and once they penetrate down to the underlying hard primer, their adhesion strength increases greatly (Townsin & Anderson, 2009). The efficacy of FCCs relies solely, if sufficiently thick, on the special nature of the surface. As a result, one drawback of current FCCs is their susceptibility to scraping or gouging during for instance

mooring, due to their elastomeric nature. Conventional biocidal antifouling coatings suffer the same fate, but since they do not rely solely on their surface properties for their efficacy, the issue is not considered to be as significant (Townsin & Anderson, 2009).

Summary

Table 1.1 displays the active lifetime, limitations, and advantages associated with biofouling protection and drag of FCCs used in today's commercial market.

Table 1.1. Active lifetime, limitations, and advantages associated with biofouling and drag of the FCCs used in today's commercial market.

Coating system	Lifetime [years]	Limitations	Advantages	Reference
Tin-free SPC	3-5 (7.5)	Lower efficiency compared to tributyltin (TBT)-based coatings	Lower cost compared to TBT-based coatings Less environmental harm compared to TBT-based coatings	Almeida et al., 2007 and Det Norske Veritas, 2010
CDP (ablative)	3	Poor self-smoothing Increasing leached layers with immersion time Biocide release not constant Little activity during idle periods Higher cost before applying new coats (sealer coating often needed)	Low cost	Yebra et al., 2004
Fouling release	5-10	Potential surface damage from in-water cleaning High risk of biofouling under static conditions.	Small environmental impact Low initial friction.	Lejars et al., 2012

Table 2.1 presents a distribution of the volume of applied FCCs and conventional biocidal FCCs for the year 2011. Presently, the use of FCCs is fairly limited, covering about 6.0 percent of the market. However, the market share of FCCs is increasing, especially in the sector of the marine market comprising larger industrial ships with larger fuel consumptions (Karunanidhi et al., 2012). Furthermore, the volume of coating needed per area for FCCs is typically less than that needed for conventional biocidal antifouling coatings. Consequently, the percentage of square meters of FCCs would be higher than the volumetric percentage shown in Table 2.1.

Table 2.1. Distribution of applied volume of FCCs in various geographical regions in the year 2011 (Karunanidhi et al., 2012). Karunanidhi et al. use the term acrylate instead of conventional biocidal antifouling coating (Karunanidhi et al., 2012).

Geographical region	Fouling release coatings [%]	Conventional biocidal antifouling coatings [%]
China	3.20	38.28
Asia Pacific	1.01	30.48
Japan	0.79	10.16
Western Europe	0.22	7.30
North America	0.28	4.32
Eastern Europe	0.39	3.09
Middle East and Africa	0.028	0.22
Latin America	0.0056	0.22
World	5.93	94.07

Fundamental fluid mechanics related to flow of water over ship hulls

Frictional forces act against the forward direction of any moving object, relative to the fluid velocity. In other words, frictional forces arise due to the fluid flowing over the surface. The properties of an FCC system are, therefore, essential for the friction of a ship, as they impact the forces acting in opposition to its forward motion. Typically, the drag forces from seawater are divided into form drag forces and skin friction, (i.e., frictional forces or frictional drag). In the field of FCCs, the objective is to minimize the drag caused by water flowing over the surface (skin friction).

Drag on a ship hull

Fluids flow over rough and smooth surfaces in a wide variety of situations, in both natural environments and engineering applications (e.g., vehicles, pumps, wind turbines, pipelines, and ships). As a result, extensive research has been devoted to the drag forces induced by flow over surfaces with varying roughness. In the case of a ship, the theoretical effective power (towing power), P_E (in Watt), necessary to move a ship through water is, equation (1.1):

$$P_E = F_T U = \tfrac{1}{2}\rho C_T U^3 A_H \qquad (1.1)$$

where F_T is the total resistance, U is the speed of the ship, C_T is the total resistance coefficient, A_H is the wetted hull area, and ρ the seawater density.

The effective power necessary to move a ship through water is proportional to the ship's speed cubed and is also proportional to the total resistance coefficient. An effective (and popular) way to decrease fuel consumption over a given distance is, therefore, to decrease the speed of the ship. However, this increases the traveling time. The ship powering requirement in terms of shaft power (SP) is impacted by the overall efficiency of the propeller and shafting, equation (2.1):

$$SP = \frac{P_E}{PC} \tag{2.1}$$

where PC is the propulsive coefficient, representing the overall efficiency of the propeller and shafting (Schultz, 2007). The value of the propulsive coefficient usually ranges between 0.5 and 1 (derived from MAN Diesel and Turbo (2011)).

The total drag coefficient consists of a form drag resistance coefficient, C_R, an air resistance coefficient, C_A, and a skin friction coefficient, C_F, equation (3.1):

$$C_T = C_R + C_F + C_A \tag{3.1}$$

The form drag results from wave and wake-making, while the skin friction is due to the tangential shear stress on the ship's hull, caused by the fluid flowing over it. The air resistance force, F_A, is given by equation (4.1):

$$F_A = \tfrac{1}{2}\rho C_A U^2 A_{air} \tag{4.1}$$

where A_{air} is the cross-sectional area of the ship above water (MAN Diesel & Turbo, 2011).

The form drag force, F_R, is given by equation (5.1):

$$F_R = \tfrac{1}{2}\rho C_R U^2 A_H \tag{5.1}$$

The skin friction force, F_F, is given by equation (6.1):

$$F_F = \tfrac{1}{2}\rho C_F U^2 A_H \tag{6.1}$$

The total drag coefficient for a hull, C_H, is equivalent to equation (3.1), excluding the air resistance, (Schultz & Swain, 2000) equation (7.1):

$$C_H = C_R(Fr) + C_F(Re) \quad (7.1)$$

The form drag is a function of the Froude number, $(C_R(Fr))$, defined as, equation (8.1):

$$Fr = \frac{U}{\sqrt{g\,L}} \quad (8.1)$$

where g is the gravitational acceleration and L is the water line length of the ship.

The Froude number is used to determine the form drag resistance of ships with different lengths and velocities. A high Froude number indicates a large form drag. The skin friction, in turn, is a function of the Reynolds number, $(C_F(Re))$, defined as, equation (9.1):

$$Re_s = \frac{U\,L}{\vartheta} \quad (9.1)$$

where ϑ is the kinematic viscosity.

The Reynolds number of a ship relates to its surface friction, so a large Reynolds number results in a high surface friction. The opposite is true for the skin friction coefficient, which typically decreases slightly when the Reynolds number increases. Equation 8.1 clearly shows that, as the Froude number decreases (i.e., the form drag decreases), the length of a ship increases when the speed is constant. Equation (9.1), in turn, reveals the fact that the Reynolds number increases (i.e., the surface friction increases) when the length of a ship increases, if a ship is maintaining a constant speed (Amfilokhiev & Conn, 1971). In general, a larger ship has a larger total resistance than a smaller ship. However, when the total resistance divided by the length of the ship is evaluated, the resistance per hull meter decreases as the ship increases in length. Therefore, the use of larger ships is beneficial when moving goods, as the power per mass of goods decreases compared to smaller ships. Practical constraints, such as the size of the Suez Canal and the structural integrity of larger ships do, however, limit the size of ships (Paik & Frieze, 2001).

The relative contribution to the total resistance from the form drag and skin friction of a typical naval ship is shown in Figure 1.1. At low to moderate velocities (Fr< 0.25), the skin friction is the largest component of the total drag (Salta et al., 2010). At higher velocities, however, the form drag, designated by the sum of form and wave-making in Figure 1.1,

becomes dominant. Figure 2.1 shows the resistance in tons as a function of speed (knots) for the destroyer Yudachi. Noticeably, both the skin friction (frictional resistance in the figure) and form drag (residual resistance in the figure) increase with increasing speed, although the skin friction increases relatively slowly, as opposed to the form drag.

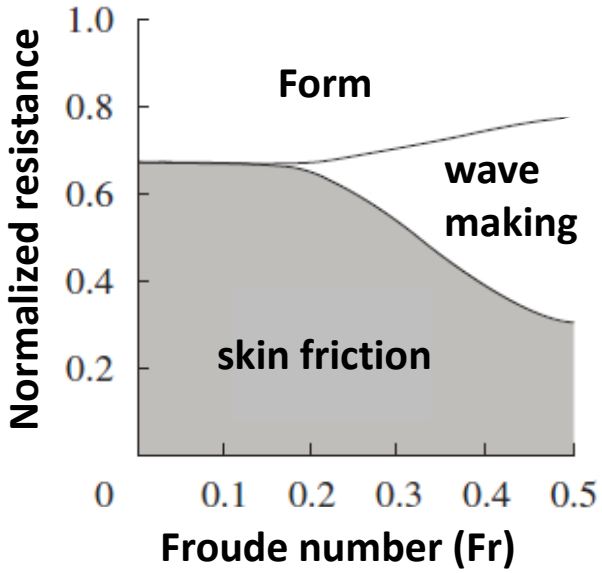

Figure 1.1. Normalized resistance (resistance between 0 to 1) of a ship hull as a function of the Froude number (modified from Salta et al. (2010)).

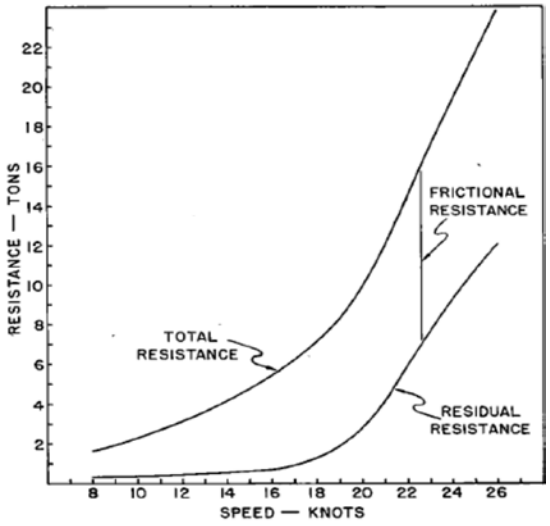

Figure 2.1. Total resistance, form drag (shown here as residual resistance), and skin friction (shown here as frictional resistance) of the destroyer Yudachi in tons versus speed (modified from U.S. Naval Institute (1952)).

In short, the hull resistance is the summation of the forces in the direction of motion of the tangential stresses that the water produces on the hull; apart from the viscosity and density of water, the hull resistance primarily depends on the area, length and roughness of the wetted area of the hull, as well as the speed of the ship (King, 1982). It is significant to note, however, that an increase in mechanical roughness or biofouling exerts a greater relative influence at low to moderate velocities than at high speed (Schultz, 2007). Since mechanical damage or biofouling cause an increase in skin friction, leading to a higher total drag, the development of low-friction FCCs is essential, especially the development of FCCs that can prevent or limit biofouling at these lower speeds where marine organisms can attach more easily.

The operation of ships at maximum speed can be estimated from a ship's Froude number. Most conventional ships do not have sufficient power to operate at velocities associated with a Froude number greater than 0.4 (Parnell & Kofoed-Hansen, 2001). A ship equipped with the power to operate up to a Froude number of 0.4 and having a water line length of

300 m, would, therefore, have a maximum moving speed of approximately 22 m/s (≈40 knots). Figure 3.1 provides an example of a wake (at stern) and wave (along hull) pattern, which is responsible for the form drag, for a model of the KRISO container ship (KCS) with a Froude number of 0.26 (Kim et al., 2001). The Cartesian co-ordinates (X, Y) are used to display the data, where X denotes the downstream direction, and Y the starboard. The origin of the coordinates is located at midship on the free surface. All the coordinates are non-dimensionalized by the length between perpendiculars of the model ships, that is, the approximate water length of the ship.

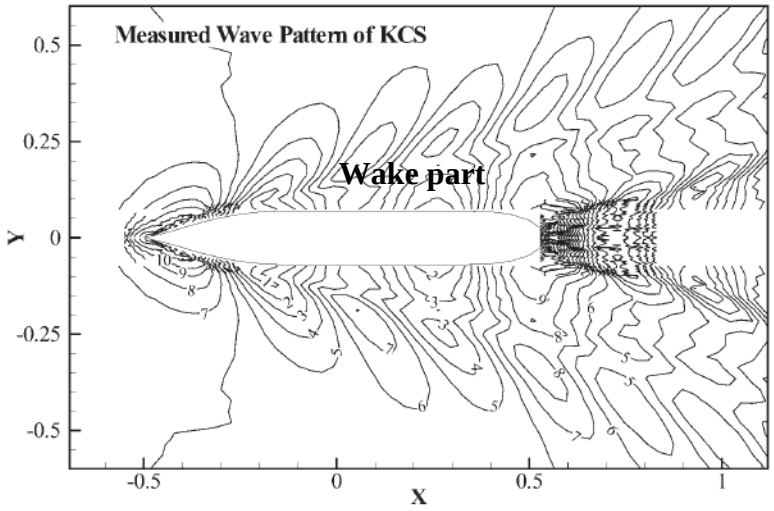

Figure 3.1. Measured wave and wake patterns of the model of the KRISO container ship (KCS) with a Froude number of 0.26 (modified from Kim et al. (2001)).

Figure 4.1 presents a schematic flow regime along a ship hull which determines the magnitude of the skin friction. From the bow and along the first part of the hull, the flow will be laminar, followed by a short transition region which, further downstream, develops into a highly turbulent region with a steadily increasing boundary layer thickness. The turbulent flow region covers the vast majority of a hull at typical traveling velocities. Turbulent wake flows start occurring at the separation point, a certain distance before the stern.

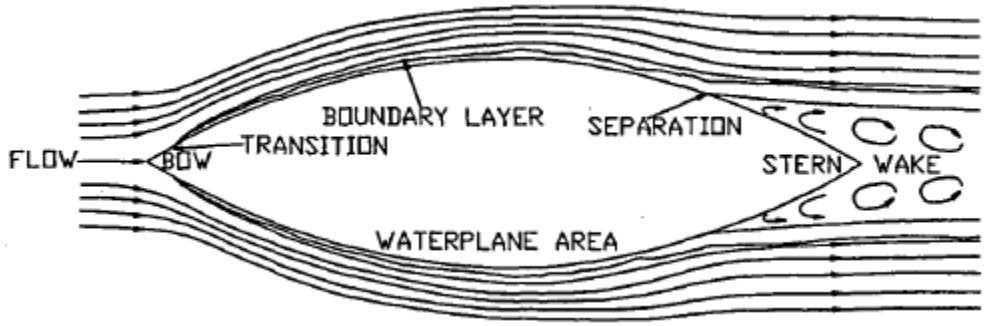

Figure 4.1. Schematic of the flow regime along a ship (Schultz & Swain, 2000).

The form drag and skin friction are the primary resistances responsible for the fuel consumption where only the skin friction is significantly affected by biofouling on the hull surface. The increased annual fuel cost of a biofouled hull compared to a clean hull can be estimated. Several factors must be assumed: (a) the form drag, air drag, and skin friction contributes with 28%, 2%, and 70% to the total drag for a clean hull of a bulk carrier, respectively; (b) for a biofouled hull, the form and air drag remains constant, while the skin friction increases by 40% due to biofouling (MAN Diesel & Turbo, 2011)); (c) a bulk carrier in clean condition uses 30 tons of fuel oil per day when traveling (Kiil et al., 2001); (d) the fouled and clean bulk carriers travel for 80% of the year, and (e) the fuel oil price for both carriers is $600 per ton. Given these assumptions, the price of fuel oil per year for a bulk carrier with a clean hull would be 10.51 million dollars, and the price of fuel oil per year for a bulk carrier with a biofouled hull would be 11.98 million dollars per year. Therefore, based on this example, a biofouled hull costs an additional 1.47 million dollars annually, compared to a clean hull. Clearly, this example demonstrates the necessity of developing and applying FCCs that limit or prevent biofouling.

Parameters impacting total drag

From a design point of view, the ship design (ship geometry); propulsion system (propeller and engine); and surface condition, which is related to the choice and condition of the coating system, are the three main parameters that influence the overall fuel efficiency of a ship. For newly built ships, all three parameters must be considered in order to minimize fuel consumption. For existing ships, the FCC system is the only one that usually influences their efficiency, because ship geometry and propulsion are rarely subject to change after a ship has been built. Therefore, apart from retrofitting, the only means to enhance fuel efficiency

for the existing fleet is by reducing the skin friction. The main parameters identified to affect skin friction are:

- Speed
- Seawater parameters (i.e., temperature and salinity of seawater)
- Weather parameters (i.e., wind, waves, and currents)
- Coating surface conditions (e.g., the presence of biofouling, roughness, and potential mechanical damage)

The following sub-sections briefly detail the influence of the first three parameters with respect to skin friction, while the coating surface conditions are addressed in the section 'Impact of the coating surface condition on drag forces'.

Speed

A ship's speed largely impacts (a cubed dependency) its necessary towing power, as noted earlier. However, the speed of a ship also influences the degree of biofouling. The speed distribution (e.g., maximum speed, average speed, frequency of idle periods, and duration of idle periods) influences the degree of biofouling development, and subsequently, the skin friction over time. Idle periods will cause more biofouling, compared to periods when a ship is traveling. In fact, the fouling organisms normally encountered on ship hulls cannot colonize on ships traveling at velocities above 4-5 knots. For this reason, it is considerably easier to protect the hulls of high-speed ships and those that are rarely in port, than the hulls of slower, more idle ships (Almeida et al., 2007).

Temperature of seawater

The temperature of the seawater is a critical parameter because fluid properties and biofouling activity change with temperature. Table 3.1 displays the dynamic viscosity and density of standard seawater (ITTC, 2011). As the temperature increases from 1°C to 30°C, the dynamic viscosity of water reduces by more than 50%, while the density decrease is very limited (≈0.5%). Lackenby stated that, for a smooth turbulent flow, the net effect is a reduction in resistance of approximately 2.5 % for a rise in temperature of 10 °F (≈5.6 °C), which is due primarily to changes in the viscosity (Lackenby, 1962).

Table 3.1. Dynamic viscosity and density for standard seawater (ITTC, 2011).

Temperature T [°C]	Dynamic viscosity mμ [mPa·s]	Density ρ [kg/m^3]
1	1.843	1028.09
5	1.620	1027.72
10	1.397	1027.00
15	1.220	1026.02
20	1.077	1024.81
25	0.959	1023.39
30	0.861	1021.77

Shear stress consists of viscous and turbulent shear stress. The viscous shear stress is proportional to the dynamic viscosity, whereas the turbulent shear stress is proportional to the density of the fluid. The density of seawater changes only slightly within the temperature range expected to be encountered by ship hulls. Ships typically operate in the transitional or rough regime, causing the turbulent shear stress to be much greater than the viscous shear stress. Therefore, the temperature changes impacting the turbulent shear stress are of minor importance. Furthermore, since the viscous shear stress contribution is relatively small in the transitional or rough flow regime, the temperature changes that would affect it are of little significance to the total shear stress. It must be stated that this relationship is complex and the dependency of the total shear stress on temperature must be verified experimentally. However, it is well known that the total shear stress will decrease slightly as temperatures increase.

The temperature is also important for ship performance over longer periods of time because it affects various coating properties, such as the rate of chemical reactions in the binder and the dissolution rates of biocides (Kiil et al., 2001; Kiil et al., 2002). In addition, a high temperature typically leads to higher biofouling intensity. The temperature is rarely considered in the performance analyses by ship owners or operators, although the temperature does have some influence on drag (Munk et al., 2009). The lack of interest in temperature influence on drag might also be because it is given by the traveling route and, therefore not, subject to be changed by design.

Salinity of seawater

Capurro defined salinity as ‘the total of solid materials in grams in 1 kilogram of sea water when all the carbonate has been converted to oxide, the bromine and iodine replaced by

chlorine, and all organic material completely oxidized'(Capurro, 1970). In other words, the concentration of the dissolved salts is designated as a single solute. The salinity of the world's oceans is fairly uniform, with an average of approximately 3.5 wt%, corresponding to 0.6 M. However, local variations in the salinity may exist, for instance, near river mouths. The relative amounts of various salt components in seawater are practically constant, with NaCl being the most abundant compound (Capurro, 1970). The fluid properties affected by salinity are density and, therefore, viscosity (ITTC, 2011), which influence the drag of an object moving through water. Since larger ships are expected to spend the vast majority of their time in oceans, where the salinity does not differ substantially from 3.5 wt%, the small variation in salinity is not expected to influence the total drag over longer periods. The salinity does, however, affect self-polishing rates and biocide release rates and, consequently, the ability to prevent or limit biofouling. It was, for instance, found that when the salinity decreases from 0.55 M to 0.28 M, the leached layer thickness decreases from 7.2 µm to 4.9 µm in steady state conditions for an SPC coating. Furthermore, that same decrease in salinity corresponds to a decrease in the release rate of Cu^{2+} from approximately 120 µg/(cm^2·day) to 45 µg/(cm^2·day) (Kiil et al., 2002). The influence of salinity on drag for FCCs has yet to be investigated in depth. FCCs are, ideally, chemically inert; therefore, the influence of salinity is expected to be of minor importance, as the chemical surface structure is expected to remain identical, even in cases of varying levels of salinity typically encountered by traveling ships. From a drag point of view, the variation in salinity has not been given much attention, most likely due to the parameter's small variation as well as the fact that the salinity is given by the traveling route and, therefore not, subject to be changed by design.

Weather parameters: wind, waves and currents

Wind, waves, and currents vary along traveling routes. Although they influence drag, the parameters are not subject to design influence. Weather routing of ships can, however, be used to establish the shortest time route or the most economical route by applying available information about the weather conditions with regard to the wind, waves, and currents (e.g., Padhy et al. (2008)) However, because the performance of FCCs has little, if any, significant impact on the drag arising from wind, waves, and currents, these parameters are

not factors worthy of consideration in the FCC design process. For an introduction to the topic of wave resistance, see Havelock (1940), Kinsman (1965), Mei (2005) and Newman (1977).

Experimental setups for determination of skin friction

Full- and small-scale measurements are used to determine the drag impact of the parameters listed in the section 'Parameters impacting total drag'. Experimental setups applied to measure skin friction on FCCs described in the following sections include rotating disks, rotating cylinders, towing tanks, water tunnels, static and dynamic panel exposure tested on a boat, pipes, and optical methods. The task of accurately converting small-scale skin friction coefficients (C_f) into full-scale ones for either clean or biofouled FCCs is very complex; in fact, to the authors' knowledge, no small-scale test has ever been conducted with subsequent full-scale testing. Furthermore, even if the conversion of small scale results were considered accurate for biofouled FCCs, the actual fouling pattern on a ship would likely be much more heterogeneous, which would complicate the up-scaling. Differences in the intensity and type of biofouling over a hull can be caused by various factors, including light-shade effects, larval zonation in the water column, differences in the flow patterns and stresses along the hull, and the color of the coating system (Dobretsov, 2013; Visscher, 1928). The drag comparison of FCCs via small-scale measurements can, however, be useful, as they can indicate differences in fuel-saving capabilities, although estimations may be linked with some uncertainty. Small-scale measurements are advantageous because they are more economical than full-scale experiments; they allow experiments to be conducted faster and they are capable of varying only one or a few parameters at a time, which is useful when determining the FCC's drag performance. Static experiments have been conducted where, for example, flat plates and disks have been immersed in oceans or rivers with subsequent 'true' biofouling. However, although relevant, such methods only realistically resemble a static body, such as a stationary ship at port conditions, without consideration of the mechanical shear stress encountered by a moving ship. Zargiel and Swain stated that dynamically grown biofouling, which better mimics ship conditions, should be used when addressing biofouling's influence on drag, because static and dynamic exposures differ in the

diversity of the species and the mass of biofouling attached to FCCs when compared at otherwise similar conditions (Zargiel & Swain, 2013). The first means of accurately determining the surface friction via a small scale setup was done by the English engineer William Froude in the latter part of the 19th century where he invented a towing tank setup for this purpose (e.g., Froude (1872)).

Rotating disks

The friction disc machine (FDM) has been used by several authors to measure the drag induced by surfaces (e.g., Granville (1982), Haslbeck and Bohlander (1992), Holm et al. (2004) and Loeb et al. (1984)). Granville used rotating disks to determine the skin friction coefficient of rough surfaces (Granville, 1982). The indirect method described involves measuring the torque and rotations per minute (RPM) of a rotating disk uniformly covered with the roughness under investigation. Figure 5.1 illustrates an FDM, including the most important parts therein. The FDM used by Holm et al. employed disks of 22.86 cm in diameter and 0.3 cm in thickness (Holm et al., 2004). The disks were immersed in a cylindrical test chamber of 25 cm in height and 33 cm in diameter. The disks were then spun from 700 RPM to 1500 RPM, with changes of 200 RPM. The FCC disks were statically exposed for a time period ranging between 21 and 24 days. In all cases, the FCCs experienced an increase in drag. An ablative antifouling coating resulted in the lowest increase, 9%, whereas three fouling-release coatings experienced increases of 17%, 27%, and 29%, based on their skin friction coefficient development (Holm et al., 2004).

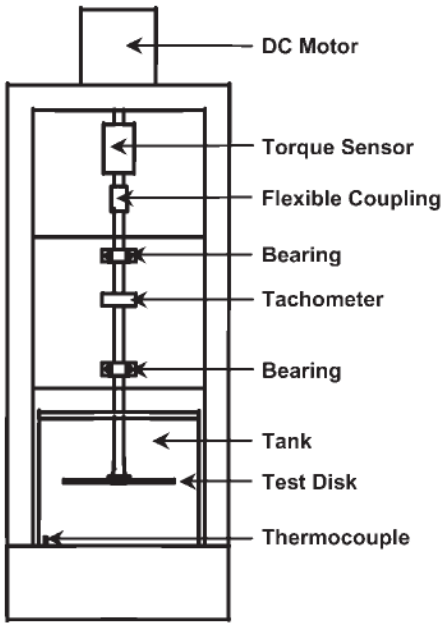

Figure 5.1. Schematic illustration of the friction disk machine (Holm et al., 2004).

Figure 6.1. Friction disk machine at TNO, Den Helder (Klijnstra, 2014).

As depicted in Figure 7.1, along the disk surface, three regions can be distinguished: a laminar flow region, a transient region, and a turbulent flow region.

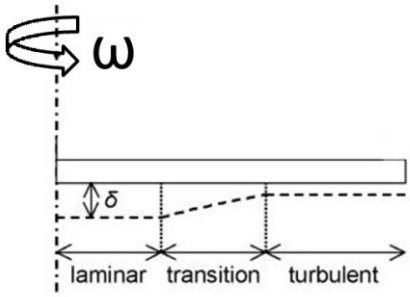

Figure 7.1. Schematic illustration of flow regions (laminar, transitional, and turbulent) along a rotating disk. Only half of the disk is shown (modified from De Jong et al. (2002)).

Several authors have successfully applied the FDM to correlate roughness with drag. An interesting feature of the FDM is that the shear stress on the investigated disk changes as a function of the radius. The FDM test method will, therefore, determine results for the investigated surface with different shear stresses applied, as opposed to, for example, the sides a rotating cylinder in a Coutte flow (see section 'Rotating cylinders'). This can be considered an advantage because it will allow for the evaluation of the drag performance of the FCC under a wide range of shear stresses. The FDM is also beneficial because the coating layer is simple to apply due to the flat geometry and the drag for the investigated surface can be quickly measured. Furthermore, a visual inspection is possible for an investigation of

the surface. The varying shear stress could, however, be considered a limitation because it prevents the application of a uniform shear stress to the disk surface. The shear stress in the center of the disk is small, and it increases as the radius increases. Additionally, the constrained flow in a tank could potentially cause uncertainties regarding the actual speed of the disk relative to the fluid. This uncertainty can be limited by either a setup with unconstrained flow (e.g., a very large tank), or the determination of the swirl factor, which accounts for the wall effect.

Rotating cylinders

In order to measure the drag induced by surfaces, several authors have used a rotary setup, in which an inner cylinder rotates inside a static cylinder (e.g., Candries et al. (2003b), Ghani et al. (2010), Kawaguchi et al., Mirabedini et al. (2006) and Weinell et al. (2003)). A rotating cylinder system and its most essential parts are shown in Figure 8.1. In this case, the inner (rotating) cylinder, where test samples were applied, had a diameter of 30 cm and a height of 17 cm. The diameter of the outer, static cylinder was 38 cm, and its height was 17 cm. The water tank's volume was 400 l, and its temperature could be controlled using a heat exchanger. The tangential velocity of the cylinder surface ranged between 10 knots and 35 knots for the experiments conducted by Weinell et al. (2003).

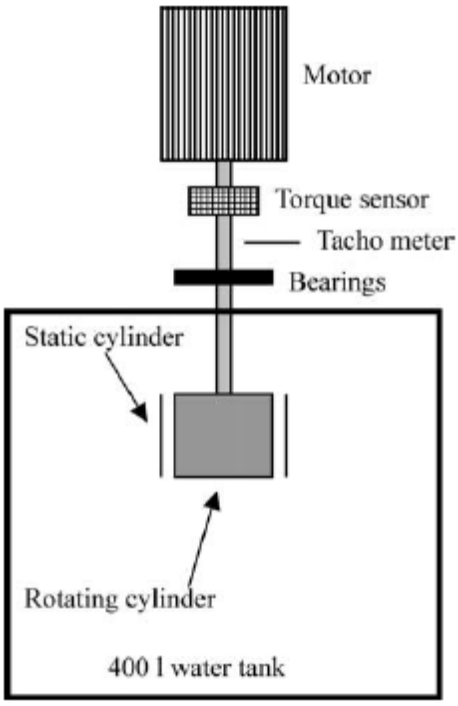

Figure 8.1. Schematic illustration of a laboratory-scale, rotary setup (rotating cylinder). Test samples can be applied to the surface of the rotating cylinder. The maximum tangential velocity applied was 35 knots (Weinell et al., 2003).

Figure 9.1 Laboratory-scale rotary setup.

Weinell et al. determined the skin friction coefficient of surfaces by means of a rotating cylinder (Weinell et al., 2003). This indirect method described involves measuring only the torque and the RPM of the cylinder under investigation. The rotating cylinder setup has proven to be effective in measuring differences between the resistance of smooth and rough surfaces; indeed, this type of setup is used in the FCC industry and at scientific institutes (e.g., Candries et al. (2003b) and Weinell et al. (2003)). The advantages of the apparatus are its low operating cost, easy maintenance, compact size, and simple construction. In contrast to friction planes (e.g., flat plate tests in towing tanks), the rotating cylinder setup offers a distinct advantage because it does not suffer from complications associated with the development of a boundary layer along the length of a test section. One disadvantage of the rotor is caused by the end effects, which occur at the top and bottom, where the flow regime makes the transition from 'cylinder' to 'disc' flow. A further disadvantage could potentially be related to the difficulties of obtaining the same FCC smoothness as that of plane surfaces, which bear a closer resemblance to hull surfaces than cylinders do. The rotor setup could, therefore, possibly measure a rougher surface than flat plates would measure

(Candries et al., 2003b). Furthermore, the rotating cylinder system produces results that are difficult to interpret accurately, mainly due to the formation of the Taylor-Couette flow. The term Couette flow describes the flow between two surfaces that are in close proximity, such that the flow is dominated by viscous effects, and inertial effects are negligible. When considering flow in an annulus, the Navier-Stokes equations can be solved exactly by analytical techniques, but when subject to a number of significant assumptions, particularly that of laminar flow, the application of the resulting solution is severely limited. In practical applications there is a need to quantify the power required to overcome the frictional drag of a rotation shaft at angular velocities, which far exceed the velocities at which laminar flow occurs. When it is not possible for the radial pressure gradient and the viscous forces to dampen out and restore changes in centrifugal forces caused by small disturbances in the flow, the fluid motion is unstable, resulting in a secondary flow, named the Taylor-Couette flow. Although the Taylor-Couette flow occurs at sufficiently high rotational velocities, it can also occur at lower rotational velocities if the gap between the cylinders is too large. The interpretation of the Taylor-Couette flow's impact on the skin friction coefficient is complex; although it already has been subject to a vast number of scientific studies, further studies are needed in order to determine its impact (Childs, 2010).

Towing tanks

Of all the test facilities, towing tanks are one of the most frequently employed to estimate ships' resistance to motion. Indeed, many authors have used towing tank tests to investigate friction (e.g., Candries (2001) and Schultz (2002)). Essentially, the setup consists of a long, open-topped tank of rectangular cross section containing water. A rail runs along the top of each side of the wall for the total length of the tank. A carriage, supported by wheels running on the side rails, usually spans the water. The carriage, to which either a flat plate or ship geometry is attached, can be driven either by motors situated 'onboard,' driving the wheel, or by a motor located next to the towing tank driving a long cable, fixed to the carriage. Between the carriage and the flat plate or ship geometry, a drag force gage is placed to measure the drag forces in the longitudinal direction. Figure 10.1 provides an example of a towing tank with a ship model. Typically, a flat plate is used when determining

skin friction, and a ship model is used when determining the form drag of a specific ship geometry.

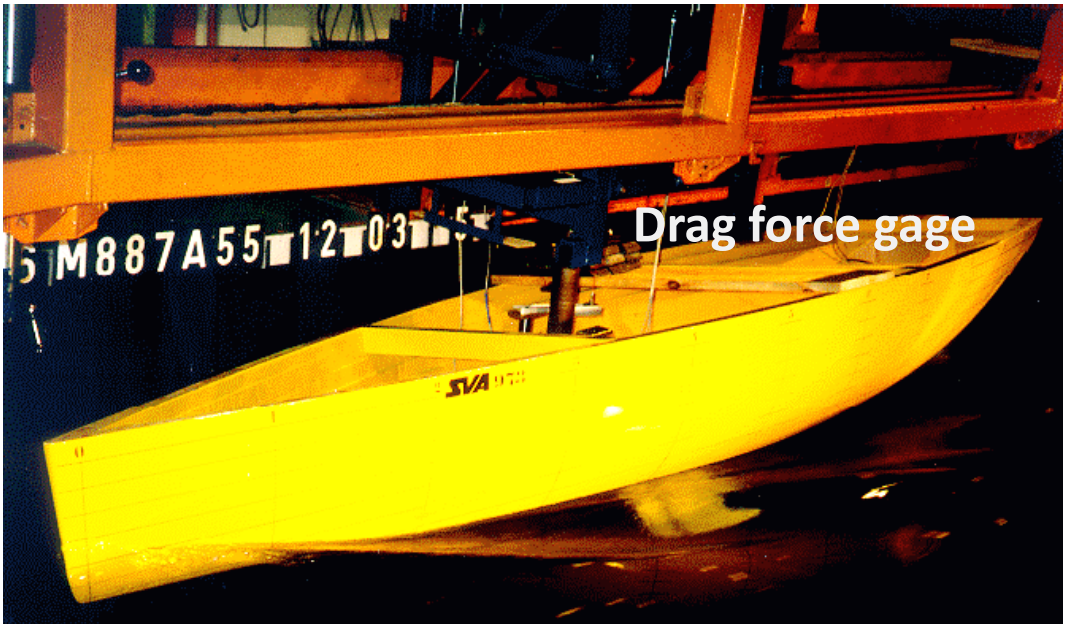

Figure 10.1. Towing tank used for friction and form drag measurements (modified from Hochkirch and Brandt (1999)).

There are several advantages to using a towing tank with a flat plate. For instance, the flow over a flat plate has been studied a great deal; therefore, many correlations exist for this geometry. Furthermore, a flat plate, as compared to a profiled body, has a minimal form drag effect (wake and wave); thus, these effects are reduced to a minimum causing the effect of skin friction to stand out. Compared to a profiled body, a flat plate more accurately simulates large ship hulls with respect to friction. On a flat plate, there are no pressure gradients parallel along the flow direction, affecting the boundary layer. Plates are relatively cost-effective, easy to manufacture, and simple to handle. Finally, FCCs can easily be applied to a flat plate. However, experiments carried out in a towing tank also do suffer some drawbacks. A long tunnel is, for instance, needed to obtain reliable results, due to the development of steady flow scenarios. The development of a boundary layer along the length of the test section will only form as the initial part of a hull, without including the effect from further downstream of the hull. Applying roughness at the leading edge can, however, provoke a turbulent flow, thereby mimicking flow conditions further downstream of a hull. Hydrodynamic similarities between the size of the models and the ships are widely applied (e.g., Schultz (2007)) to minimize this drawback, although uncertainties in the up-

scaling are bound to occur. Finally, end effects at the edge of the plate, where the flow regime makes the transition, causes changes to the local skin friction coefficients at the edges. However, a wider plate results in a less significant transition influence from the edges.

Water tunnels

Water tunnels are widely used and, in principle, they provide identical results to the towing tank. Whereas towing tanks necessitate the movement of the test section through the water, a water tunnel requires only that water move over the test section. Barton et al. provided an example of a water tunnel used to measure drag, shown in Figure 11.1 (Barton et al., 2011).

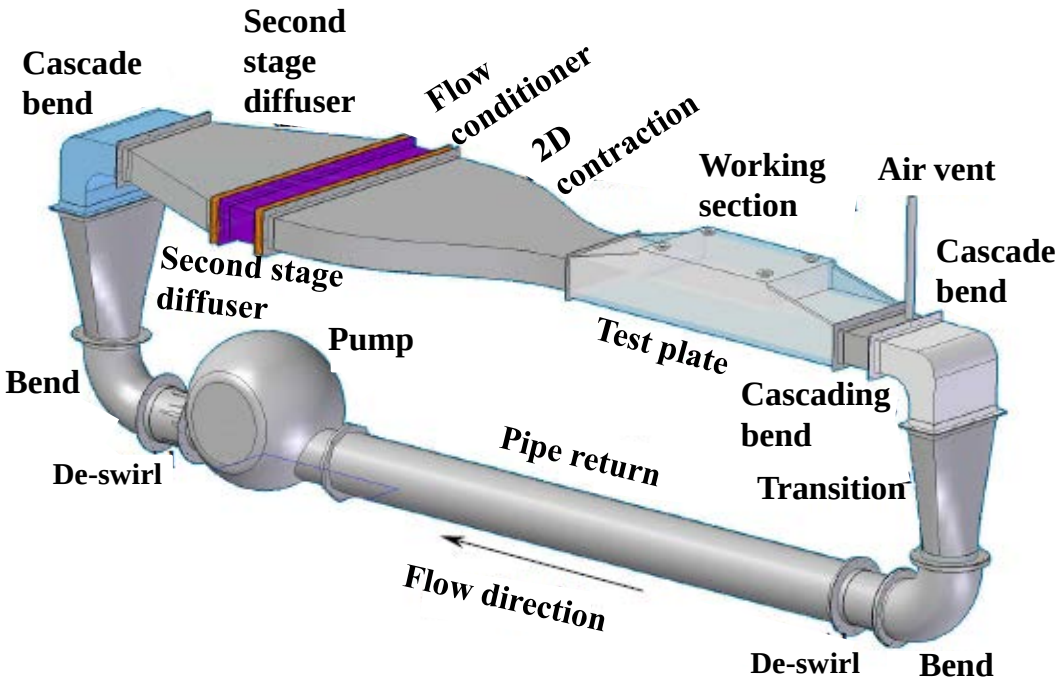

Figure 11.1. Schematic illustration of a water tunnel setup (modified from Barton et al. (2011)). The working section is 220 cm long, 20 cm high, and 60 cm wide (Barton et al., 2011).

The test setup consisted of a closed loop, recirculating water in a tunnel built specifically for the controlled and detailed measurement of local skin friction, drag, and general boundary layer research. A number of components needed to be specially designed to achieve controlled and uniform flow conditions within the working section, which is where the friction and flow properties were measured. The bulk flow velocity through the working section of the tunnel ranged from 0.3 m/s to 2 m/s, yielding a Reynolds number ranging from approximately $5 \cdot 10^5$ to $2 \cdot 10^6$ (equation (9.1)) with the length parameter being the

length of the working section.57 In the water tunnel setup provided by Barton et al. (2011), the working section was 220 cm long, 20 cm high, and 60 cm wide. Additionally, the test surface within the working section measured 99.7 cm long, 59.7 cm wide, and 0.3 cm thick.

A water tunnel offers several advantages, compared to a towing tank. It is often much smaller, and it allows for the incorporation of components that will obtain a controlled flow, such as a honeycomb structure, thereby creating a laminar flow, even at high velocities. Furthermore, optical equipment (see the section 'Optical methods for drag measurements') can be installed at a fixed position in order to investigate the flow patterns for the FCCs under investigation. The relatively small working section and relatively low Reynolds number are amongst the few disadvantages of using a water tunnel when compared to a towing tank.

Static and dynamic panel exposure tested on a boat

The setup described in this section was developed by Swain et al. at the Florida Institute of Technology, USA (Swain et al., 2007). The test consists of a combined static and dynamic exposure of panels followed by drag measurements using a small boat. Panels measuring 25x30 cm2 were exposed in natural seawater conditions at the static immersion site located in the Indian River Lagoon, FL. Figure 12.1 depicts the dynamic test setup, where up to 4 panels could be exposed simultaneously. A rotating stirrer was installed in the bottom of a deep circular tank, measuring 5 ft in diameter and 4 ft deep. The stirrer was maintained at a rate of 60 RPM, resulting in a velocity of water of approximately 5 m/s moving over the panels.

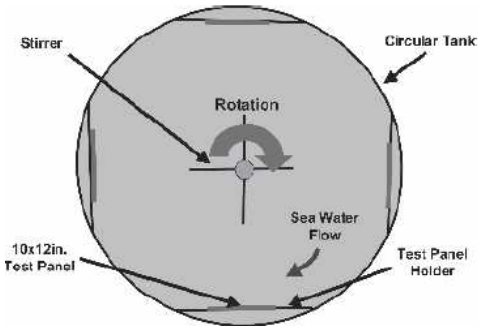

Figure 12.1. Top view of the dynamic test tank (Swain et al., 2007). Reprinted with kind permission from Journal of Ship Production.

Figure 13.1 illustrates the hydrodynamic test facility, consisting of a wet well built into the aft section of the hull of a modified, 9 m Chris Craft Commander.

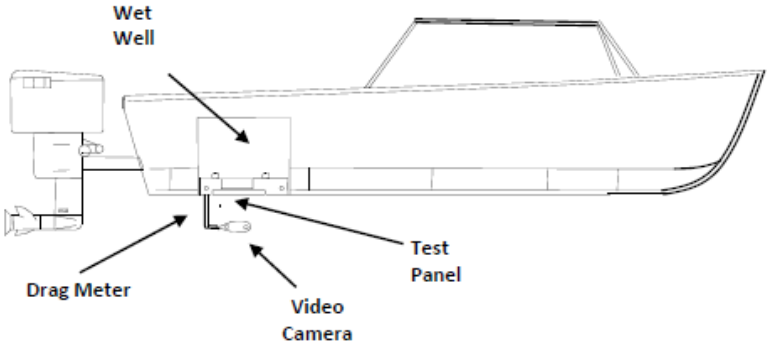

Figure 13.1. Schematic illustration of a hydrodynamic test facility in the form of a boat with a wet well, test panel, video camera, and drag meter. The maximum speed is 17 m/s (Swain et al., 2007). Reprinted with kind permission from Journal of Ship Production.

The boat was capable of testing at velocities of up to 17 m/s and local Reynolds numbers of approximately 5.5 x 107. The test panels were statically and dynamically exposed prior to drag testing. They were mounted on a through-hull instrument. The instrument was equipped with a floating element force gauge that measures drag forces on the FCC; it is also equipped with a video camera, which could observe the FCC surface condition and biofouling communities (Figure 14.1). Figure 14.1 displays a drag meter installed in the well of a boat, where drag forces are applied to the test panels.

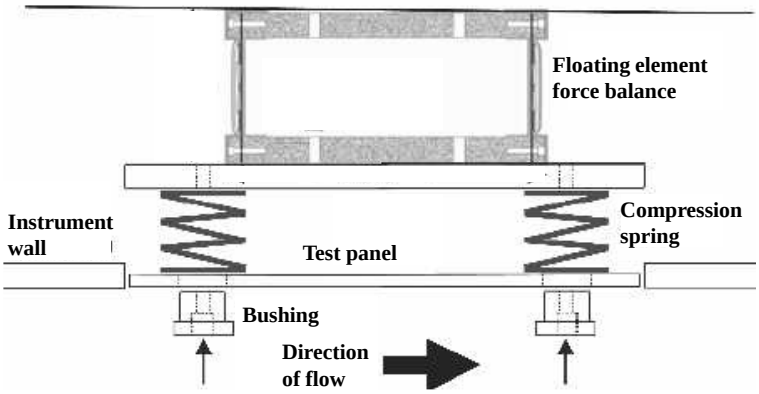

Figure 14.1. Drag meter, which measures drag forces on the coating (Swain et al., 2007). Reprinted with kind permission from Journal of Ship Production.

In the study by Swain et al. (2007), the coatings were subjected to one cycle of 60 days' static immersion and 15 days' dynamic immersion (Swain et al., 2007). One important advantage of this setup is that the panels were exposed to natural seawater during every part of the test. The static immersion resembled the conditions a ship is exposed to in port, while the dynamic exposure, providing water velocities of up to 5 m/s (≈10 knots), resembled the shear stress some ships experience along their hulls, although it can be argued that the velocity is an insufficient representation of the majority of the larger commercial ships. The drag measurement facility could provide velocities of up to 17 m/s (≈33 knots), providing a wide range of dynamic testing possibilities. The setup was also capable of varying the static and dynamic immersion periods, resembling in-port and traveling conditions, respectively, which offers a large degree of flexibility. This method provides an excellent side-by-side comparison, as the panels are exposed to very similar conditions, which is useful when determining the optimal choice of FCC. However, it can be argued that the lack of a continuous intake of seawater, since no new intake occurs during the dynamic exposure, is insufficient to represent actual biofouling conditions during the dynamic exposure. Furthermore, sunlight does not enter the tank; therefore, this aspect of the aging process only partially resembles natural conditions.

Pipes

Flows in pipes are relevant to the FCC industry because resistance in pipes is related to surface properties and, therefore, related to the frictional resistance of FCCs. Experimental tests and flow modeling in pipes has been conducted by several authors (e.g., Brett (1980), Leer-Andersen and Larsson (2003) and Picologlou et al. (1980)). Figure 15.1 shows an

example of a pipe system used to determine the skin friction of FCCs, as described by Leer-Andersen and Larsson (Leer-Andersen & Larsson, 2003). The equipment consisted of a tank, which was a large vertical polyvinylchloride (PVC) cylinder; a cylindrical pipe connected smoothly to the tank; and a pumping system capable of pumping water from a large basin into a tank. The pipe test section could be split axially in order to coat its inside and join it afterward. Before the pressure drop of the 1.5 m long test section was measured, 3.0 m of coated pipe was used to attain a fully developed flow. The pipe in the setup had a diameter of 6.7 cm. Leer-Andersen and Larsson (2003) measured the skin friction coefficients for three types of coated surfaces, known as fiberflocs, and ten coated surfaces with barnacles (Leer-Andersen & Larsson, 2003).

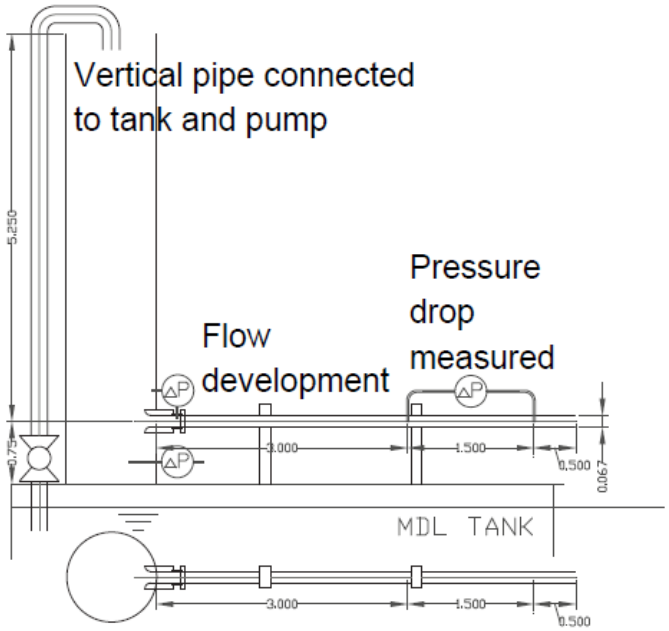

Figure 15.1. Design of the pipe friction measurement equipment (modified from (Leer-Andersen & Larsson, 2003). All dimensions are relayed in meters.

There are several advantages to the test setup used by (Leer-Andersen & Larsson, 2003). The setup is simple with minimal construction and maintenance cost needed. Large increases in the skin friction coefficient can be measured quickly and accurately via simple pressure drop measurements. Furthermore, extensive literature exists regarding the flow in pipes related to mechanical roughness. However, some disadvantages of the test setup have been identified by Leer-Andersen & Larsson (Leer-Andersen & Larsson, 2003). For instance, in this setup the outlet is too close to the test section. A fully developed flow is not attained at the test section because the pipe length is too short. A poor alignment of the pressure taps

influences the differential pressure gauge measurement causing skin friction coefficient uncertainties. A non-uniform pipe diameter causes pressure differences and, therefore, uncertainty. Additionally, accuracy of the measuring equipment is limited, due to low diameter tolerance. PVC material was chosen partly because only pipe material that can be split and joined is applicable. The tolerance of the PVC pipes used was 0.6 mm and the diameter was 6.7 cm; a substantial portion of the uncertainty in the measurements can be explained by the diameter tolerance. Finally, a reduction in the available tube cross section was evidenced due to biofilm, barnacle, or other material accumulation. General disadvantages occur for FCCs, with regard to any pipe setup such as: the closed system creates difficulty with the examination (e.g., roughness, biofilm growth, and the velocity profile inside the pipe); the FCC cannot easily be applied in the same manner as on a ship or flat plate, which causes uncertainties in the upscale to full-scale or the comparison with other experiments where flat geometries are used.

Optical methods for drag measurements

Laser Doppler Anemometry (LDA), also known as Laser Doppler Velocimetry (LDV), is a non-intrusive technique used to measure fluid flow patterns in a high resolution. One advantage of LDA is the fact that precise and reliable flow properties such as boundary layer measurements can be obtained and then used to determine frictional drag over FCCs. Furthermore, measured flow patterns combined with surface roughness might prove useful to discerning the relationship between surface roughness and drag. The fundamental principle of LDA revolves around the Doppler Effect, which causes changing wave frequencies for a moving body relative to a stationary body. Particles that scatter laser light (e.g., polystyrene in water, with a typical size interval between 5 µm to 100 µm) can be immersed in a fluid, and then the reflected light can be used to obtain the velocity profile. If three different lasers are applied, all three velocity components can be obtained. Although several authors have employed LDA to investigate surface friction (e.g., Candries & Atlar (2005), Schultz (2000) and Ünal et al. (2012)), its application has only recently been applied to determine FCC's drag performance. In fact, Candries and Atlar (2005) stated that, to the best of their knowledge, theirs was the first publication in open literature regarding LDA measurements on FCCs.

An LDA setup has several advantages. It allows systems involving complex flows to be easily studied, as the method is non-intrusive. It also prevents flow disturbance, as compared to a pitot-tube, for example. Furthermore, a vast amount of information regarding the flow can be obtained (e.g., boundary layer thickness, displacement thickness, momentum thickness, and instantaneous velocity components in all three directions). The LDA setup also allows very localized measurements of the mean velocity and fluctuating flow properties to be determined, even for a turbulent flow. The flow measurements are extremely precise with LDA, although some sources of errors do exist, as with any measurement technique. One main disadvantage of the LDA setup is the high cost of its commercial instruments. Also, LDA only measures velocity in smaller volumes of fluid; thus, larger flow patterns are impossible to detect. Table 4.1 presents the advantages and disadvantages of LDA for the determination of FCC's drag performance. Hopefully, this technique can be applied in the near future to further enhance the knowledge of the drag performance of FCCs.

Table 4.1. Advantages and disadvantages of LDA in determining FCC's drag performance.

Advantages	Disadvantages
Accurate measurement of flow velocities	High cost of equipment
Applicability with direct drag measurements	Extensive knowledge required
Non-intrusive technique	Indirect estimation of friction

Summary

In short, the ideal properties of a method to determine the drag performance of FCCs include:

- Accurate skin friction coefficient determination
- Correct and feasible conversion to full-scale
- Potential short- and long-term drag performance determinations
- Investigation of several FCCs under identical and ship-like conditions
- Low cost
- Easy use
- Low maintenance and manual work
- Reliable

Every method of determining the drag performance of FCCs has advantages and disadvantages. No clear definition of the best method exists, as each method can be viewed

from various perspectives; nonetheless, Table 5.1 indicates advantages and disadvantages of the methods explored along with specific scientific data for an example of each setup.

Table 5.1. Advantages and disadvantages along with design values for specific test set-ups. The measured range of skin friction coefficients and Reynolds numbers and the estimated uncertainties are also presented for specific test set-ups.

Test set-up	Rotating disk	Rotating cylinder	Towing tank	Water tunnel	Static and dynamic panel exposure tested on a boat	Pipes	Optical methods for drag measurements
Advantages	Small size Easy application of coatings Fairly low cost	Small size Fairly low cost	No pressure gradients Resemblance to ship geometry Vast amount of literature for flow over flat plates	Small size Controlled flow	Flexible immersion conditions (static and/or dynamic)	Vast amount of literature for flow in pipes	Accurate flow pattern measurements
Disadvantages	Varying shear stress over the test surface	Complex interpretation of friction coefficient	Large tank necessary	Complicated flow stability to two- and three-dimensional controlled disturbances	Dynamic immersion could deviate some from actual hull conditions of a moving ship	Large uncertainty Complicated visual inspection	Expensive equipment Indirect drag evaluation
Range of skin friction coefficients	$2.0 \cdot 10^{-3}$ to $1.2 \cdot 10^{-3}$	$2.3 \cdot 10^{-3}$ to $2.7 \cdot 10^{-3}$	$3.5 \cdot 10^{-3}$ to $6.0 \cdot 10^{-3}$	Drag coefficient, C_D, interval of $1.9 \cdot 10^{-3}$ to $1.1 \cdot 10^{-3}$	Drag coefficient C_D interval of $3.0 \cdot 10^{-3}$ to $7.0 \cdot 10^{-3}$	$3.0 \cdot 10^{-3}$ to $2.0 \cdot 10^{-2}$	$2.5 \cdot 10^{-3}$ to $6.0 \cdot 10^{-3}$
Test panel size and shape	Disk diameter of 22.86 cm and 0.3 cm thick	Rotated cylinder diameter was 30 cm and the height was 17 cm.	The flat test plate measured 1.52 m in length, 0.76 m in width and 3.2 mm in thickness	Stainless steel plates measuring 997mm long by 597 mm wide by 3 mm thick, or an acrylic plate of the same area but 5 mm thick	25 × 30 × 0.625 cm aluminum test panels	Pipe length of 1.5 m and 6.7 cm in diameter	LDV equipment shall be used in combination with other setups. In Candries & Atlar (2005) the water tunnel "Emerson Cavitation Tunnel" was used in combination with LDV. A

							1 m long, 0.8 m wide and 3 mm thick flat mild steel plate was used as test surface.
Size	Cylindrical test chamber was 25 cm in height and 33 cm in diameter	Cylindrical test tank with a volume of approximately 400 l. Outer static cylinder was 38 cm in diameter and 30 cm in height	Towing tank was 115 m long, 7.9 m wide and 4.9 m deep.	The working section where test plates were mounted for the study section was constructed of 30 mm thick acrylic sheeting, and measuring 2.2 m long, 0.2 m high and 0.6 m wide.	Motor boat to test panels. A 5 ft diameter and 4 ft deep high-density polyethylene circular tank used to dynamically age coatings.	6 m pipe in vertical direction and 5 m pipe in horizontal direction	7.69 m high and 10.79 m long. The rectangular measuring test section was 1.22 m wide by 0.81 m high and 3.10 m long.
Water velocity or object velocity	Rotational velocity of disk at the edge ranged from 2.66 m/s to 5.70 m/s (700 to 1500 rpm)	Cylinder velocity of 5.14 to 18.0 m/s (317 rpm to 1109 rpm)	The towing carriage had a velocity range of 0–7.6 m/s. In the present study, the towing velocity was varied between 2.0 m/s and 3.8 m/s	The bulk flow speed through the working section of the tunnel ranged from 0.3 m/s to over 2.0 m/s	Boat speed of 13 m/s	7 m/s was the design maximum average flow velocity	Water velocity of, 2, 3, 4, 5 and 6 m/s
Uncertainty	Moment coefficient C_m was determined to approximately ± 2%	The relative uncertainty of M_c was found to be ~ 10–15% at low speed decreasing to ~ 1–2% at high	Overall uncertainty in C_f ± 2%	Uncertainty of 2.7 % (with confidence 95%) in C_D	Not provided for drag measurements	The uncertainty depended on the surface. For a fully rough surface the error was	The uncertainty of C_f for the smooth walls was ±1.4% for the Clauser method, ±4.5% for the Reynolds stress method, and ±2.4% for the Hama

		speed.				estimated to $0.43 \cdot 10^{-3}$	method. For the rough walls it was ±2.5% for the Reynolds stress method and ±3.1% for the Hama method.
Method to measure or determine skin friction or frictional resistance	A sensor installed on the shaft measured the torque produced when the disk rotated	A 50 Nm strain gauge transducer picked up the torque	Overall drag of the plate was measured using a modular variable-reluctance displacement force transducer	A strain-gauge force balance arrangement was used for the total drag measurements	A floating element force gage measured drag on the test panels	Pressure drop over the test section of 1.5 m was used to determine the friction	Laser Doppler velocimetry via the Hama method, Reynolds stress method and the Clauser method
Reynolds number	10^9 to 10^{10}	$7.5 \cdot 10^4$ to $2.6 \cdot 10^6$ (length scale was the gap between the inner and outer cylinder)	$2.8 \cdot 10^6$ - $5.5 \cdot 10^6$	$8.3 \cdot 10^5$ to $3.2 \cdot 10^6$	$5.5 \cdot 10^7$		Momentum thickness Reynolds number of approximately $7.3 \cdot 10^3$ to $3.1 \cdot 10^4$
Reference	Holm et al., 2004	Weinell et al., 2003	Schultz & Myers, 2003	Barton et al., 2011	Swain et al., 2007	Leer-Andersen & Larsson, 2003	Candries & Atlar, 2005

Impact of the coating surface condition on drag forces

The results found in the literature from both full-scale ship trials and small-scale tests document that biofouling and mechanical damages lead to significant increases in the frictional drag (e.g., Haslbeck and Bohlander (1992), Weinell et al. (2003) and Schultz (2004)). Skin friction caused by the hull condition can be divided into three main categories (Figure 16.1): smooth, mechanically rough, and biofouled (micro-fouled and macro-fouled). A smooth hull condition is typical after a dry-dock operation; the duration of this condition varies, however, depending on the quality of the applied FCC and the conditions it encounters during operation. The boundaries between smooth (unfouled), micro-biofouled and macro-biofouled are vague, leading to unclear definitions.

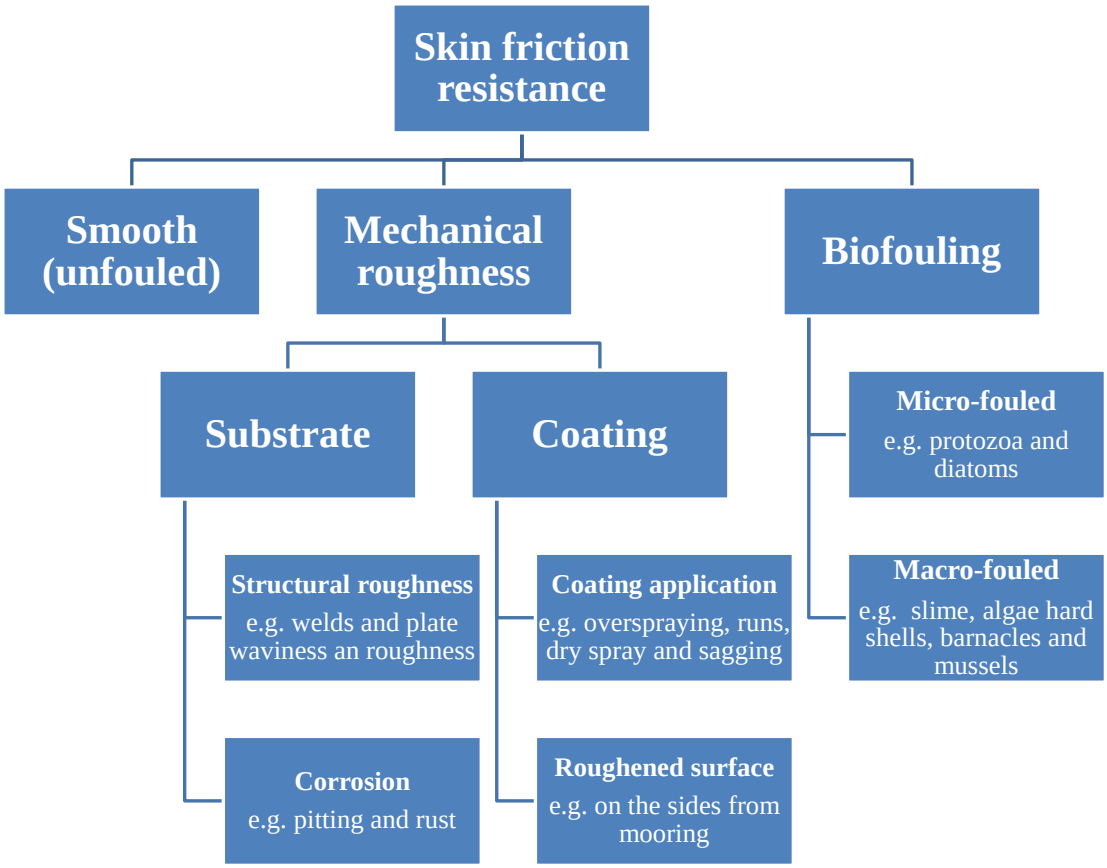

Figure 16.1. Factors affecting the skin friction of smooth, mechanically rough, and biofouled FCCs.

Mechanical roughness is a relatively rigid surface roughness, which can occur due to structural roughness (welds and plate waviness), a poor coating application (e.g., overspraying, runs, and sagging), mechanical damage, corrosion (pitting and rust), and

coating failures (e.g., blistering). Biofouling is substantially different than mechanical roughness in both origin and form; it is caused by the accumulation of micro-organisms, plants, or animals on man-made structures, such as a hull or other subsea structure. Biofouling typically consists of complex biological species from the following main categories: bacteria, diatoms, tunicates, bryozoans, tubeworms, algae, barnacles, and mussels. Micro-fouling forms the primary film of biofouling on subsea structures. The life forms responsible for micro-fouling generally consist of bacteria, protozoa, fungi and diatoms (Figure 17.1). Macro-fouling, on the other hand, occurs when biofouling organisms that are sufficiently large to be seen with the naked eye attach to subsea structures. These usually consist of green, brown, or red algae, or animals such as barnacles (Figure 18.1).

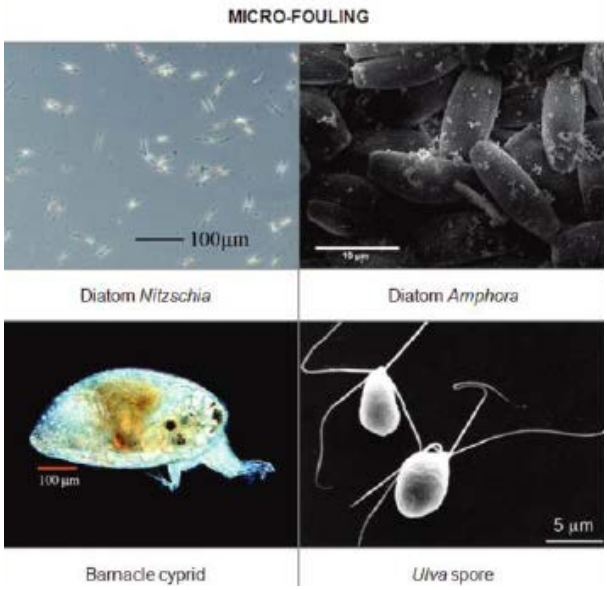

Figure 17.1. Micro-fouling organisms attaching to ship hulls, except the barnacle cyprid which is classified as macro-fouling. Diatom Nitzshia. Reprinted from Lejars et al. (2012). Copyright 2010, with permission from Elsevier. Barnacle cyprid. Reprinted from Lejars et al. (2012), with permission from The Royal Society Interface. Ulva spore. Reprinted from Lejars et al. (2012), with permission from Springer.

Figure 18.1. Macro-fouling organisms attaching to ship hulls. Reprinted from Lejars et al. (2012). Copyright 2011 American Chemical Society.

Biofouling, and in particular marine biofilms, are quite different compared to mechanical roughness, as they are neither uniform nor rigid. They consist of microbial cells that attach to a substrate and then proceed to grow, reproduce, and synthesize extracellular polymeric substances (EPS) dominated by polysaccharides (Christensen & Characklis, 1990). Their coverage ranges from fairly uniform to patchy, and the scale of the component organisms

ranges from bacteria (micrometers) to filamentous algae (centimeters). The complexity of marine biofilms is obvious. A surface coated with a heterogeneous, compliant polymer with entrapped organisms is much more complex than a homogeneous sand roughness.

The frictional drag increase due to biofouling depends on many parameters, including the type of organisms, their location on the ship, the percentage of the hull covered with biofouling, the type of ship, and the ship's speed. Likewise, the biofouling settlement on an FCC varies according to many parameters, including the ship's speed, hull geometry, intensity of sunlight reaching the hull's surface, water depth, and water temperature. Hull treatment in dry dock is known to reduce friction due to the surface treatment. For instance, a fully sandblasted hull and a new coating scheme establish a relatively smooth surface while eliminating biofouling and mechanical damages and potentially restoring the ship's hull to a new-build condition. Figure 19.1 provides an example of the decrease in resistance due to dry-docking treatment and the post period in which resistance steadily increases for a container ship. The hull and propeller developed an added resistance of less than 0.5% per month in this case (Munk et al., 2009). The increase in resistance is primarily explained by the increase in roughness from damages and biofouling, which developed over time.

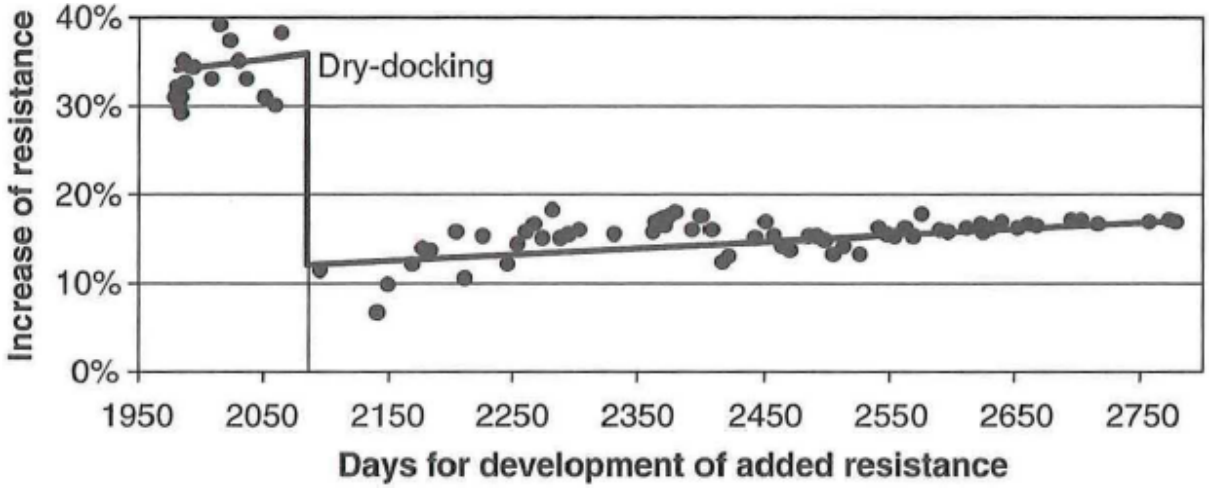

Figure 19.1. Increased resistance diagram illustrating the decrease in resistance due to a dry-docking hull treatment (Munk et al., 2009). Reprinted with permission from Elsevier.

Mechanical surface roughness

Mechanical roughness impacts skin friction and is commonly correlated with ships' drag. Furthermore, it influences the settlement and attachment of biofouling, deeming it a significant parameter in the evaluation of the expected biofouling attachment to FCCs.

Several authors have investigated the topic of roughness and its impact on skin friction (e.g., Schultz (2002), Moody (1944), Schlichting (1968) and Flack et al. (2012)). Roughness is usually defined as the texture of the surface, for example, highest peak to lowest valley, kurtosis, and skewness. Several researchers have attempted to correlate drag with surface structure; the most common for ships is the Rt(50) roughness, which is the maximum peak to valley over a sampling length of 50 mm, as exemplified in Figure 20.1.

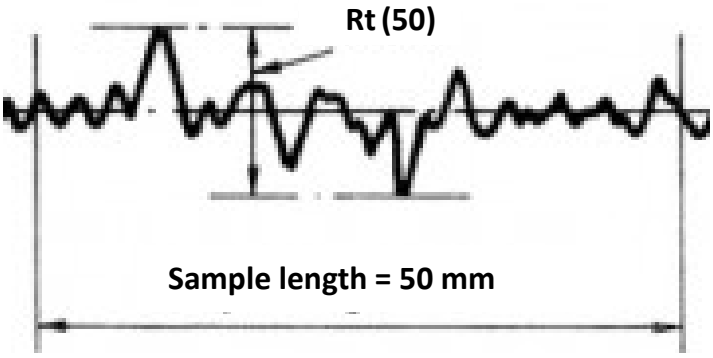

Figure 20.1. Rt(50) is the maximum peak to valley over a sampling length of 50 mm (modified from Molland (2008)).

Other roughness parameters, such as the arithmetic average roughness, R_a; the root mean square roughness, R_q; the skewness roughness, R_{sk}; and the kurtosis roughness, R_{ku}, have also been applied to correlate with drag (e.g., Candries and Atlar (2005), Schultz (2002) and Flack et al. (2012)). The arithmetic average roughness is a mean of the surface roughness, which gives a general description of the height variations without being sensitive to small deviations from the mean line. The root mean square roughness represents the standard deviation of the distribution of the surface heights. Compared to the arithmetic average height, it is more sensitive to large deviations from the mean line. The skewness of a profile is sensitive to occasional deep valleys or high peaks, and it can be used to distinguish between two profiles that have the same R_a or R_q but different shapes. The kurtosis roughness describes the sharpness of a surface profile. If $R_{ku} < 3$, the distribution is said to be platykurtoic, with relatively few high peaks and low valleys. Conversely, if $R_{ku} > 3$, the distribution curve is said to be leptokurtoic, with many high peaks and low valleys. For a thorough introduction to the various roughness parameters, see e.g., Gadelmawla et al. (2002) and Blunt and Jiang (2003). Table 6.1 displays an example of the roughness parameters for 220-grit sand paper (rough surface), a copper-based biocidal antifouling coating, and an FCC. The FCC was found to have slightly less skin friction, although this

determination did not correlate well with R_q. However, the smoother surface, which, in this case, is the FCC, generally exhibits lower skin friction.

Table 6.1. Roughness statistics for 220-grit sand paper, an antifouling copper coating, and a silicone FRC (Flack et al., 2012).

Specimen	Peak to valley roughness [μm]	R_q [μm]	R_{sk}	R_{ku}
220-grit sand paper	305	36.9	0.10	2.84
Biocidal antifouling coating (copper based)	152	20.8	0.05	2.75
FRC (silicone)	135	10.0	0.13	3.13

Measurement of surface roughness usually requires removing the waviness portion from the measured profiles in order to focus on the surface features of interest through the selection of different cut-off lengths for filtering. In general terms, waviness represents the larger irregularities, whereas roughness is comprised of the smaller irregularities of the surface. The cut-off filter is a short-pass filter that allows the high wave-number components through, thereby separating the waviness from the roughness. More waviness features are included in the surface roughness profiles when a longer cut-off length is used in the filtering. The values of the investigated roughness parameters and their correlation with respect to drag are affected by the selection of the cut-off length (Chang et al., 2004). Unfortunately, many of the published works regarding surface roughness and FCCs do not mention the cut-off length; therefore, their results cannot be compared (Howell & Behrends, 2006). Although Schultz (2002) stated that waviness has little effect on drag, Townsin (2003) asserted that induced waviness caused by the flow over a pliable surface, that is, a biofouled coating, must be considered. However neither Schultz (2002) nor Townsin (2003) addressed the absolute impact of mechanical waviness and induced waviness on biofouled surfaces. No universal relationship has been found that is capable of linking a geometric surface description to the frictional behavior, although several attempts have been made (e.g., Schlichting's equivalent sand roughness (Schlichting, 1968). For all such methods, the surface friction will diverge increasingly from the surface friction obtained for a given surface structure as the surface geometry changes. Therefore, for surfaces with large deviations in surface geometry compared with known measurements, experiments are still the only adequate solution (Leer-Andersen & Larsson, 2003). One of the fundamental difficulties in this respect is the fact that, from a hydrodynamic or geometric point of view, a non-smooth surface cannot be described solely by a single parameter such as the average roughness

height (peak to valley); therefore, surface optimization through modeling is complicated. Several other descriptive parameters, such as R_a, R_q, R_{sk}, and R_{ku}, are needed to describe the roughness; indeed, even with these parameters defined, predicting the drag has still proven to be a complicated matter (Leer-Andersen & Larsson, 2003).

In addition to impacting drag, surface structure impacts mechanisms whereby fouling organisms attach to a substratum. This process occurs via a bioadhesive, which flows into surface imperfections and cures in order to create a secure mechanical lock (Berglin et al., 2001). In this way, surface roughness can promote organism settlement (Thouvenin et al., 2002). For instance, Aldred et al. (2010) stated that cyprids not only actively choose to settle on surfaces with the maximum number of attachment points, but it also increased the attachment strength. Theoretically, therefore, rougher coating surfaces are more likely to be biofouled than smooth surfaces (Holm et al., 2004), and their biofouling release requires higher traveling speeds compared to smoother surfaces. The least preferred topographies with the lowest number of attachment points offer a diminished settlement and growth of the propagules and larvae of fouling organisms (Scardino et al., 2008); in addition, they favor the release of biofouling from surfaces (Aldred et al., 2010). It has also been suggested that micro-topographies might influence fluid dynamics very close to the surface and, thus, micro-hydrodynamically prevent settlement (Howell & Behrends, 2006). In fact, Scardino et al. (2011) found that the roughness skewness has a higher impact on biofouling prevention than the mean waviness, which has a higher impact than the mean roughness. While topographical studies show that the surface structure influences the settlement and attachment in the marine environment, the underlying mechanism responsible for reduced biofouling still remains unclear.

Newly applied fouling control coating condition

The effect of surface roughness on the frictional drag of clean or newly applied FCCs has been investigated by several authors (e.g., Candries and Atlar (2005), Schultz (2002), Grigson (1982) and Musker (1980-198)). Candries and Atlar (2003b), Mirabedini et al. (2006), Candries and Atlar (2005), and Flack et al. (2012) investigated the initial (unfouled) drag performance of FCCs based on two rotor set-ups, a towing tank, and a water tunnel,

respectively. The investigated FCCs were FCCs and tin-free SPC coatings. A summary of the findings is presented in Table 7.1 for various test methods. Table 8.1 displays the results obtained with LDA derived from both the Hama (Hama, 1954) and Reynolds Stress (e.g., Schultz (2000)) methods for determining the skin friction coefficients when FCC systems were compared to smooth, uncoated surfaces.

Table 7.1. Initial (unfouled) skin friction measurements for FRC and biocidal antifouling coating.

Test set-up	Comments about skin friction	Reference
Rotating cylinder	FCC skin friction coefficient vs. the one of a smooth test cylinder: a) 4.3% increase for sprayed FRC. b) 5.7% increase for rollered FRC. c) 8.0% increase for tin-free SPC coating.	Candries et al., 2003b
Rotating cylinder	9% – 22% lower skin friction coefficient for the FRC (silicone) than the SPC coating.	Mirabedini et al., 2006
Water tunnel	2% – 20% lower skin friction coefficient for the FCCs (depending on the quality of the application) than the tin-free SPC coating.	Candries & Atlar, 2005
Water tunnel	The difference in skin friction between the fouling release and biocidal antifouling coating was within experimental uncertainty.	Flack et al., 2012

Table 8.1. Increase in skin friction coefficients for newly applied FCCs compared to a smooth surface determined by use of LDA (Candries & Atlar, 2005).

Fouling control coating system	Skin friction coefficient derivation method	ΔC_F compared to smooth unpainted reference surface.
Tin-free SPC coating	Reynolds Stress method	13.4%
FRC applied by roller	Reynolds Stress method	12.8%
FRC	Reynolds Stress method	10.0%
Tin-free SPC coating	Hama method	14.7%
FRC applied by roller	Hama method	12.4 %
FRC	Hama method	10.1%

Flack et al. (2012) detected only a minor difference in the skin friction coefficient for the initial friction of FCCs and biocidal antifoulings; indeed, the difference was within experimental uncertainty. Weinell et al. found that the investigated FCCs (two fouling release and four biocidal antifouling coatings) displayed similar frictional drags at lower velocities (10 – 20 knots), but at higher velocities (25 – 35 knots), the frictional drag of the coatings became significantly different (Weinell et al., 2003). The FRCs with lowest micro-roughness showed the lowest drag, and the biocidal antifouling coatings showed a slightly higher drag. Mirabedini et al. (2006) compared the skin friction coefficient between an FRC and three biocidal antifoulings. They determined that the skin friction coefficient for the FRC was between 9% and 22% lower. Furthermore, the largest difference in the skin friction

coefficient for a newly applied FCC condition for the SPC coatings was 3.5% (Mirabedini et al., 2006).

Weinell et al. (2003) tested two SPC coatings in a biofouling-free environment with respect to skin friction coefficients over a period of 5 months. Both coatings showed a tendency to smoothen until a steady state was reached after approximately two months. The initial friction of the SPC coatings might, therefore, decrease slightly for a period of time following dry-docking, if they remain free of biofouling.

Biofouled fouling control coating condition

Biofouling starts from the moment a ship is immersed in sea water. The hull surface rapidly accumulates dissolved organic matter and molecules such as polysaccharides, proteins, and protein fragments (Fitzsimmons & Ellis, 1990). This accumulation is typically followed by the accumulation of micro-organisms (biofouling). Figure 21.1 presents an example of a hull with severe macro-fouling.

Figure 21.1. A hull with severe macro-fouling (Yebra et al., 2004). Reprinted with permission from Progress of Organic Coatings.

Presently, the fluid mechanisms affecting the drag of a ship suffering from soft macro-fouling (e.g., slime) are not well understood (Schultz & Swain, 2000). A significant amount of research has been conducted to investigate the effects of soft macro-fouling on frictional drag (e.g., Barton et al. (2011), Swain et al. (2007), Andrewartha et al. (2010) and Khor and Xiao (2011)). Slime may be thought of as constantly varying stream wise roughness, not only in height but also in morphology (e.g., Schultz (2000) and Picologlou et al. (1980)), which is one of the difficulties of modeling slime skin friction. Researchers have also conducted substantial research regarding drag predictions related to hard macro-fouling (e.g., barnacles

and shells) (e.g., Weinell et al. (2003) and Leer-Andersen and Larsson (2003)). Unfortunately, there is currently no method available to accurately predict the drag for a particular ship based on its trade route, choice of FCC, biofouling distribution on the hull, type of biofouling, or mass of biofouling. Additionally, to the authors' knowledge, there is presently no means of accurately measuring and characterizing micro-fouling or soft macro-fouling, which correlate well with frictional drag. Therefore, a ship operator cannot accurately estimate the impact that an eventual removal of soft macro-fouling via underwater hull cleaning will have on the fuel efficiency of his ship. Table 9.1 presents the literature data describing the differences in skin friction increases (ΔC_f) due to various soft macro-fouling conditions. The evidence clearly shows that slime formation significantly contributes to an increase of skin friction.

Table 9.1. Increases of small-scale friction coefficients due to soft macro-fouling.

ΔC_f %	Comments	Reference
10%	Pre-roughened discs were tested before and after exposure to slime formation.	Loeb et al., 1984
10%–20%	Soft macro-fouling (slime films) on a rotating disc.	Loeb et al., 1984
4%–11%	Uniformly distributed nylon tufts attached to a rough flat plate resembling slime compared to a rough plate.	Adapted from Candries et al. (2003b)
9%–29%	A friction disk machine was used. Disks were exposed under static conditions for approximately 3 weeks. The ΔC_f increase was 9% for Cu-ablative, 17% for FR-1, 27% for FR-2, and 29% for FR-3.	Holm et al., 2004
58%–68%	Drag was measured in a towing tank using a flat plate. The biofouling coverage on a SPC TBT system after 287 days of exposure resulted in 70% slime coverage in accordance with ASTM D3623.	Schultz, 2004
33%–190%	Non-coated plates were exposed for 6, 14 and 17 days in an aquaculture facility. The average increase in C_f for slime films with a mean thickness of 160 µm was 33%; for a mean thickness of 350 µm, it was 68%; for a surface dominated by filamentous algae (Enteromorpha spp) with a mean thickness of 310 µm, it was 190%.	Schultz & Swain, 1999

Table 10.1 presents data from the literature, showing differences in skin friction (ΔC_f) due to hard macro-fouling for full-scale ships. The literature shows that macro-fouling offers a vast contribution to skin friction; generally, the ΔC_f is significantly higher for hard macro-fouling than for soft macro-fouling. However, Table 9.1 and 10.1 are not directly comparable because the exposure and test conditions were not identical.

Table 10.1. Increased small-scale friction coefficients due to hard macro-fouling.

Type of measurement	ΔC_f %	Comments	Reference
Towing tank (pontoon)	85%	75% coverage with barnacles of 4.5 mm height.	Townsin, 2003
Flat plate in towing tank	300%–400%	FRCs had extensive coverage of barnacles.	Schultz, 2004
Flat plate in towing tank	87%–138%	Ablative copper and SPC copper systems had 1% – 4% of barnacle coverage.	Schultz, 2004
Rotating cylinder	100%	3% coverage of barnacles doubled the drag.	Weinell et al., 2003

Table 11.1 displays the data from the literature regarding differences in skin friction (ΔC_f) and shaft power (ΔSP) due to different biofouling conditions for full-scale ships. The percentage increases of shaft power are not directly comparable to those of the skin friction, since the skin friction constitutes a different relative contribution to the total resistance compared to the shaft power. Full-scale ship trials show that the frictional drag changes due to biofouling represent an important parameter with respect to the total resistance of a ship and the need to minimize a ship's drag increase.

Table 11.1. Changes in skin friction (ΔC_f) and shaft power (ΔSP) due to different biofouling conditions for full-scale ships.

Increased skin friction (ΔC_f) or shaft power (ΔSP)	Comments	Reference
ΔC_f: 0.5% per day	Biofouling on full-scale ships increased resistance by 0.5% per day while at dock.	Adapted from Schultz and Swain (2000)
ΔC_f: 5% over 40 days	A hull was allowed to foul for 40 days on a coating of bituminous aluminum which, over a speed ranging from 5 to 15 knots, resulted in a frictional increase in resistance of 5%.	Conn et al., 1953
ΔC_f: 8%–14%	Added resistance due to slime formation.	Watanabe et al., 1969
ΔC_f: 25% after 240 days and 83% after 600 days	The 23 m fleet tender hull had a non-polishing antifouling. After 240 days of operation, a thin slime layer had developed, and after 600 days, a 1-mm thick slime film had developed. A 15% reduction in ship speed was further noted over a 2-year exposure.	Lewthwaite et al., 1985
ΔC_f: 100% over 375 days	Towing tests were conducted at 16 knots without a propeller on Yudachi, a 234-foot Japanese ex-destroyer. The fouling condition is not reported, but fouling is known to have developed while Yudachi remained at anchor.	U.S. Naval Institute, 1952
ΔSP: 24%	Power trials on a frigate with a fouled hull suffering from incipient tube worm growth with coverage of 10%–20% showed an increase of 24% shaft power to maintain a speed of 7.7 m/s compared to the clean condition.	Adapted from Schultz (2007)
ΔSP: -8% and -18% (decrease due to hull cleaning)	A frigate coated with an ablative antifouling (cuprous oxide and a TBT-based cobiocide) had been exposed at Pearl Harbor, Hawaii, for 22 months. Hull inspections indicated the presence of a fairly heavy slime film with little to no calcareous biofouling. Power trials due to the hull cleaning of the fouled condition showed a decrease in the required shaft power of 8% at a ship's speed of 16 knots and of 18% at 25 knots.	Haslbeck & Bohlander, 1992

Full-scale experiments have the obvious advantage compared to small-scale experiments: their FCCs experience an ageing and biofouling process on the entire hull, not only on a small area, which typically occurs for small-scale tests. If the ship is traveling, it also experiences varying biofouling intensities on the hull, instead of a similar intensity, which is often the case for small-scale experiments. Furthermore, full-scale experiments are often carried out over longer time periods, resulting in long-term evaluations. Subsequently, changes in parameters such as roughness, biofouling, and shaft power can be measured, indicating the effect of changes in the coating surface condition, although this process is admittedly complicated and linked with uncertainties. In comparison, full-scale drag prediction via

small-scale experiments is certainly bound to be encumbered by limitations and uncertainties. Full-scale experiments are affected by disadvantages, as well. For example, evaluating the impact of a single parameter, such as the choice of an FCC, is complicated. Furthermore, reproducing experiments with similar conditions is quite difficult due to the ever-changing parameters during voyage (e.g., temperature, biofouling intensity, salinity, and season), resulting in uncertain statistical errors that further complicate the drag performance estimation of FCCs.

Drag performance development over time

Few experimental methods have been developed to specifically determine the drag performance of FCC systems over time in conditions similar to that experienced by operating ships, i.e., presence of marine biofouling and partly dynamic exposure of FCCs. However, Swain et al. did conduct one such study (Swain et al., 2007). Four coatings were investigated when they were newly applied (unfouled), after 60 days of static immersion, and again after an additional 15 days of dynamic immersion. The coatings consisted of one copper-containing SPC coating (Cu-SPC), a copper-containing ablative coating (Cu-Abl), and two early silicone-based FRCs (FR-1 and FR-2). The skin friction was measured at a boat speed of 25 knots and a Reynolds number of $5.5 \cdot 10^7$ (See the section 'Static and dynamic panel exposure tested on a boat' for a detailed description of the experimental method). Table 12.1 shows the performance of the coatings relative to each other. Based on the evidence, the best-performing FCC varies for each of the conditions (newly applied, static immersion, and dynamic immersion) tested. Clearly, test conditions are of the utmost importance when evaluating the FCC's drag performance, as the performance rating was largely influenced by these conditions. In this study, FRC-2 was the best-performing coating at the end of the entire exposure cycle.

Table 12.1. Side-by-side comparison (ranking from 1 to 4, where 1 refers to best performance) in terms of skin friction coefficients at a boat speed of 25 knots and $Re=5.5\cdot10^7$ at newly applied, static exposure and dynamic exposure conditions. Modified from Swain et al. (2007).

Fouling control coating	Newly applied	60 days static	15 days dynamic
FRC-1	1	4	4
FRC-2	3	3	1
Cu-Ablative	2	1	2
Cu-SPC	4	2	3

Comparison between biocidal antifouling coatings and fouling release coatings

Small and full-scale experiments have generally shown that FRCs can better reduce skin friction compared to conventional biocidal antifouling coatings in newly applied conditions (e.g., Candries et al. (2003b), Candries and Atlar (2005) and Schultz (2004)). However, when the measurements have been performed after periods of static exposure to biofouling, the early FRCs often show a higher drag than the conventional biocidal coatings. This can be explained in part because the primary mechanism of early FRCs is based on the prevention of biofouling attachment through low adhesion strength and the subsequent release of biofouling due to water flowing over the surface; clearly, this mechanism is not fully utilized during static immersion. The biocidal antifouling coatings only partly rely on this principle. No decisive advantage could be obtained for either of these coating technologies tested after combining a static immersion with a dynamic immersion, due to the limited number of published results and the indecisive conclusions of those published. Table 13.1, 14.1, and 15.1 compare the early FRCs and the conventional biocidal antifouling coatings when they are newly applied, statically immersed, and dynamically immersed, respectively.

Table 13.1. Drag comparison between fouling release and biocidal antifouling coatings in newly applied or cleaned conditions.

Type of measurement	Lowest drag	Coating condition	Reference
Rotating cylinder	FRC	Newly applied	Candries et al., 2003b
Rotating cylinder	FRC	Newly applied	Weinell et al., 2003
Rotating cylinder	FRC	Newly applied	Ghani et al., 2010
Rotating cylinder	FRC	Newly applied	Mirabedini et al., 2006
Flat plate in towing tank	Elusive drag conclusion; results depended on the specific type of biocidal antifouling coating and FRC.	Cleaned condition (after 287 days of static exposure)	Schultz, 2004
Flat plate in towing tank	FRC	Newly applied	Schultz 2004
Water tunnel	FRC (2%–20%)	Newly applied	Candries & Atlar, 2005
Water tunnel	FRC (although within statistical uncertainty)	Newly applied	Flack et al., 2012
Static and dynamic panel exposure tested on a boat	FRC	Newly applied	Swain et al., 2007

Table 14.1. Drag comparison between fouling release and biocidal antifouling coatings after static immersion.

Type of measurement	Lowest drag	Static exposure time	Reference
Friction disk machine	Biocidal antifouling	Three weeks, with a subsequent removal of hard biofouling.	Holm et al., 2004
Flat plate in towing tank	Biocidal antifouling	287 days	Schultz, 2004
Static and dynamic panel exposure tested on a boat	Biocidal antifouling	60 days	Brett, 1980

Table 15.1. Drag comparison between fouling release and biocidal antifouling coatings based on full-scale measurement of static and hydrodynamic exposure condition.

Type of measurement	Lowest drag	Comment	Reference
Static and dynamic panel exposure tested on a boat	Elusive drag conclusion; results depended on the specific type of biocidal antifouling coating and FRC.	One FRC had the lowest drag while another had the highest. The two biocidal coatings were neither the best nor the worst in performance.	Swain et al., 2007
Fuel consumption on high-speed catamaran ferry	FRC	With same service speed, a lower fuel consumption was detected for the FRC compared to the biocidal antifouling.	Millett & Anderson, 1997

Although small and full-scale measurements have been carried out for conventional biocidal antifouling coatings and FRCs, further investigations are needed to clarify the conditions that

determine the optimal choice of coating, that is, the one with the lowest skin friction over a typical dry-dock period and a potential gain of fuel savings. From Table 13.1, it can be argued that early FRCs typically result in less drag in a newly applied condition. From Table 14.1, in turn, it can be argued that biocidal antifouling coatings typically result in less drag after static immersion. Candries and Atlar (2005) explained that the drag differences for the newly applied fouling release and biocidal antifouling coatings were caused by the differences in surface texture. The surface textures from an FRC and a tin-free SPC coating are displayed in Figure 22.1 and 23.1, respectively. It is significant to note that the fouling release surface texture is much less spiky, and it has a lower peak-to-valley distance. The smoother FRC surface compared to the tin-free SPC antifouling coating is the explanation given for the lower drag of FRCs.

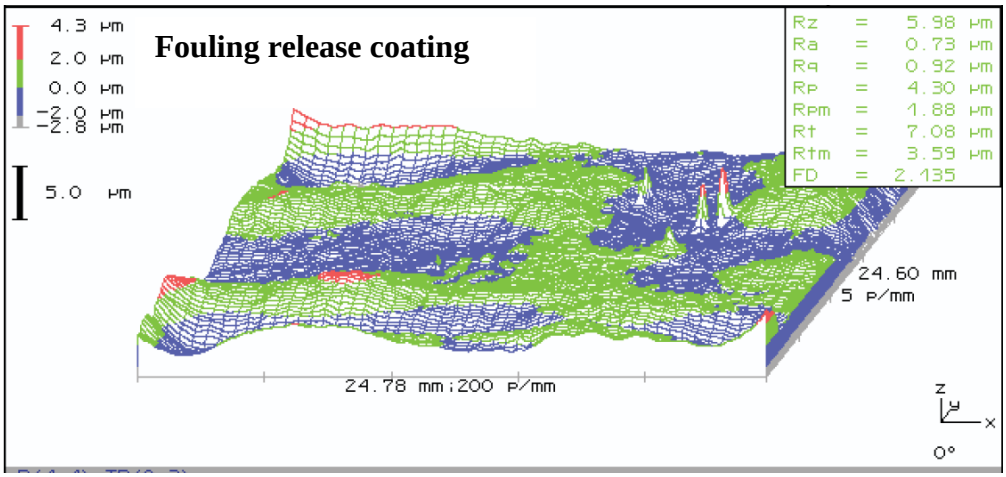

Figure 22.1. Surface texture from a fouling release coated surface. The surface structure is smooth, with small peak to valley values (modified from Candries and Atlar (2005)).

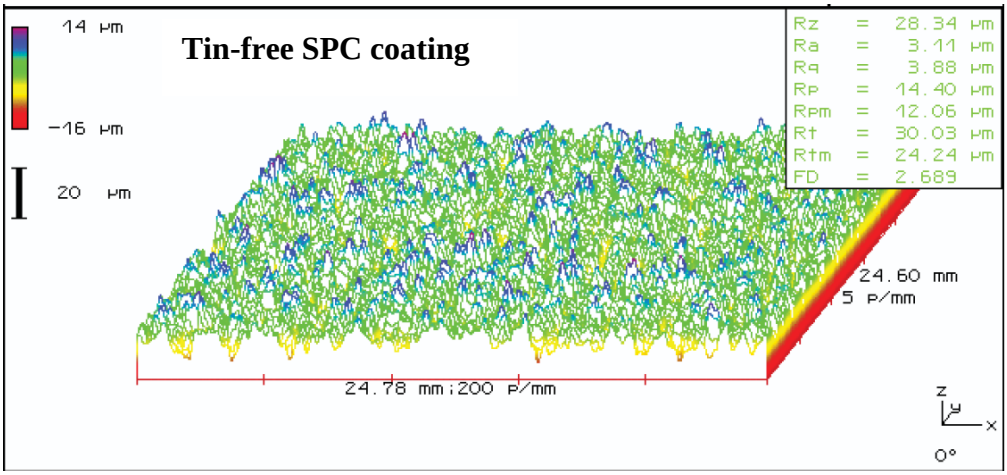

Figure 23.1. Surface texture from a tin-free SPC antifouling coated surface. The surface structure is spiky and rough (modified from Candries and Atlar (2005)).

FRCs are appealing due to both their potential fuel savings and their lack of harmful effects to the marine environment, since only small amounts of toxic components, if any, are released into the surrounding seawater. It can be anticipated, therefore, that FRCs will increasingly capture market shares of the industrial marine coating market, as the potential for drag reduction and biofouling control is considerable. This effect could be further enhanced through the minimization of the primary drawbacks, such as mechanical surface vulnerability, high price, and limited efficacy for slow and idle ships.

The impact of ships' fouling control coating conditions on drag

Surface friction influences ship operating parameters such as maximum speed, fuel consumption, and maneuverability. This section presents correlations and experimental results between FCC conditions and their impact on drag for full-scale ships. Various authors have investigated the impact of surface properties on drag for full-scale ships (e.g., Schultz (2004), Malone and Little (1980) and Townsin and Byrne (1980)). Hull performance tests for full-size ships over time can be conducted in several ways. However, one of the major challenges is to isolate the impact of the FCC surface condition from all other parameters, such as the propeller, machinery, water temperature, and sea state, in order to determine the effect of the changes in FCC conditions over time. Another challenge with full-scale tests is the inherent difficulty in obtaining a fair side-by-side comparison of different FCCs, due to the ever-changing exposure conditions that a ship hull experiences. One common method of testing is to directly compare one FCC over the full lifetime of its in-service ship's

performance (e.g., fuel consumption, shaft torque, or number of propeller revolutions per nautical mile) to that of another system. Although this approach is useful, any increase in resistance cannot be attributed solely to the coating condition; therefore, the absolute value of the FCC's drag performance cannot be determined accurately. The effects of other parameters on the ship's performance can be minimized by propeller cleaning, minimization of machinery changes, optimal machinery maintenance, and tests in calm waters. However, ships are bound to experience different conditions. The parameters impacting drag will practically always be subject to individual variations; consequently, the determination of the FCC's drag performance is bound to be a complicated matter. Figure 24.1 outlines a side-by-side comparison of two FCCs. The comparison is based on the changes in fuel consumption, speed, and shaft torque over two 60-month periods, where a new and different type of FCC is applied after the first 60-month period. Based on the changes regarding the in-service ship performance (e.g., fuel consumption) between the first and second period, the FCC performances can be estimated. For instance, the in-service ship performance method resulted in a fluoropolymer FRC, compared to a tin-free polishing antifouling, and acquired a fuel savings of 0.56% for a container ship, 11% for a tanker, and 22% for a bulk cargo ship (Corbett et al., 2011).

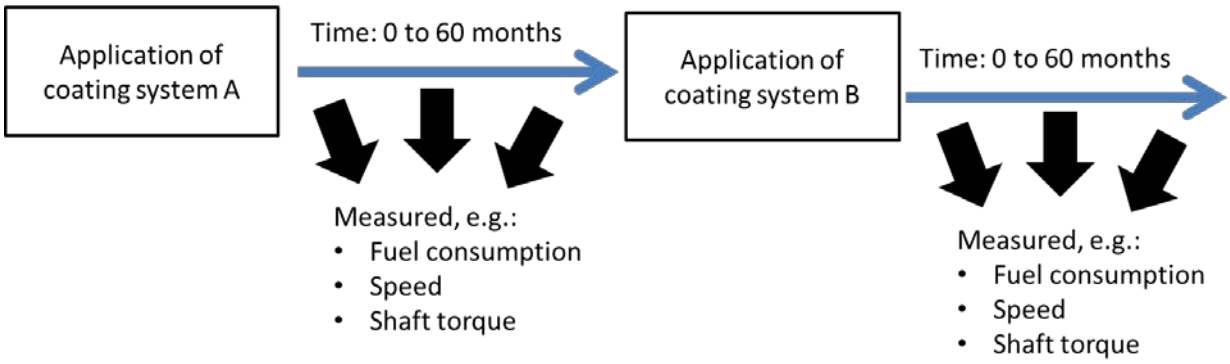

Figure 24.1. Comparison of the FCC performance of two FCC systems.

A quicker, simpler method is the widely used Rt(50) roughness measured at ship yards and laboratories to obtain an initial estimate of the FCC's drag performance. The Rt(50) roughness found at ship yards does not, however, offer indications of an FCC's capability for biofouling prevention, development of mechanical roughness, or, therefore, long-term drag performance. An average hull roughness (AHR) can be determined by evenly distributing a number of mechanical roughness measurements (e.g., 100) over the hull with for instance

Rt(50) measurements. As the roughness height distribution is random, a sufficient number of measurements must be taken in order to obtain an accurate AHR (Townsin & Byrne, 1980). Townsin presented a method to calculate the skin friction based on the mechanical FCC roughness measurements for a relatively unfouled FCC surface (Townsin, 2003). The AHR is ascertained by determining a large sample of Rt(50) values. Equation (10.1) shows the increase in the skin friction coefficient based on the Rt(50) roughness measurements, compared to a smooth surface:

$$1000\Delta C_f = 44\left(\left(\frac{AHR}{L}\right)^{1/3} - (Re_s)^{-1/3}\right) + 0.125 \quad (10.1)$$

where ΔC_f is the skin friction coefficient increase, L is the ship length, and Re_s is the ship's Reynolds number at a specific speed U. The model is only valid if the AHR is below 230 µm. Diver inspections will typically be used to monitor and evaluate the performance of a coating system when it is out of dry-dock. However, this method only evaluates the biofouling that is visual to the naked eye, and therefore, only provides basic indications of the performance in terms of areas covered and approximate degrees of fouling, which prevents accurate drag evaluations. Schultz presented a model to predict the change in a full-scale resistance coefficient for a hydraulically smooth surface, typical as applied FCC condition, and biofouled FCC condition (micro- and macro-fouled), based on towing tank tests on a flat plate (Table 16.1) (Schultz, 2007).

Table 16.1. Predictions of the change in total resistance (ΔC_T) and corresponding increase in shaft power (ΔSP) for an Oliver Hazard Perry class frigate (FFG-7) with a range of representative coating and biofouling conditions at a speed of 7.7 m/s (15 knots) and 15.4 m/s (30 knots) (Schultz, 2007).

Description of condition	ΔC_T U_s=7.7 m/s	ΔC_T U_s=15.4 m/s	ΔSP U_s=7.7 m/s	ΔSP U_s=15.4 m/s
Hydraulically smooth surface	-	-	-	-
Typical as applied FCC coating	2%	4%	2	4
Deteriorated coating or light slime	11%	10%	11	10
Heavy slime	20%	16%	21	16
Small calcareous biofouling or weed	34%	25%	35	26
Medium calcareous biofouling	52%	36%	54	38
Heavy calcareous biofouling	80%	55%	86	59

Control of biofouling by hull cleaning

When a ship's hull is sufficiently fouled, causing severe increase in drag, removal of the biofouling on the hull by an underwater hull cleaning may be a worthy consideration. Waterborne hull cleaning allows for the removal of biofouling accumulations on hulls and propellers during idle periods, such as mooring and harboring. The appropriate use of these cleanings can improve the drag performance of an FCC system for a period of time and potentially delay dry-docking and its associated costs. Hull cleaning can reduce friction substantially by removing biofouling; indeed, at times it may restore the level of friction to its former condition, when the ship left dry-dock (e.g., Schultz (2004), Millett and Anderson (1997) and Schultz et al. (2010)). Admittedly, the long-term effect of hull cleaning on ship performance is not well-established. The ship operator, therefore, must balance the cost and inconvenience of underwater cleaning for a biofouled hull with the uncertainty of the performance gain. Biofouling is typically removed by an underwater procedure where divers apply an impeller system with rotating brushes against the FCC, thereby removing the biofouling. Other methods for biofouling removal include water jets and cavitation systems. However, the majority of these methods use diver-operated machines fitted with rotating brushes (Figure 25.1). The extent of the area that receives waterborne cleaning varies; for example, it can include the entire underwater hull, selected areas of the underwater hull, propellers, shafts, struts and rudders, and all openings.

Figure 25.1. Example of an underwater hull cleaning with a rotating brush system, operated by a diver (modified from Bohlander and Zealand (2009)).

Hull cleaning offers several distinct advantages. The process is relatively fast, often taking less than a day to complete. It can be conducted when the ship is in port or stationary for other reasons. Additionally, the decrease in friction often reaches a level approaching that of the ship when it left the dry-dock after being newly painted. A negative result of the process is the fact that the cleaning actions are likely to impact the environment, as toxic compounds from biocidal antifouling coatings often are removed during the cleaning process. Another major disadvantage of hull cleanings is the fact that the coating may be mechanically damaged during the process, especially if hard fouling is present. If a cleaning occurs before the seaweed biofouling is reached, then very soft brushes can be used, and the FCC system is not likely to be damaged.32 If mechanical damage does take place, the rate of biofouling accumulation will likely increase substantially faster than it would have before the hull cleaning. Clearly, the decision to employ hull cleaning is often a trade-off between reduced biofouling and the risk of a potentially increased rate of biofouling. Figure 26.1 provides an example of the effect that hull cleaning (hull brushing) and propeller polishing (two times) has on drag performance (designated as resistance in the figure). In this case, the increase of resistance due to hull cleaning drops from the reference point by an approximate factor of 1.23 to 1.15. Based on the figure, the drag performance just before the hull cleaning was carried out (5700 days) is reached approximately at day 6150. Simply stated, within

approximately 1.2 years, the resistance returns to the same level as it had been before the hull cleaning.

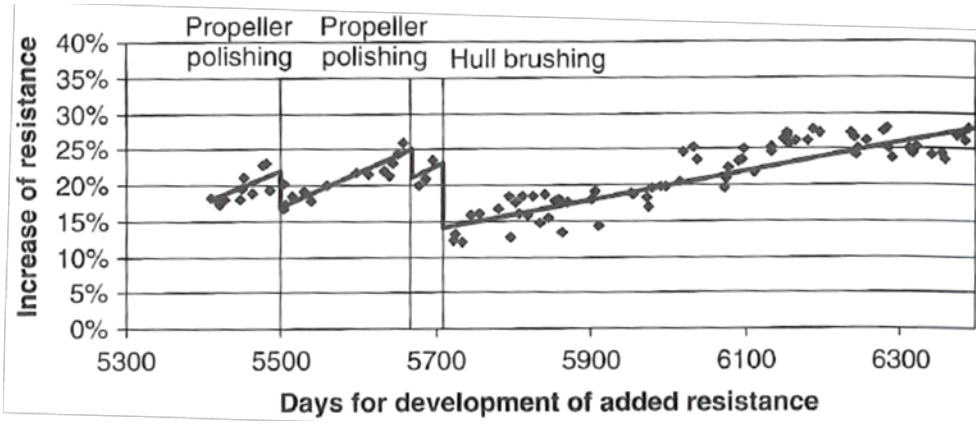

Figure 26.1. Increase of resistance diagram illustrating the decrease in resistance due to propeller polishing (two times) and hull cleaning (Munk et al., 2009). Reprinted with kind permission from Elsevier Books.

In short, the physical removal of biofouling by typical hull cleaning methods is relatively efficient and cost effective, but it is also a relatively short-term method for drag reduction. Therefore, hull cleaning should presently be considered a short term solution that can be useful during the last stage, prior to dry-docking and the application of a new FCC. The further development of hull cleaning systems, where the FCC is less likely to be damaged could be a potential means to ensure that biofouling is kept to a minimum over both shorter and longer periods.

Conclusions

Today's estimations of the drag performance of FCCs stem mainly from small-scale tests that evaluate the newly applied condition and, occasionally, perform an evaluation after static natural seawater exposure. Only one study analyzed the drag performance of FCCs through a combination of static and dynamic seawater exposure, which more closely resembles the natural ageing process of a ship's FCC.

Small-scale tests investigating newly applied FCCs are common and relevant, but they only provide limited information, since they fail to consider biofouling species, mechanical roughness, and other forms of ageing experienced by FCCs on a ship. Therefore, only the drag properties that exist shortly after a ship leaves dry-dock are studied; as a result, the evolution of a ship's drag during service is completely ignored. The static exposure tests

provide some additional information regarding the impact of ageing on FCCs, but even these are limited, because they only closely reproduce the conditions experienced by idle ships. For instance, the shear stress experienced by a moving ship and its impact on biofouling settlement and growth are not accounted for during static immersion. Furthermore, static tests can potentially provide inaccurate trends in relation to FCC performance for moving ships, especially as some technologies have a greater dependency on a certain water flow that prevents or limits biofouling (e.g., fouling release technology). Dynamic and static cycles simulating a ship's trading patterns in the presence of biofouling should, therefore, primarily be used when determining the drag performance of FCCs. It is typically reported that FRCs exhibit a lower drag when in newly applied or clean conditions, while conventional biocidal antifouling coatings (e.g., SPC) exhibit a lower drag when immersed statically in seawater for an extended period of time. In fact, no decisive conclusions have been made regarding the dynamic exposure of early FRCs and conventional biocidal antifouling coatings in seawater. There simply are no available studies that explore the most recent technologies, which have evolved significantly in the past few years, especially in the area of FRCs. Evaluating FCCs in newly applied conditions, the difference in drag performance is typically found to be relatively small, whereas it is often much larger after longer periods of static immersion. One major issue that needs to be resolved is the absence of a method that accurately determines the drag performance and associated costs (savings) of specific FCCs over a given period of time, based on conditions similar to those experienced by moving ship hulls. The prediction of drag performance based on statistical roughness parameters is complicated, since a non-smooth surface cannot be described solely in terms of a single roughness parameter. Several other descriptive parameters, such as the density of the roughness elements and shapes are needed to describe the roughness; even with these parameters, accurate predictions prove difficult. No universal relationship has been found to link a geometric surface description to frictional behavior, although several attempts have been made. Therefore, for surfaces with large deviations in surface geometry being compared to known measurements, experiments are still the only adequate solution. The drag performance prediction due to biofouling is even more complex than that of mechanically rough surfaces, especially for soft biofouling; as such, it is currently not well understood. Fortunately, drag penalties caused by hard

macro-fouling are better understood. Systematic studies comparing the drag behavior of FCCs over time in the presence of biofouling species under realistic speed and activity conditions are limited or nonexistent. Yet, they are essential to determining the optimal choice of FCC with respect to fuel efficiency. Finally, the task of converting a small-scale measurement to a full-scale ship size is difficult, especially since the literature presents only limited results and correlations verified by full-scale tests, if any. A better understanding of conversion to full-scale drag performance is necessary. One study converted flat plate drag measurements into increased shaft power consumption for a mid-sized naval surface. Compared to a hydraulically smooth surface the following shaft power increase at cruising speed of 7.7 m/s was estimated: (a) 2% for typical as applied on hull FCC; (b) 11% to 21% for deterioted coating or light to heavy slime; (c) 35% to 86% for small to heavy calcareous biofouling.

Studies comparing drag differences between FCCs in conditions similar to those experienced by ship hulls could be useful to evaluate the optimal choice of FCC and its impact on fuel consumption. Other issues that have yet to be satisfactorily addressed include the quantitative definition of biofouling coverage and, secondly, a correlation between biofouling coverage and simple predictions of resistance and powering. Due to their complexity, many parameters have been ignored to date, including biofouling settlement with regard to exposure time and traveling pattern, the location of biofouling on the hull, and the influence of self-smoothening mechanisms on a ship's drag. Developments in these areas would help to determine the optimal choice of FCC, the optimal time to conduct underwater hull cleaning (partial or complete), the optimal time between dry-dockings with new coating application and benefits of a full abrasive blasting of the hull. The economic and environmental gains associated with the latter knowledge are expected to be enormous.

Chapter 2 - Scientific hypotheses of the project

Introduction

In this chapter, the scientific hypotheses, which have been investigated, are described, along with the potential scientific and industrial gains. The project focused on measuring the drag performance of a new commercial fouling release coating with biocides incorporated, the influence of substrate roughness on drag when a full coating system (i.e., primer, tie-coat, and top-coat) was applied, and the development of a new experimental method with emphasis on long-term drag development when realistic exposure conditions were simulated for hull coatings applied to traveling ships. Furthermore, a comparison was made between the results obtained from the static exposure study (friction disk machine (FDM)) and the dynamic and static exposure study (rotor setups).

Overall aims of the work

The overall aims of the project were to both increase the scientific knowledge of the drag performance of FCCs and to develop a valuable experimental method for coating suppliers and users. The new FRC with biocides incorporated was of interest to evaluate, along with high-quality commercial top-coat products, in order to determine its potential for drag reduction in a newly applied condition, after static exposure, and after a combination of dynamic and static exposure. The purpose of investigating the impact of the substrate roughness on drag performance was to either reject or verify the substrate roughness as a significant parameter on drag. The outcome of the study on substrate roughness and its impact on final drag performance would reveal the importance of the substrate roughness and, potentially, other factors (e.g., top-coat or underlying coatings). The purpose of developing a setup that could simulate realistic exposure conditions for coatings applied to the hull of a ship was to increase the accuracy of the drag performance of FCCs applicable to voyaging ships, as opposed to only evaluating the performance in a newly applied condition after static immersion.

Scientific hypotheses

Fouling release coating with biocides incorporated

An FRC with biocides incorporated was evaluated in a series of tests with a number of commercial FCCs, in order to evaluate how this new type of FRC would perform in comparison to the other coatings. It is likely that the FRC with biocides incorporated would yield superior drag performance, compared to other similar FRCs without biocides and biocidal marine coatings, due to the well-known FRC effects and the release of biocides. The hypothesis that was investigated was whether the FRC with biocides could provide significantly lower drag than other quality top-coat products, and under which conditions (i.e., newly applied, after static immersion, and after dynamic immersion) it could do so. The drag performance over time for the FRC was determined with two different experimental setups (i.e., an FDM and a land-based rotor setup) and two different exposure conditions (i.e., static and a combination of static and dynamic). Furthermore, a detailed analysis of the surface characteristics of 5 different FCCs was made in order to reveal how this parameter would impact the initial and long-term performance. The parameters of interest to investigate are the visual biofouling, self-cleaning capabilities, drag development and its correspondence to both static and dynamic exposure, and resistance measured (i.e., torque). It is believed that the primary mechanisms for limiting biofouling and keeping the surface friction low for the FRC with biocides stems from the smooth surface and low surface energy, well-known for FRCs, but also the migration of biocides to the upper part of the coating layer, which, thereby, limits biofouling from attaching. This latter mechanism is thought to provide an extra defense mechanism, which likely is particularly useful during idle periods, when the self-cleaning mechanism of the FRCs without biocides is limited, as there is no or only limited water flow over the coated surface. The lack of water flow over the FRC would, therefore, potentially leave the FRC more vulnerable to biofouling settlement than biocidal marine coatings.

Substrate roughness

After a full dry-dock period, ships are often blasted down to the steel, leaving a non-smooth surface. The vast majority of studies investigating the frictional performance of FCCs have,

however, been carried out with smooth substrates. Studies revealing the impact of the substrate are potentially relevant for the final frictional performance of FCCs, but unfortunately such studies are missing in the literature. Researchers have yet to investigate, in depth, the impact of a smooth substrate versus a rough substrate to determine the impact that a rough substrate has on the final friction, with a full coating system applied to it. The scientific hypothesis should test if a rough substrate will lead to a higher drag than a smooth substrate, even if applied with several layers of coating, i.e., primer, tie-coat, and top-coat. For instance, Holm et al. (2004) stated, "The drag on a clean or fouled disk is a function of the roughness of the disk surface, which may be a fundamental characteristic of the coating or a result of preparation of the disk surface before painting and the care taken during paint application" (as cited in Candries et al. (2003) and Weinell et al. (2003)). To reveal the substrate's impact on the final drag performance, this study measured the initial drag performance in an FDM for two different coating systems with varying substrate roughness. Furthermore, it was of interest to identify if certain classes of marine top-coats (e.g., FRC and biocidal coatings) would be impacted differently by the underlying substrate roughness.

Rotor setup

A number of scientific studies have reported that the friction of FRCs is lower than that of biocidal marine coatings, when tested in clean and newly applied conditions (e.g., Atlar et al. (2003); Candries & Atlar (2005); Ghani (2010); Schultz (2004); and Weinell et al. (2003)). Conversely, a number of studies have reported a higher friction after static periods for biocidal marine coatings compared to FRCs (Holm et al. (2004); Schultz (2004)). Only one study based on small-scale setups with a focus on dynamic exposure has been presented in the scientific literature (Swain et al. (2007)). Unfortunately, the studies that measured the drag performance in the newly applied and clean condition and after static exposure cannot be directly compared, as the FRCs and biocidal marine coatings differ in the studies. The literature often reports a high frictional increase after static immersion, even for relatively short exposure periods; for example, Weinell et al. detected a 100% frictional increase after 5 weeks of static exposure. It is in the literature found that high drag increases found after static immersion are typically much smaller for ships where the coatings primarily have been dynamically exposed. For instance, Townsin (2003) stated that the frictional increase was

typically in the range of 5% to 25%. It is, therefore, likely that static exposure will lead to a higher frictional increase, compared to a dynamic exposure. However, the difference in frictional increase between dynamic and static exposure has to be investigated in order to verify this and to determine the difference in frictional increase arising from the different exposure conditions. A method that could expose coatings in dynamic and static conditions would be useful, as it could verify if static immersion is a more severe exposure condition than dynamic exposure, with respect to friction and biofouling development. Furthermore, the difference in friction could be investigated with such a setup. The study by Swain et al. (2007) indicated that the initial friction and the friction after static immersion were insufficient to determine the optimal choice of coating in conditions resembling those encountered by ocean-going ship hulls, because the drag performance ranking in a number of cases changed when the coatings were dynamically exposed. Commercial ships usually have a high ratio of dynamic immersion relative to static immersion. Furthermore, the time between dry-docking and, therefore, re-coating for ships is typically much longer than the exposure periods encountered in the scientific literature. To enhance the accuracy and reliability of the drag ranking performance of top-coats for voyaging ships longer in situ exposure conditions with a higher ratio of dynamic exposure compared to existing studies are needed. Studies revealing the effect of dynamic exposure over a substantial period, i.e., more than 3 months, from small-scale setups are lacking. It is, therefore, important to investigate the frictional impact of marine top-coatings when primarily dynamically immersed, because this exposure condition more accurately represents that typically encountered by FCCs on commercial ships, as opposed to a static exposure. It is, furthermore, critical to measure the frictional performance with frequent intervals over a long time period in order to obtain the average drag performance, as it is the average performance that is relevant, not only the final frictional performance. To compensate for the lack of setups that can determine the drag performance accurately under conditions representing those met by voyaging ships, a test setup with specific traits was developed. The first scientific hypothesis that was intended to investigate was if the impact of static immersion would be more severe compared to dynamic immersion from a drag performance perspective by using the dynamic rotor setup. The second hypothesis to evaluate was how

much more severe a static immersion would be compared to a dynamic immersion, if static immersion would cause a higher drag increase than dynamic immersion. The purpose of the rotor setup was, furthermore, to evaluate the drag development over a long time period, when coatings were exposed to realistic voyaging conditions from a small-scale setup, as this research is missing in the literature. If the hypothesis is that an approach with primarily dynamic exposure would yield a more accurate drag performance prediction, then the rotor setup could be further developed to gain more knowledge with scientific and industrial value. For instance, the rotor setup could be used to age coatings for a full dry-dock period and even longer to determine the impact of extended dry-dock periods. Such a study could be applied to a cost-benefit analysis to determine the optimal time period before re-coating FCCs. The setup could also be improved by one or more of the following options (see the section “Further work” for more details):

- expose more cylinders with different activity patterns;
- age FCCs in a location with high biofouling intensity;
- age FCCs in locations with varying biofouling intensity, i.e., low, medium, and high;
- use replicate samples; and
- increase the exposure period.

The dynamic in situ setup could, furthermore, be developed to continuously measure the drag from the exposed cylinders, which would provide a more detailed knowledge of the changes in drag over time and, therefore, the impact from various traveling patterns from ships. The rotor setups also have the advantage of being very flexible, because leaching and polishing rates, as well as drag performance, would be parameters that could be determined by this setup, which, therefore, would be of high value to the coating industry and academia.

Comparison of dynamic rotor setup and friction disk machine studies

One study (Swain et al. (2007)) revealed changes in the ranking of the drag performance in a number of cases when comparing the initial condition, the condition after static immersion, and the condition after dynamic immersion. A hypothesis tested if the drag performance ranking could be correctly identified via a static immersion study or for newly applied coatings or both, when compared to more realistic exposure conditions with, primarily, dynamic immersion. To investigate this hypothesis, two different setups with different

exposure conditions were used. An FDM was used to measure the drag performance of newly applied coated disks and the one after static immersion in the harbor of Den Helder, the Netherlands. In addition, a land-based rotor setup was used to measure the performance of newly applied coated cylinders after a combination of static and dynamic immersion from a seawater-based rotor setup in Roskilde Fjord, Denmark.

Chapter 3 – Measurements of drag performance of statically exposed fouling control coatings using a spinning disk

This chapter is intended for publication in a scientific and relevant journal in 2015 with the title “Measurements of drag performance of statically exposed fouling control coatings using a spinning disk”. The authors are Asger Lindholdt, Kim Dam-Johansen, Stefan M. Olsen, Diego M. Yebra, Job W. Klijnstra and Søren Kiil.

Abstract

The drag performance of fouling control coatings (FCCs) is of interest because it affects the speed or fuel consumption and the amount of harmful exhaust gases from ships. In this work, five commercial FCC systems were applied to disks with a radius of 11.45 cm and smooth substrates. The drag performance was measured using a friction disk machine (FDM) in the newly applied coating condition and after one month of static immersion in natural seawater. The four best performing coatings were re-examined for their drag performance after an additional 2.5 months of immersion. The five FCCs in the newly applied coating condition revealed a small difference and, in most cases, one that was less than the experimental uncertainty when applied on smooth substrates. After one month of static immersion, a hydrogel-based fouling release coating (FRC) with biocides had the lowest drag, while a fluorinated FRC had the highest drag. A hydrogel-based FRC without biocides and two self-polishing copolymer (SPC) coatings showed intermediate performance. After 3.5 months of immersion, the two hydrogel-based FRCs showed superior drag performances compared to the two SPC coatings. Furthermore, the drag performances of two different FCC systems with varying substrate roughness (i.e., the roughness below the coating system) were measured in the newly applied condition. An increase in the substrate roughness led to increased drag for both FCC systems, but the FRC was less impacted by the higher substrate roughness than the SPC coating.

Introduction

Due to the high cost of fuel and the environmental concerns (e.g., emission of greenhouse gases, SO_2, and NO_x) connected to fossil fuel consumption, the fuel efficiency of ships is becoming increasingly important. Commercial ships typically operate with dry-docking intervals of 3 to 5 years, although extended dry-docking of up to 7.5 years can be granted for certain ship classes. During that time, substantial biofouling can occur. Biofouling is defined as the accumulation of micro and macro-organisms, such as the settlement of bacteria, algae, slime, weed, or barnacles, on man-made structures. This accumulation adversely affects ships through the loss of speed, decreased maneuverability, higher fuel consumption leading to a higher cost of operation, emission of harmful gases, increased frequency of dry-dockings, and the translocation of invasive species (Yebra et al., 2004). Frictional resistance represents a considerable portion of a ship's resistance (Lindholdt et al., 2014). For example, frictional resistance constitutes 70% to 90% of the total resistance for slow trading ships (e.g., bulk carriers and tankers) and, occasionally, less than 40% for faster trading ships (e.g., cruise liners and container ships) (MAN Diesel & Turbo, 2011). The choice of fouling control coating (FCC) thereby affects fuel consumption significantly because it directly influences the drag on the hull. The objective of this study was to determine the drag performance of FCCs in a newly applied condition and after static immersion in natural seawater (i.e., exposure to biofouling). The drag performance of a biofouled FCC after static immersion reveals its capability to limit and release biofouling. The majority of larger industrial vessels have high traveling activity, although extensive idle periods can occur. Biofouling accumulation during static immersion is known to be more severe than during dynamic immersion (e.g., a moving ship) (Almeida et al., 2007). Therefore, the worst exposure condition for an FCC system with respect to biofouling accumulation typically occurs during static immersion. An excellent FCC system should limit biofouling adhesion, and if biofouling does attach, it should be able to self-clean due to the forces arising from the water flowing over the FCC at conditions similar to those affecting a hull when a ship is moving. In this work, these properties were examined via FCC disks in a friction disk machine (FDM) after static immersion in natural seawater. Furthermore, the substrate roughness and its influence on the drag performance of two different FCC systems, i.e., FRC and SPC, were investigated in order to assess the impact of

ship hull roughness on the final drag performance of different FCC systems prior to the coating application.

Experimental setup

Figure 1.3 displays the FDM, which was used to measure the torque of the investigated coatings. The FDM consists of a cylindrical chamber with a height of 35 cm and a diameter of 33 cm. During the drag measurements, the chamber holds filtered natural seawater from the harbor of Den Helder (the Netherlands). The coated disks have a radius of 11.45 cm and a height ranging from 0.6 to 0.7 cm (depending on the thickness of the substrate and the paint system). The experimental setup has similar dimensions to those described in Holm et al. (2004). The distance from the bottom of the tank to the disk surface was approximately 9.25 cm and from the top of the chamber to the disk surface it was approximately 25.25 cm. The disks applied with FCCs were statically immersed at the raft facilities of Toegepast Natuurwetenschappelijk Onderzoek's (TNO; now Endures BV) located in the harbor of Den Helder (the Netherlands). The average temperature of seawater from June to September, 2013, ranged from 15°C to 21°C. In the same period the salinity ranged from 2.65 wt% to 2.94 wt% (Klijnstra, 2014). The salinity was, therefore, approximately 30 wt% to 40 wt% lower than what is typically encountered at oceans, where the salinity ranges between 3.3 wt% and 3.8 wt% (Yebra et al., 2004).

Figure 1.3. Friction disk machine used to measure the drag of coated disks, located at TNO, the Netherlands. Here shown with a blue disk in the chamber, which can hold water (here without water) (Klijnstra, 2014).

Experimental drag measurement procedure

During the drag experiments, the torque and rotations per minute (RPM) were recorded. The RPM varied between 500 and 1500, with increments of 200 RPM. The torque at each speed was measured for 120 seconds, of which the average torque value of the last 60 seconds was used in the drag performance analysis. This ensured that the drag measured was based on the biofouling that was well-attached at each given RPM. The temperature was measured prior to the FDM measurements and after each run.

All of the disks had the same coating system on the back (i.e., the area facing the bottom of the tank during spinning) and the edge while the top (i.e., the area facing the water surface during spinning) was covered with the coating under investigation, see Figure 2.3. Prior to the first run, the back and the edge of the biofouled disks were mechanically cleaned to ensure a similar drag contribution from these areas on all the disks. During the mechanical cleaning, a soft wet sponge was used to remove the biofouling with minimal impact to the surface of the FCC. The different torque values should, therefore, only be attributed to the differences in the FCC applied to the top area of the disks. After each run of measurements, the chamber was emptied and refilled with filtered natural seawater to remove any released biofouling. The newly applied disks only received one run of drag measurements, whereas three runs of drag measurements were applied to the disks after static immersion. The following observations were made for the three runs:

- First run: loose biofouling detached
- Second run: only well-attached biofouling remained on disks
- Third run: prior to this last run, all biofouling was removed by hand with a soft sponge

The first run can be related to a ship's drag for a short period after it begins to move after an idle period, while the second run can be related to a ship's drag after a substantial period with movement, e.g., some minutes or a few hours. The third run can be linked to a ship's drag after a gentle hull cleaning.

Estimation of experimental uncertainty

One of the inherent challenges when determining the uncertainty of biofouled FCC surfaces is that, once the biofouled surface is exposed to a force, it is likely to release part of the biofouling, which changes the surface friction. Repeating drag measurements of biofouled surfaces is, therefore, a challenge. There were no replicate disks, which renders the uncertainty of the coating application and biofouling intensity at the test site unknown. The uncertainties from the FDM at the investigated RPMs were estimated from repeated measurements on a blank (smooth) aluminum disk. Thus, the uncertainty presented in this paper is solely based on the FDM uncertainty, while other uncertainties are not accounted for. Table 1.3 provides the experimental uncertainty, reported as one standard deviation, for the measured torque value for the smooth disk at the investigated RPMs. The uncertainty is seen to generally decrease with increasing RPM.

Table 1.3. Absolute standard deviation and standard deviation in percent for a blank (smooth) aluminum disk.

RPM	Standard deviation [Nm]	Standard deviation (%)
500	0.0077	2.41
700	0.0065	1.14
900	0.0089	0.95
1100	0.0091	0.69
1300	0.0067	0.38
1500	0.010	0.42

Fouling control coating systems

Table 2.3 lists the dry film thickness (DFT), binder technology, basic operating mechanism, and underlying substrate roughness of the investigated FCC systems. All of the disks were applied with the same FCC system, i.e., the hydrogel-based FRC with biocides applied to disk 4, on the back and outer edge of each disk. All of the disks were coated with the same epoxy

primer in two layers, with a final DFT of approximately 200 µm. One tie-coat was used for the FRCs, and another one was used for the SPC coatings. Both tie-coats are commercial products, and their DFTs were approximately 100 µm. The substrate roughness was based on Rt(50) measurements (Molland, 2008). Figure 2.3 provides an illustration of the various coatings applied to the disks.

Table 2.3. FCC systems, approximate DFT, binder technology, operating mechanism, and Rt(50) substrate roughness.

Disk #	Top-coat	Approxi-mate top-coat DFT [µm]	Binder technology	Operating mechanism	Rt(50) substrate roughness
1	Antifouling (SPC)	200	Silylated acrylate	Biocide release and self-polishing	Smooth
2	Antifouling (SPC)	200	Acrylate-based binder	Biocide release and self-polishing	Smooth
3	Fouling release (FRC)	150	Polydimethylsiloxane	Hydrogel-based surface	Smooth
4	Fouling release (FRC)	150	Polydimethylsiloxane	Hydrogel-based surface and biocide release	Smooth
5	Fouling release (FRC)	150	Polydimethylsiloxane	Amphiphilic surface via perfluorinated copolymers	Smooth
6	As disk 4	As disk 4	As disk 4	As disk 4	211 µm
7	As disk 1	As disk 1	As disk 1	As disk 1	211 µm
8	As disk 4	As disk 4	As disk 4	As disk 4	322 µm
9	As disk 1	As disk 1	As disk 1	As disk 1	322 µm

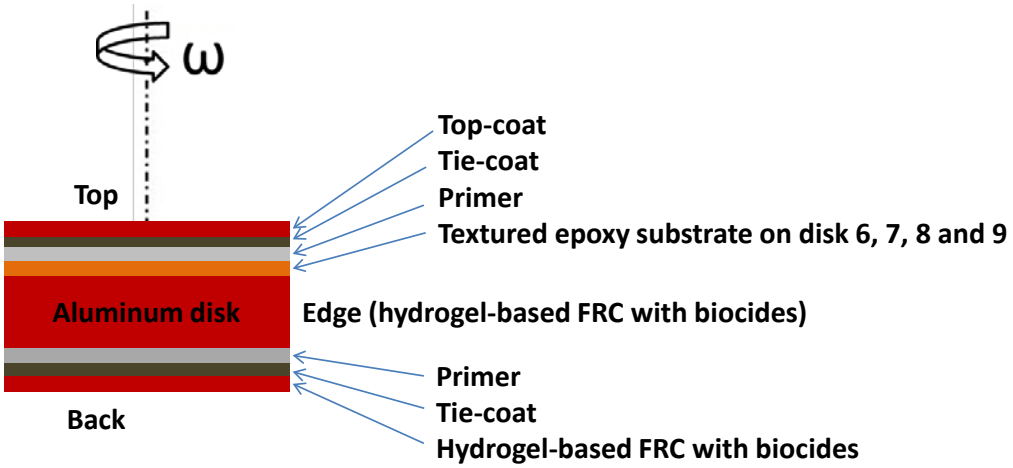

Figure 2.3. Generic top, back and edge description of the coating systems applied on the rotating disks.

Measurement scheme

All of the disks (i.e., 9 in total) were examined for their newly applied drag performance in the FDM. Subsequently, disks 1 to 5 were statically immersed in seawater from June 6, 2013 to July 8, 2013 (i.e., 31 days); afterward, new measurements of their drag performances in the FDM were performed. Disks 1 to 4 were then re-immersed in their mechanically cleaned condition for an additional period from July 16, 2013 to October 6, 2013 (i.e., 82 days), resulting in a total of 113 days of immersion. Disks 1 to 4 were, after the additional immersion, examined for their drag performance once again.

Surface characterization

The substrate roughness parameters were measured before coating application and the top-coat surface roughness parameters were measured after application. The surface roughness and waviness parameters of the newly applied FCC condition were measured using laser profilometry for every disk on an area of 50 mm x 45 mm (i.e., 22.5 cm^2). The applied cut-off length was 0.8 mm. The substrate roughness was measured with a Total quality control (TQC) hull roughness analyzer DC9000 (TQC, 2012), which provides the Rt(50) roughness. The Rt(50) measures the maximum peak-to-valley height over a 50 mm length of the surface (Molland, 2008). Several Rt(50) measurements were made to obtain an average Rt(50) roughness value.

In Figure 3.3, a picture of a disk with a high substrate roughness prior to the coating application is shown. The substrate placed on the disk was made of epoxy. A roughness

calibration template (similar to a muffled plastic plate) with a high and well-defined Rt(50) roughness was used to create a silicone cast of the roughness profile. The silicone cast was then used to make epoxy substrates with the same roughness profile. After curing, the epoxy substrate was removed from the silicone cast, to which it did not adhere. Finally, the epoxy substrate was glued and cut to fit the aluminum disk. By using the same silicone cast, identical levels of epoxy substrate roughness were achieved. The substrate roughness measured with a TQC hull gauge roughness analyzer (TQC, 2012) resulted in a substrate roughness of the two silicone casts in average Rt(50) values of 211 µm and 322 µm.

Figure 3.3. Picture of disk with high substrate roughness prior to coating application.

Results and discussion

The measured torque is converted into a non-dimensional torque coefficient, C_m, using the following equation

$$C_m = \frac{2M}{1/2\rho R^5 \emptyset^2 \omega^2} \quad (1.3)$$

where M is the recorded torque, ρ is the density of the seawater in the test chamber, R is the radius of the disk, Ø is the swirl factor, and ω is the angular velocity. The swirl factor, which takes the wall effect into account, was reported by Loeb et al. (1984) to have a value of 0.854 over a wide range of $Re\sqrt{C_m}$, which coincides with the dimensions in this study. This value of Ø was, therefore, used in the present study. The Reynolds number (Re) for a FDM is shown in the following equation

$$\mathrm{Re} = \frac{\emptyset \omega R^2}{\vartheta}, \quad (2.3)$$

where ϑ is the kinematic viscosity of the fluid (Loeb et al., 1984).

The FDM measurements were conducted at a temperature ranging from 12.3°C to 20.5°C. Filtered seawater was taken directly from the Den Helder harbor and used with its current temperature in order to preserve the biofouling in the best possible way as the biofouling on the disks had experienced this temperature prior to the drag measurements. The torque coefficients were converted so they could be compared at identical Reynolds numbers, despite the temperature differences during the FDM measurements. The conversion to the same Reynolds number at each of the investigated RPM was found by making a second order polynomial that fit the C_m as a function of the Reynolds number determined for the measured temperature and RPM. The second order polynomial was then used to determine the C_m at the desired Reynolds numbers. The second order polynomials described the C_m well based on R^2 (i.e., coefficient of determination) values varying from 0.94 to 0.98. The average C_m of the disks in the newly applied coating condition applied to smooth substrates was used as the reference torque coefficient, $C_{m,ref}$. The reference torque coefficient was used to calculate the change in C_m, ΔC_m, after static immersion at the investigated Reynolds numbers. Table 3.3 shows the investigated Reynolds numbers, which are based on the viscosity of seawater at 16.3°C for the FDM, used for comparison with the torque coefficients after static immersion.

Table 3.3. RPM and corresponding Reynolds number used for comparison of the torque coefficients after static immersion and the reference torque coefficients. The Reynolds numbers are based on the viscosity of seawater at 16.3°C (ITTC, 2011)

RPM	Corresponding Reynolds number ($\cdot 10^5$)	$C_{m,ref}$ ($\cdot 10^2$)
500	5.35	3.46
700	7.48	3.20
900	9.62	3.00
1100	11.8	2.85
1300	13.9	2.76
1500	16.0	2.72

The change in C_m, ΔC_m, was determined as

$$\Delta \mathrm{C_m} = 1 - \frac{\mathrm{C_m}}{\mathrm{C_{m,ref}}} \cdot 100\% \quad (3.3)$$

where $C_{m,ref}$ and C_m were determined at the same Reynolds number and C_m is the torque coefficient determined after static immersion.

The average torque coefficients based on the three highest Reynolds numbers, $\bar{C}_{m,H}$, was calculated as

$$\bar{C}_{m,H} = \frac{C_m(Re=1.18\cdot10^6)+C_m(Re=1.39\cdot10^6)+C_m(Re=1.60\cdot10^6)}{3}, \quad (4.3)$$

where $C_m(Re = 1.18 \cdot 10^6)$, $C_m(Re = 1.39 \cdot 10^6)$ and $C_m(Re = 1.60 \cdot 10^6)$ are the torque coefficients at the three highest RPMs (i.e., 1100, 1300 and 1500 RPM). The uncertainty at the higher Reynolds number is lower and, therefore, the average value of C_m at high Reynolds numbers provide a higher certainty than those at lower Reynolds numbers.

Roughness measurements

Table 4.3 displays the average roughness (R_a), total roughness (R_t), average waviness (W_a), and total waviness (W_t) for each of the top-coats (final coating layer) in the newly applied condition, including their standard deviations. The averages for waviness and roughness are determined from the average deviation from the centerline height, while the total roughness and total waviness are calculated from the maximum peak to valley height. For a detailed description of the roughness and waviness parameters, see ISO 1996.

Table 4.3. R_a, W_a, R_t, and W_t surface parameters and the standard deviation of the newly applied coating condition.

Disk #	Top-coat	R_a [µm]	R_t [µm]	W_a [µm]	W_t [µm]
1	Silylated acrylate SPC coating	1.44 ± 0.06	13 ± 2	11 ± 2	64 ± 8
2	Acrylate-based SPC coating	0.63 ± 0.02	7 ± 2	9 ± 2	52 ± 8
3	Hydrogel-based FRC without biocides	0.33 ± 0.02	5 ± 1	9 ± 2	46 ± 7
4	Hydrogel-based FRC with biocides	0.23 ± 0.03	6 ± 6	8 ± 2	41 ± 8
5	Fluorinated FRC	0.17 ± 0.03	6 ± 4	6 ± 2	25 ± 15
6	Hydrogel-based FRC with biocides	0.34 ± 0.03	6 ± 4	24 ± 4	134 ± 22
7	Silylated acrylate SPC coating	1.8 ± 0.2	16 ± 2	29 ± 4	161 ± 22
8	Hydrogel-based FRC with biocides	0.62 ± 0.08	6 ± 4	40 ± 5	209 ± 26
9	Silylated acrylate SPC coating	1.41 ± 0.08	12 ± 3	53 ± 6	267 ± 25

The FRCs consistently resulted in a lower R_a and R_t than the SPC coatings when evaluated at the same substrate roughness. As shown in Table 4.3, the FRC containing biocides had a lower W_a and W_t than the SPC coating when applied to both a smooth substrate and an equally rough substrate. Increasing the substrate roughness caused the W_a and W_t to increase for both FCC systems. In short, the substrate roughness influenced both the final

FCC roughness (R_a and R_t) and waviness parameters (W_a and W_t), but the FRC resulted in a smaller increase of these parameters compared to the SPC coating. Furthermore, a poor correlation between the investigated roughness and waviness parameters was found.

Newly applied coating condition and impact on drag

The newly applied FCC condition is typically considered to be the best possible condition with respect to the drag performance of an FCC throughout its lifetime on a ship hull, although the self-smoothening effects of SPC coatings and water uptake might provide a drag reduction if the coating can remain free of biofouling (Weinell et al., 2003). Due to surface degradation, damage, corrosion or biofouling, the drag performance of the newly applied FCC systems decreases with time after seawater immersion, but the rates of degradation can differ significantly. Figure 4.3 displays the torque coefficients of the newly applied FCC systems and a blank aluminum disk. The torque coefficients, and therefore the drag resistance, were within the experimental uncertainty in most cases. Only the silylated acrylate-based SPC coating gave a torque coefficient that was significantly higher than the acrylate-based SPC coating and the hydrogel-based FRC with biocides when evaluated as the average torque coefficient from the three highest Reynolds numbers ($\bar{C}_{m,H}$). The finding of primarily insignificant differences for newly applied coatings is opposite to many other studies where significant differences are reported (e.g., Lindholdt et al. (2014)). However, this study and other ones are not directly comparable due to different coatings being evaluated.

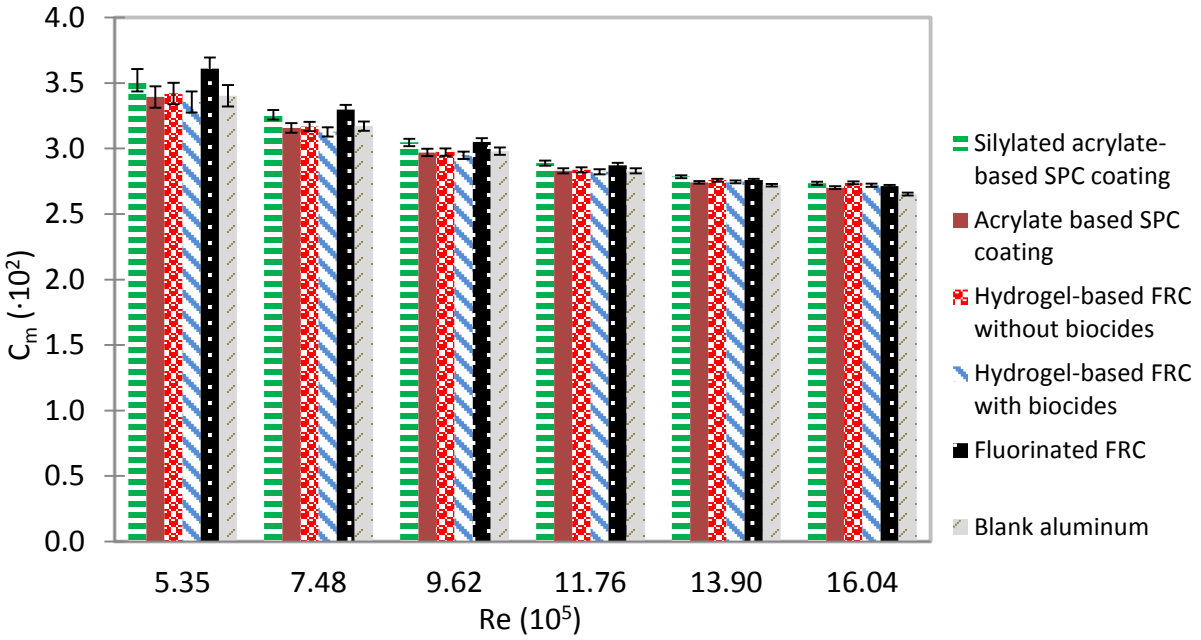

Figure 4.3. C_m times 10^2 at various Reynolds numbers times 10^5 in the newly applied coating condition.

Long-term static immersion and impact on drag

One month of static immersion

The drag performance and, therefore, potential fuel savings due to smoothness can be negated if an FCC system becomes biofouled (Lejars et al., 2012). Thus, the newly applied drag performance of an FCC is only important as long as it is capable of remaining free of biofouling. Figure 5.3 provides the difference in torque coefficients compared to the reference value, ΔC_m, of the FCCs after the first run, following one month of static immersion. The fluorinated FRC clearly performed worse than the other FCCs, even though it showed a similar drag performance to the other coatings in the newly applied condition and a low initial roughness. The FRC with biocides incorporated showed the lowest drag after one month of static immersion. The hydrogel-based FRC without biocides resulted in a torque coefficient slightly lower than the acrylate-based SPC coatings at the higher Reynolds numbers, where the uncertainty is lowest. The silylated acrylate-based SPC coating revealed the second highest torque coefficient at the majority of the investigated Reynolds numbers.

Figure 5.3, 6.3, 10.3, and in particular 7.3 present drag values that are lower than the reference value. The decrease in the torque coefficients compared to the reference value based on the newly applied coatings could be due to mechanical cleaning or seawater uptake, which could make the coating surfaces smoother. Mechanical cleaning occurred on

the back and the side of the discs after static immersion and also on the top part after the third run. However, the decrease in drag compared to the newly applied coating condition could also occur from measurement uncertainty from the FDM. The reported values, which are lower than the reference values, are primarily only slightly lower and within or close to one standard deviation from the reference value. Furthermore, the majority of the observations with drag values below the reference values occur at the lower Reynolds number where the uncertainty is highest. It is, therefore, believed to be primarily an uncertainty from the FDM measurement and less due to changes in the surface roughness that some values are observed below the reference values. However, self-smoothing effect and water uptake could potentially have caused lower drag, which was reported for two SPC coatings in a biofouling free environment by Weinell et al. (2003).

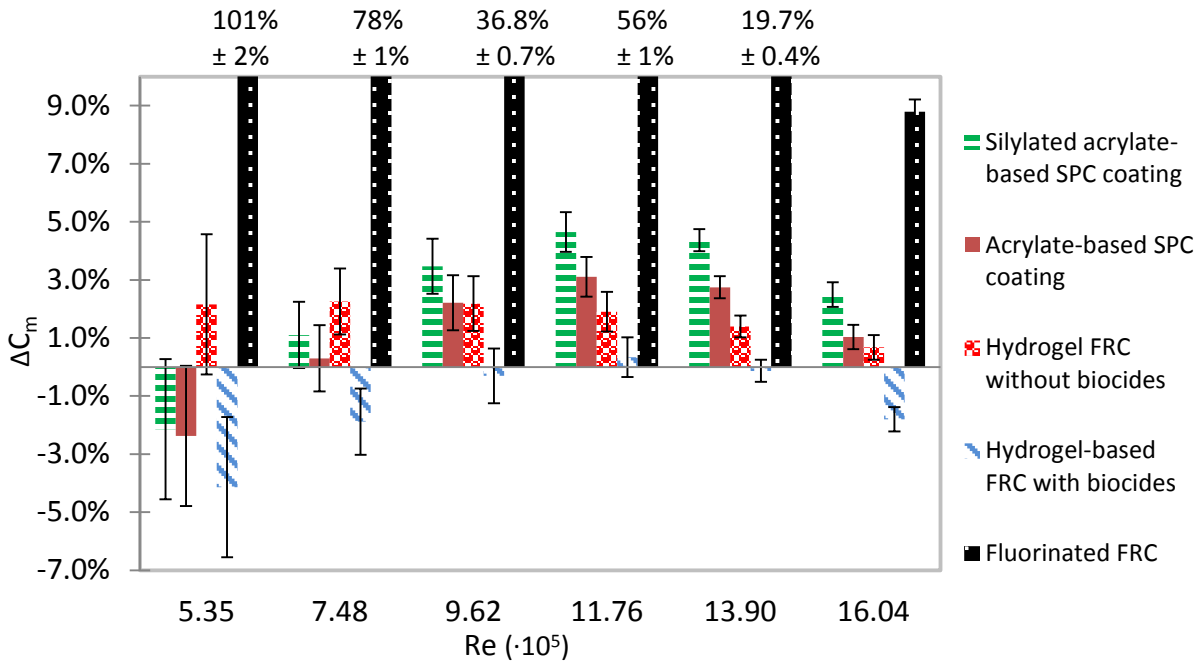

Figure 5.3. ΔC_m at various Reynolds numbers times 10^5 from the first run, after one month of static seawater immersion. The bar of fluorinated FRC is cut due to the high values; these values are shown at the top of the bar instead. ΔC_m is defined from equation 3.3.

Figure 6.3 shows the difference in torque coefficients compared to the reference value of the FCCs from the second run. The same ranking of the FCCs is seen for the first and second run at the higher Reynolds numbers. Due to the release of biofouling in primarily the first run, the differences in torque coefficients were lower in the second run. In many cases, the drag differences were within the experimental uncertainty, thereby complicating the

distinction between the coatings. Indeed, the only clear distinction was the fact that the fluorinated FRC performed significantly worse than the other coatings over the entire range of investigated Reynolds numbers.

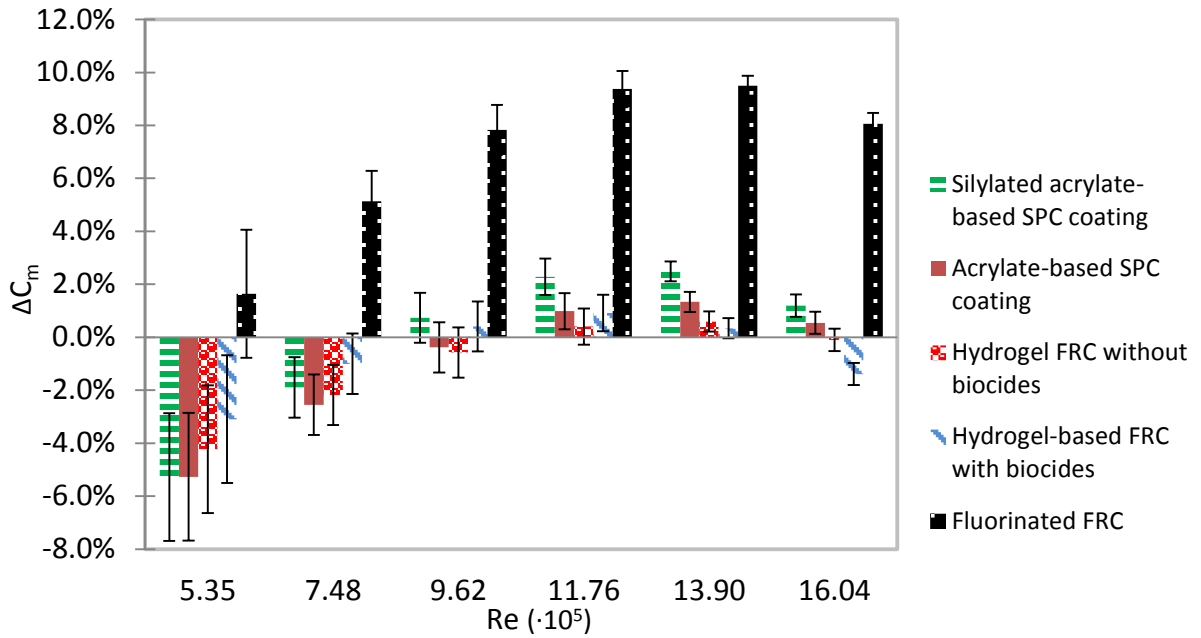

Figure 6.3. ΔC_m at various Reynolds numbers times 10^5 from the second run, after one month of static seawater immersion. ΔC_m is defined from equation 3.3.

Figure 7.3 shows the difference in torque coefficients compared to the reference value from the third run, when mechanical cleaning of the FCCs had taken place prior to the measurements. In the mechanically cleaned condition, the fluorinated FRC was no longer the worst performing FCC. In fact, the ranking of the coatings varied with the Reynolds number; none of the coatings had a significantly lower drag over the entire range of investigated Reynolds numbers. Thus, the difference in the drag performance in the mechanically cleaned condition after one month of static seawater immersion was at a similar level for all the FCCs.

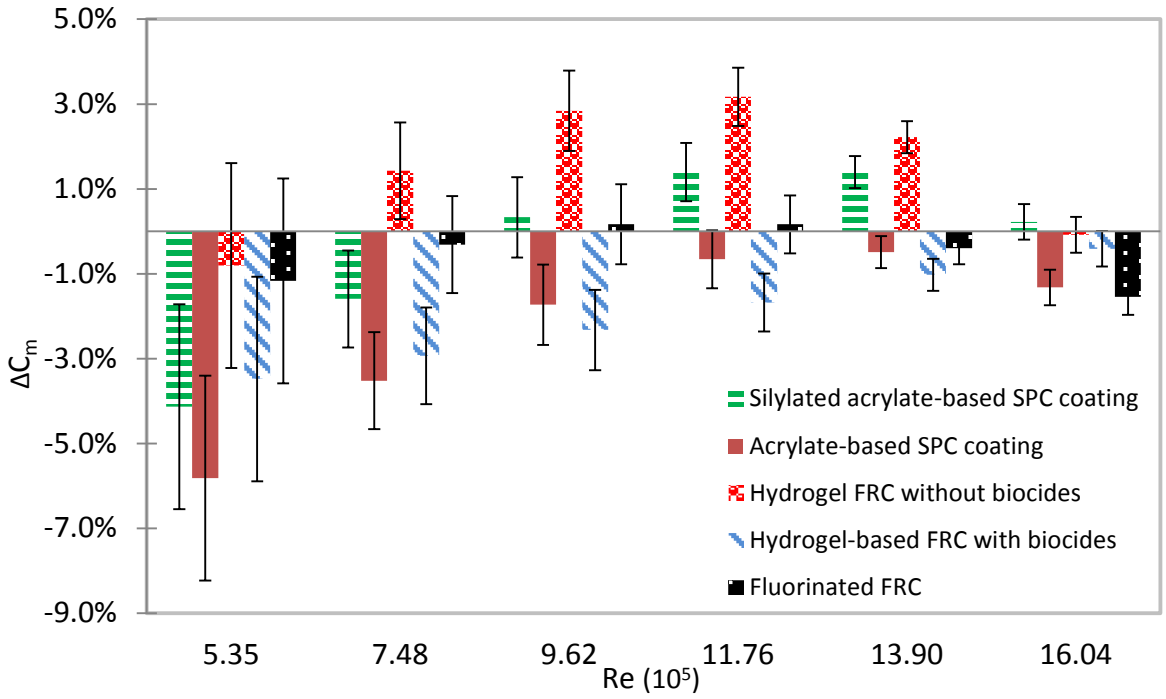

Figure 7.3. ΔC_m at various Reynolds numbers times 10^5 from the third run, after one month of static seawater immersion. Mechanical cleaning with a soft sponge had been carried out prior to these torque measurements. ΔC_m is defined from equation 3.3.

In short, the difference between the FCCs was most significant during the first run. Smaller differences in torque coefficients were found for the second run, and these often occurred within the experimental uncertainty, leaving the ranking between the intermediate performing coatings unknown. The smallest difference was, as expected, seen in the mechanically cleaned condition; the ranking of the drag performance of the coatings in this condition remained largely uncertain. The hydrogel-based FRC containing biocides showed a significantly lower drag than other coatings after one month of static immersion. In contrast, the fluorinated FRC showed the highest drag, but after mechanical cleaning, it regained a drag performance similar to the other coatings. The four coatings aside from the fluorinated FRC were in many cases within the experimental uncertainty after one month of static seawater immersion.

3.5 months of static immersion

The four FCCs that had shown the lowest drag after one month of static immersion in the first and second runs, i.e., the two SPC coatings and the two hydrogel-based FRCs, were statically immersed for an additional 2.5 months (i.e., a total of 3.5 months, but with a mechanical cleaning after one month). Figure 8.3, 9.3, and 10.3 depict the differences in

torque coefficients compared to the reference value during the first, second, and third runs, respectively. Figure 8.3 reveals that the two FRCs had similar and significantly lower drag than the SPC coatings, which also showed a similar level of drag.

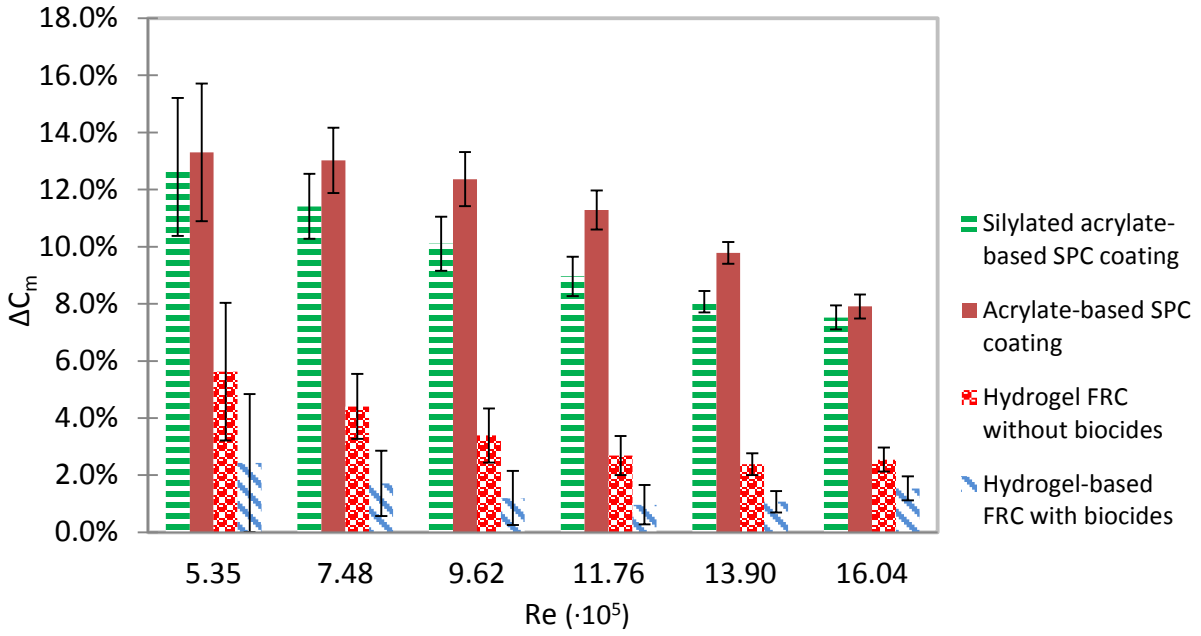

Figure 8.3. ΔC_m at various Reynolds numbers times 10^5 for the first run, after 3.5 months of static seawater immersion. ΔC_m is defined from equation 3.3.

The second run shown in Figure 9.3 displays that the FRCs' drag is still lower than that of the SPC coatings. However, in the second run, the ΔC_m values are significantly lower, which is explained by the release of biofouling.

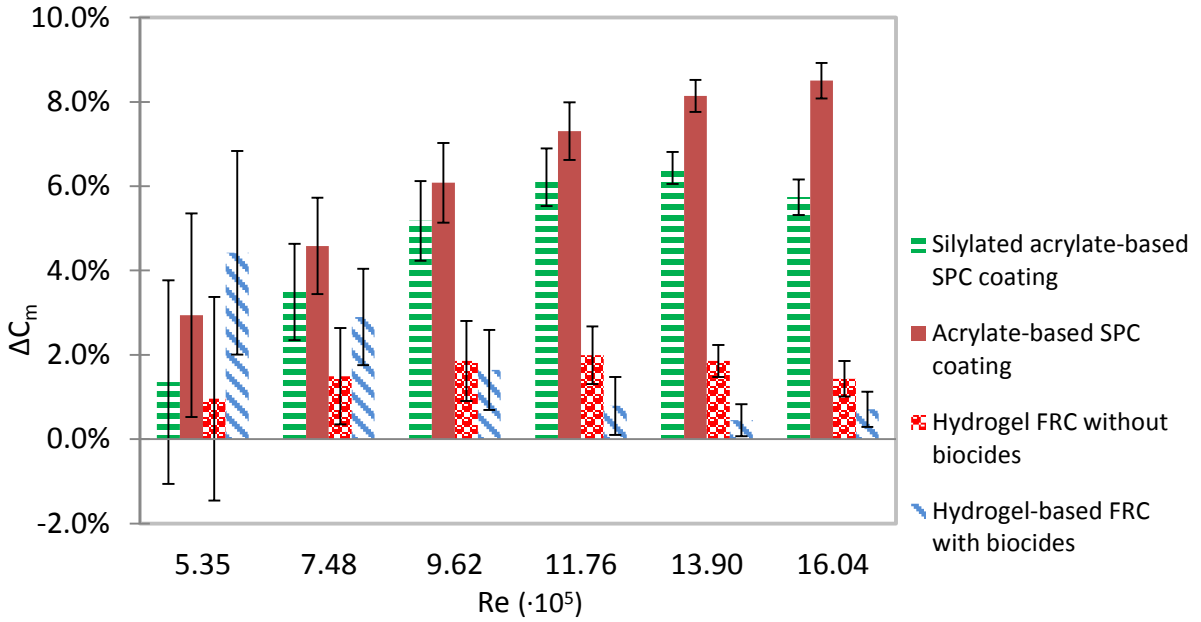

Figure 9.3. ΔC_m at various Reynolds numbers times 10^5 for the second run, after 3.5 months of static seawater immersion. ΔC_m is defined from equation 3.3.

The mechanically cleaned condition represented in Figure 10.3 shows that the FCCs had similar performances when evaluated over the investigated range of Reynolds numbers.

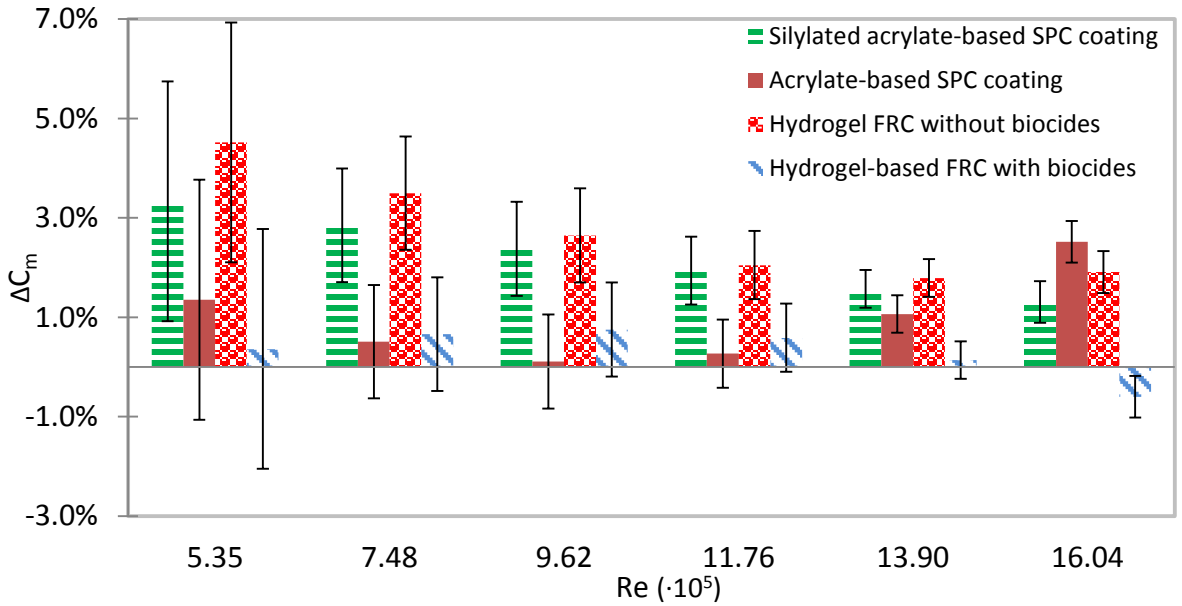

Figure 10.3. ΔC_m at various Reynolds numbers times 10^5 for the third run, after 3.5 months of static seawater immersion. Prior to the third run, mechanical cleaning had taken place. ΔC_m is defined from equation 3.3.

Summary of long-term static immersion

In most cases, the difference in drag performance of the FCCs in the newly applied condition was smaller than the experimental uncertainty from the FDM, whereas it was larger and often significant after one month of static immersion. The difference in drag decreased after

the first run of measurements, which is explained by the release of some of the biofouling. In the mechanically cleaned condition, the difference in drag was again typically smaller than the experimental uncertainty. The same tendency of increasing differences in drag performance after immersion was observed after an additional 2.5 months of immersion. Interestingly, the hydrogel-based FRC without biocides, which revealed a drag resistance within the experimental uncertainty compared to the acrylate-based SPC coatings after one month of static immersion, showed a significantly lower drag than that of the two SPC coatings after 3.5 months. One month of static seawater immersion is, therefore, not sufficient to reveal the correct long-term drag performance ranking of FCCs when statically immersed. Table 5.3 displays the FCC ranking based on the average torque coefficients from the second run, at three highest Reynolds numbers ($\overline{C}_{m,H}$) as defined in equation 4.3. The second run was chosen to rank the coatings because only firmly adhered biofouling was assumed to have remained on the disks after the first run, which presumably left a biofouling condition that was more representative of a moving ship. The higher velocities were chosen because of the higher Reynolds numbers providing a lower uncertainty on the torque values. From Table 5.3, it is seen that the drag performance ranking can change from the newly applied condition and the immersed condition. Furthermore, the ranking can change depending on the time of immersion. It is, therefore, essential to measure the drag of FCCs over a substantial amount of time, i.e., at least some months, and with frequent intervals in order to obtain the correct drag performance ranking; in this way, the coating system with lowest drag during a typical dry-dock period (i.e., 3–5 years) is likely to be estimated correctly for a ship with frequent and long idle periods. It should, however, be noted that the difference in drag performance in most cases was close to or within the statistical uncertainty.

Table 5.3. Ranking of drag performance of FCCs from the second run based on the average torque coefficient values measured at three highest Reynolds numbers. The ranking is based on "1" representing the best performance (lowest drag) with decreasing performance and "5" representing the worst performance (highest drag).

Top-coat	Newly applied	1 month of static immersion	3.5 months of static immersion
Silylated acrylate SPC coating	3-5	3-4	3
Acrylate SPC coating	1-5	2-4	4
Hydrogel-based FRC without biocides	1-5	1-3	1-2
Hydrogel-based FRC with biocides	1-5	1-2	1-2
Fluorinated FRC	1-5	5	-

Visual impact

Ideally, a visual evaluation of the biofouling level could provide a rough estimate of the drag resistance of an FCC surface. Schultz (2007) provided an estimate of the relationship between the visual biofouling level and its impact on the powering needs of a naval ship. The fluorinated FRC and the FRC containing biocides had the highest and the lowest biofouling level respectively, which also translated into the highest and lowest drag resistance. In this case the visual inspection was a correct predictor of the drag performance. However, Table 6.3 shows the observed biofouling level of the other FCCs prior to the torque measurements, where the correlation to their drag resistance is not so clear. For example, the hydrogel-based FRC without biocides and the two SPC coatings showed a similar drag level after one month of static immersion, despite dissimilar biofouling species and coverage were observed. This means that the drag performance and the biofouling level observed on the disks prior to the torque measurements were sufficient to rank the FCCs in terms of drag in some cases, although small differences in biofouling did not necessarily correspond to a difference in drag. For instance, the silylated acrylate-based SPC coating showed a lower drag than the acrylate-based SPC coating, even though it had 20% more slime coverage. This could be due to different biofouling release properties or experimental uncertainty or a combination. After static exposure, the biofouling release properties are not revealed by visual evaluation which, however, is partly, included in the drag measurements. Drag measurements are, therefore, necessary when a more accurate estimate of the drag performance of an FCC system is needed, especially since providing an accurate visual determination of the surface coverage, type of biofouling attachment, and thickness of biofouling is complicated.

Table 6.3. Biofouling level of statically immersed FCCs after one month and after 3.5 months including biofouling description, prior to drag measurements.

	Biofouling rating according to ASTM D3623 (ASTM D3623, 2012)		Biofouling level (surface coverage and type)	
Top-coat / exposure time	One month	3.5 months	One month	3.5 months
Silylated acrylate SPC coating	0	20	80% Medium thick slime 20% Diatoms	80% Medium thick slime
Acrylate SPC coating	30	40	60% Thin slime 10% Diatoms	60% Medium thick slime
Fluorinated FRC	0	N/A	60% Medium thick slime 10% Barnacles 30% Young barnacles	N/A
Hydrogel-based FRC without biocides	67	90	30% Very thin slime 3% Barnacles	10% Hydroid biofouling
Hydrogel-based FRC with biocides	45	75	50% Very thin slime 5% Diatoms	25% Thin slime

Impact of substrate roughness on drag performance

A vast amount of work has been conducted to investigate the drag performance of FCC systems on substrates with low roughness, which often does not represent a ship hull surface prior to its coating application in dry-dock. Significantly less work has been conducted to determine the impact of the underlying substrate and its roughness on the drag performance of FCC systems. In this study, these properties were investigated for a hydrogel-based FRC containing biocides and a silylated acrylate SPC coating. Figure 11.3 shows the average torque coefficients at the three highest Reynolds numbers, $\overline{C}_{m,H}$, for both FCCs with varying substrate roughness. A significant increase was noted in the torque coefficients (drag) for both FCC systems when the substrate roughness increased. The drag was higher for the SPC coating than the FRC, and the difference increased as the substrate roughness increased. The self-leveling, i.e., the ability to make a smooth coating surface, of the FRC was better than that of the SPC coating; this was revealed by both the FDM measurements and the lower levels of roughness and waviness. Based on the drag measurements with varying substrate roughness, it is assumed that a ship hull surface with a high roughness will be less negatively impacted if an FRC system is applied, compared to an

SPC system. If a ship owner chooses to full-blast, a significant amount of fuel savings can be expected regardless of the chosen FCC system, because a substrate with low roughness obtained from full-blasting is expected to result in a lower roughness of the top-coat (upper layer). If full-blasting does not occur and the ship hull surface is rough, the smallest increase in drag is expected when applying an FRC system, compared to an SPC coating.

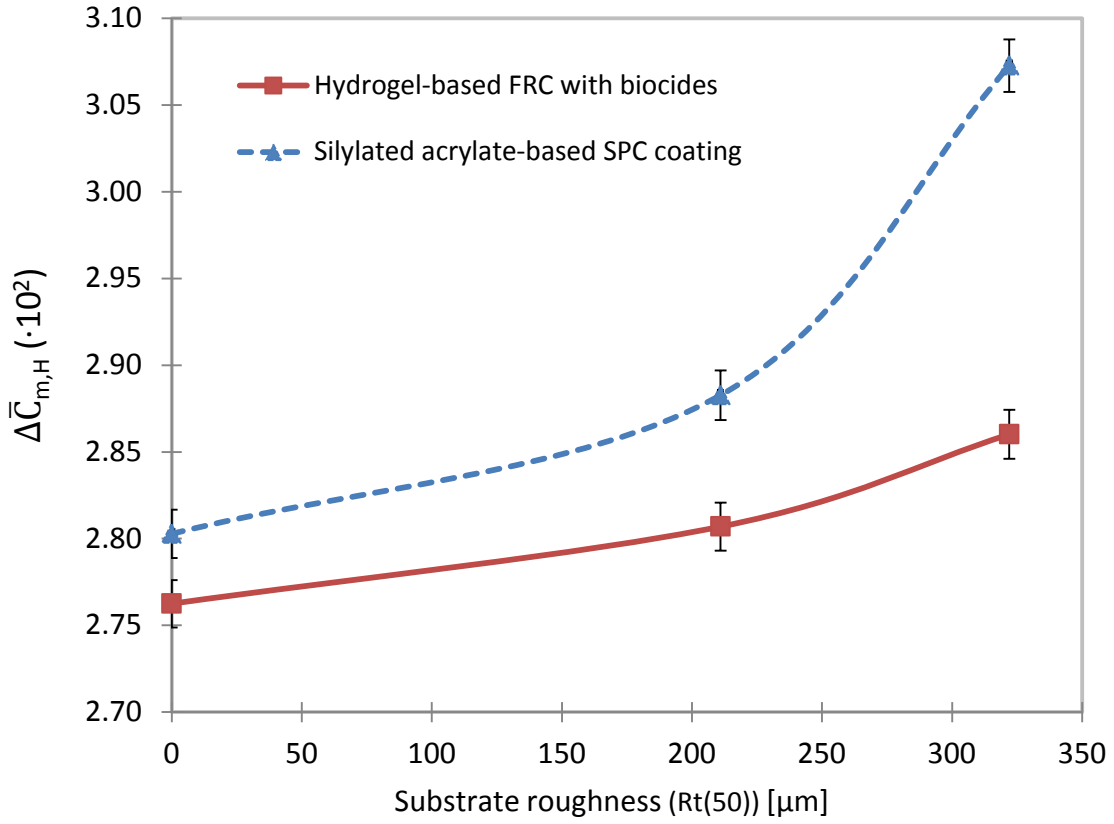

Figure 11.3. Average torque coefficients at three highest Reynolds, i.e., $\bar{C}_{m,H}$, numbers as defined in Equation 4.3. An FRC system and an SPC system with varying Rt(50) substrate roughness is shown.

Conclusions

The drag performance of five different FCCs applied on smooth disks, consisting of two SPC coatings and three FRCs, were examined in their newly applied condition and after one month of static immersion in natural seawater; four of them were re-examined after an additional 2.5 months. Despite significant differences in roughness and waviness parameters between the FCCs, significant differences in torque coefficients were in most cases not observed for the newly applied condition. In other words, most of the coatings revealed drag differences smaller than the experimental uncertainty. On the other hand, the same coatings

in many cases deviated significantly in their long-term drag performance. The value of drag measurements for coatings in a newly applied condition is, therefore, limited, especially if a coating quickly biofouls.

The hydrogel-based FRC containing biocides was superior in performance after one month of static immersion and after 3.5 months of static immersion. The incorporation of biocides in the FRC is believed to increase the biofouling prevention significantly, which was also revealed by a lower biofouling accumulation during the static immersion, compared to the otherwise similar hydrogel-based FRC without biocides. The fluorinated FRC performed as well as the other coatings in the newly applied condition, but it accumulated significant amounts of biofouling after one month of static immersion. Even though the fluorinated FRC had the same binder as the other FRCs, it provided a poorer performance after the static immersion. The copolymers incorporated into the coating, even though typically only between 1 wt% and 10 wt% for FRCs (Lejars et al., 2012), are believed to be the main factor responsible for the difference in performance between the hydrogel-based FRC without biocides and the fluorinated FRC. The hydrogel-based FRC without biocides revealed a significantly lower drag than the two SPC coatings after 3.5 months of static immersion. The SPC coatings performed similarly after one month of static immersion, but the acrylate-based SPC coating performed better than the silylated acrylate-based SPC coating after 3.5 months.

The impact of the substrate roughness for an SPC coating and a hydrogel-based FRC system with biocides was also investigated. Both FCCs showed that increasing the substrate roughness increased drag. It was, however, found that the hydrogel-based FRC system with biocides was capable of minimizing the impact of a high substrate roughness better than the SPC coating; this was revealed from both the drag measurements and the lower final top-coat roughness and waviness. This discovery would provide an extra incentive for ship owners to apply an FRC system, especially if full-blasting of the ship is not carried out, as the drag gains compared to the SPC increased with increasing substrate roughness.

Chapter 4 – Estimation of long-term drag performance of fouling control coatings using an ocean-placed raft with multiple dynamic rotors

The content of this chapter was accepted for publication in the Journal of Coatings Technology and Research (JCTR) May 2014 with the title "Estimation of long-term drag performance of fouling control coatings using an ocean-placed raft with multiple dynamic rotors". The authors are Asger Lindholdt, Kim Dam-Johansen, Stefan M. Olsen, Diego M. Yebra and Søren Kiil. There have been minor changes compared to the journal article in order to match the format of this thesis, but otherwise it remains as presented in the JCTR.

Abstract

An experimental setup was designed and built to estimate changes in the skin friction of fouling control coatings (FCC) over an extended period of time in conditions simulating the vast majority of ship profiles (regarding speed and activity) in the present market. The setup consisted of two separate parts: one aged FCCs directly in seawater in a dynamic manner by simulating the exposure condition of a ship's hull, and a second, laboratory part measured the torque (drag) of aged coatings in a rotary setup. From the spring to the autumn of 2013 and 2014, four commercial FCCs were exposed for 53 weeks in Roskilde Fjord, Denmark, which is characterized by relatively cold seawater and a salinity of approximately 1.2 wt%. The in situ immersion seawater conditions consisted of five-week cycles divided into two weeks of static immersion and three weeks of dynamic immersion, during which time the cylinders were rotated at a tangential velocity of 8.1 knots. The skin friction was found to generally increase more during the static period, compared to the dynamic ones. Over the course of the entire exposure period, the skin friction of the investigated FCCs decreased in the following: fluorinated fouling release coating (FRC) (highest skin friction), hydrogel-based FRC without biocides, silylated acrylate self-polishing copolymer (SPC) coating, and hydrogel-based FRC with biocides (lowest skin friction). However, the differences in skin friction between the latter three coatings were minor and often within the range of experimental uncertainty. The average surface roughness of the FCCs in the newly applied and

mechanically cleaned condition, determined as the Rt(50) and R_z parameters, was evaluated as poor predictors of skin friction.

Introduction

Due to the high costs of fuel and environmental concerns (emissions of greenhouse gases, SO_2, and NO_x), the fossil fuel efficiency of ships is becoming increasingly important. Commercial ships typically experience dry-docking intervals of 3 to 5 years, although extended dry-docking of up to 7.5 years can be granted for certain ship classes. During that time, substantial biofouling, defined as the accumulation of micro- and macro-organisms (e.g., bacteria, algae, slime, weed, or barnacles) on man-made structures can occur. This accumulation adversely affects ships through the loss of speed, decreased maneuverability, higher fuel consumption leading to a higher cost of operation, emission of harmful gases, frequency of dry-dockings, and translocation of invasive species (Yebra et al., 2004).

Frictional resistance nearly always represents a considerable portion of a ship's total resistance (Lindholdt et al., 2014). For example, frictional resistance constitutes 70% to 90% of the total resistance for slow trading ships (e.g., bulk carriers and tankers) and, occasionally, less than 40% for faster trading ships (e.g., cruise liners and container ships) (MAN Diesel & Turbo, 2011). The choice of fouling control coating (FCC) thereby affects fuel consumption significantly because it directly influences the drag on the coated hull.

In this paper the term "fouling control coatings (FCC) cover all marine top-coats below the waterline of a ship with the purpose of minimizing friction arising from water flowing over the coated hull. The term "fouling release coatings" (FRC) rely on a working mechanism with a dual mode of action, that is, non-stick properties and a biofouling release behavior. The general idea of FRCs is to minimize the adhesion between fouling organisms and the surface, so that the biofouling can be removed by hydrodynamic stress during navigation or by a simple mechanical cleaning (Lejars et al., 2012). Most of the present FRCs are based on cross-linked poly-dimethylsiloxanes (PDMS). Conventional biocidal antifoulings cover "self-polishing copolymer coatings" (SPC), "controlled depletion polymer" (CDP) coatings and other top-coats which primary working mechanism consists of releasing biocide to minimize

biofouling. SPC coatings are characterized by a controlled biocide release, which allows a fairly constant leaching rate over time at constant seawater conditions (Yebra et al., 2004).

It is well-known that biofouling can cause severe drag increase; therefore, an FCC with low drag in newly applied and unexposed conditions can prove to be a poor choice if it easily biofouls. Thus, the value of the drag performance for a newly applied coating condition is limited unless the coating can stay completely clean (Lindholdt et al., 2014). Static exposure reproduces the biofouling pressure on an idle ship quite well, but the vast majority of larger commercial ships are primarily moving, experiencing only relatively short idle periods. Zargiel and Swain (2013) showed that biofilm adhesion, abundance, diversity, and community composition were impacted differently when exposed either statically or dynamically; thus, it was concluded that, rather than statically grown biofilms, dynamically grown biofilms should be used to address the influence of biofilms on drag and the associated costs. The current drag performance estimation is often based on the newly applied coating drag performance and is typically followed by drag measurements after static immersion.

The literature generally reports that fouling release coatings (FRCs) exhibit a lower drag, compared to conventional biocidal antifouling coatings in the newly applied condition (e.g., Schultz (2004), Candries and Atlar (2003b), Swain et al. (2007), Weinell et al. (2003), Ghani et al. (2010), Flack et al. (2012) and Mirabedini et al. (2006)). However, it has generally been reported that when FCCs are exposed statically, conventional biocidal antifouling coatings exhibit lower drag than FRCs (e.g., Schultz (2004), Swain et al. (2007) and Holm et al. (2004)). However, one study reported superior performance of FRCs compared to conventional biocidal antifoulings when examined after 3.5 months of static exposure (Lindholdt et al., 2015a). Since the results for exposure conditions resembling larger commercial ships are limited, it is yet uncertain whether FRCs or conventional biocidal antifouling coatings perform better under realistic conditions. Millett and Anderson (1997) reported that the use of an FRC led to a 12% lower fuel consumption in all weather conditions for an aluminum catamaran when compared to a low-copper TBT-free biocidal antifouling coating.

According to the results in Swain et al. (2007), the relative performance between the four coatings tested, i.e., two FRCs, one copper ablative and one copper SPC, varied with the test condition, i.e., newly applied, after static immersion, and after dynamic immersion (Swain et al., 2007). The test conditions clearly impacted which coating had the lowest friction. For instance an FRC exhibited the lowest drag coefficients after dynamic exposure while the best performing coating under static conditions was a Cu-ablative coating (Swain et al., 2007). It is, therefore, of utmost importance to determine the frictional performance in exposure conditions, which to the best possible extent simulate those a ship hull encounters during voyage to determine the optimal choice of coating with respect to friction. For this reason a new approach, which simulates exposure conditions of ships realistically, has been developed in this work to provide an accurate determination of an FCC's drag performance in ship like conditions. The work presented in this paper include experiments with FCCs during a long exposure period (approximately 53 weeks) with frequent drag measurements during the entire experimental period, a land-based and an in situ rotor setups in a combination not previously used and FCCs exposed to a high percentage of dynamic immersion (60%), as opposed to the more common experiments performed after primarily static immersion.

Experimental setup

The experimental setup used in this study consisted of two parts. One part of the setup, a laboratory-placed rotor, was used to determine the drag performance (torque) of FCCs. The other part employed coated cylinders that could be rotated in the seawater from a raft. This latter setup was used to age coatings in conditions simulating those that FCCs typically encounter during voyages. For a period of 53 weeks, the drag performances of the coated cylinders were measured every two or three weeks in conditions resembling those of slow to fairly fast ocean-going ships. After 25- and 53-week exposures, the coatings were mechanically cleaned by hand with a soft wet cloth. The release of biofouling was removed with a light stroke over the FRCs, while the SPC coating needed a somewhat firm stroke to remove the biofouling. The coated cylinders used in this study were transferred from the raft to the laboratory rotor for drag performance measurements to be taken; afterward, they

were returned to the raft for further aging. It should be noted that a typical dry-dock period is five years; therefore, the 53-week immersion period represents only some of the time between two dry-dockings.

Drag performance measurement setup

To measure the drag performance, a laboratory rotor setup in which an inner cylinder was rotated inside a static cylinder was used. This setup was originally developed to study the polishing and leaching rates of chemically active antifouling coatings (Kiil et al., 2001). It is common to use a rotary setup to measure the drag induced by FCC surfaces (e.g., Weinell et al. (2003), Candries et al. (2003b), Ghani et al. (2010), Kawaguchi et al., Mirabedini et al. (2006)). Figure 1.4 displays the laboratory rotating cylinder system. The inner rotating cylinder, coated on the outside, had a diameter of 31 cm and a height of 30 cm. A smooth PVC disk was attached to the top and bottom before the torque measurements. Both disks had a height of 0.5 cm; thus, the total height of the rotating cylinder was 31 cm. The outer static cylinder shell had a diameter of 38 cm and a height of 31 cm. The volume of the seawater tank was approximately 600 L. The gap distance between the inner rotating and the outer static cylinder was 4 cm. The two bearings ensured the mechanical stability of the shaft to which the rotating cylinder was attached. The mechanical stability was needed due to vibrations from the rotary setup when operated at high rounds per minute (RPM).

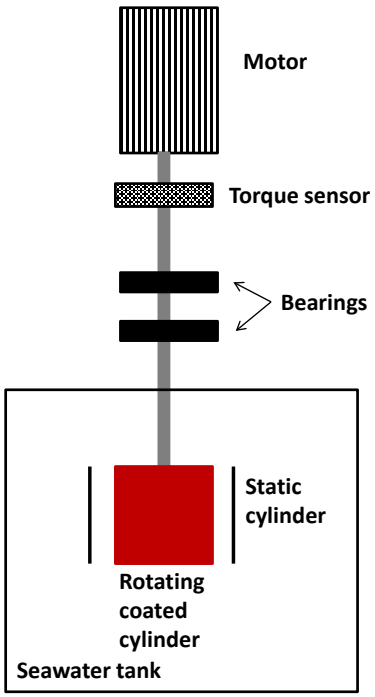

Figure 1.4. Schematic illustration of the laboratory rotor used for drag (torque) measurements. Maximum tangential velocity applied was 15.8 knots.

Figure 2.4. Laboratory rotor with a coated cylinder detached from the shaft.

The tangential velocity applied to the coated cylinders ranged from 3.2 knots to 15.8 knots (i.e., 100 RPM to 500 RPM), while measuring the torque. The measurements were carried out in natural seawater transported from Roskilde Fjord, Denmark, in order to maintain the biofouling in the best possible condition and to determine the drag performance of the FCCs in conditions that closely resembled those encountered during ageing. Two 0.5-cm (unexposed) smooth PVC disks were mounted to the end parts, i.e., top and bottom, of the cylinders in order to ensure identical top and bottom contribution for every cylinder. In this way, a constant contribution from the top and bottom was achieved, and the differences in drag between the FCCs and their development over time should, therefore, only originate from the changes occurring on the sides of the cylinders.

Aging setup

The purpose of the aging setup was to simulate the conditions encountered by the hull of an ocean-going ship during voyage, in order to ultimately predict the long-term drag performance of different FCCs on a ship. The raft with four rotor setups was located in Roskilde Fjord in Denmark at the DTU Risø campus (Lat: 55.692626 and Lon: 12.079442).

Figure 3.4 and 4.4 show the raft with the main parts: engines, coated cylinder, shafts, bearings, protection against floating objects, and electronic control box.

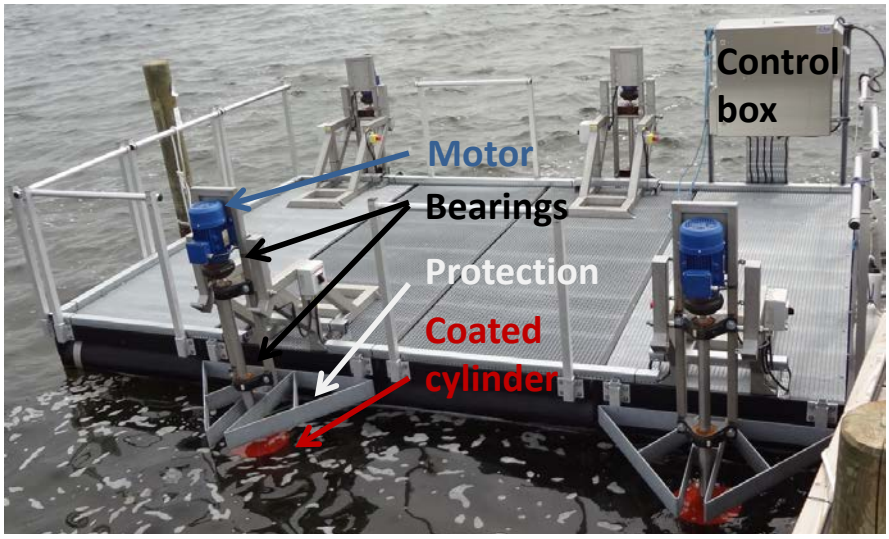

Figure 3.4. Photo of the aging setup where four coated cylinders can be rotated. The tangential velocity during the dynamic aging was 8.1 knots. The accessible raft is 3.5 m long and 2.4 m wide.

Figure 4.4 Photo of a cylinder out of the water at the aging setup.

Dick and Nowacki (1978) also used a rotor setup, as in this study. Advantages and disadvantages of their rotor compared to the one employed in this study are worth discussing. 18 different coating systems with different substrates, pretreatments, anticorrosive coatings, and top-coats were investigated for 51 months by Dick and Nowacki (1978). Curved panels of 6 × 6 inches were applied on drums exposed to seawater near Daytona Beach, Florida (USA). The plastic drums were three ft in diameter. The coatings were exposed in monthly cycles: one month with dynamic immersion at a tangential velocity of 20 knots was followed by one month of static immersion. Complete inspections were made after the first, third and fifth cycles, and afterward, one each year was made. Blank panels were also inspected both during the entire exposure period and each new season to determine the biofouling intensity of each season. The antifouling performance was rated with respect to total biofouling and in terms of the specific biofouling present (e.g., barnacles, mollusks, annelids, filamentous and encrusting bryozoan, hydroids, and algae). Their aging setup was, in many ways, similar to the one described here, with the main differences being that the setup of Dick and Nowacki (1978) used a smaller test area, a much longer exposure period, different exposure cycles, more coatings in the investigation and much warmer seawater (i.e., a higher biofouling intensity was expected). The main

advantages of the setup used by Dick and Nowacki (1978) were that more coatings could be investigated and the coatings did not have to be moved to another setup. Thus, it avoided the risk of impacting the biofouling that might have occurred when removing it from the seawater (discounting a presumably short inspection period on the site), and avoided the risk of mechanical damage during transportation. The main drawback was that the coatings could only be evaluated via visual inspection; a visual inspection is, at best, only an approximate indication of the drag performance, whereas a laboratory rotor setup of the present work provides accurate drag measurements. The visual inspection is, furthermore, likely to be subjective, making comparisons to other experimental data inaccurate. Another setup similar to the one employed by Dick and Nowacki (1978) was the one used by Swain and Zargiel (2013). A drum of 1 m rotating at 6 knots was used to investigate micro-fouling during static and dynamic immersion. The same advantages and disadvantages mentioned above are valid for this setup. Swain et al. (2007) used a static test site to expose panels of 10 × 12 inches and subsequently exposed them in a land-based tank with a stirrer to simulate dynamic exposure. Finally, after a cycle of static and dynamic immersion the drag induced by the panels on a boat was measured. This setup exposed the coatings in a dynamic and static manner, which could be representative of certain ships. Indeed, a useful approach towards realistic FCC exposure. However, the dynamic exposure would, ideally, occur in situ and not in a land-based tank with a once-through seawater supply.

Biofuling intensity at aging setup

The natural seawater present at the aging setup is relatively cold, i.e., ranging between approximately -5°C and 25°C during the year. The salinity is approximately 1.2 wt% at the test site (Pedersen, 2010). Figure 5.4 provides a close-up view of the bottom of the raft after 6 months of exposure. The uncoated PVC material at the bottom of the raft had received significant biofouling in the form of a thick slime layer, a vast number of mussels, long seagrass, and some barnacles.

Figure 5.4. Close-up of the raft bottom after approximately 6 months of immersion in Roskilde Fjord. The end of the horizontal cylinder had been cleaned to show the PVC substrate.

One of the inherent challenges when comparing FCCs is that biofouling intensity is subject to changes over time and location. No apparent difference in biofouling intensity was found on the bottom of the raft, however; indeed, a similar biofouling intensity was noted around the raft and, therefore, also at the four rotor setups on the raft. However, to reduce any systematic uncertainty the position of the coated cylinders changed every week to minimize any differences in experienced biofouling intensity during exposure.

Measurement procedure

Prior to seawater immersion, drag measurements were carried out for the coated cylinders in the newly applied coating condition. Subsequently, two weeks of static immersion took place followed by additional drag measurements. After the static immersion, three weeks of dynamic immersion with subsequent drag measurements were conducted. This cycle of two and three weeks of static and dynamic immersion, respectively, followed by drag measurements, was applied from the spring of 2013 to the autumn of 2014. The exact periods were from May 21, 2013 to November 13, 2013 (25 weeks) and from April 1, 2014 to October 22, 2014 (28 weeks), resulting in a total exposure time of 53 weeks. After the end of each season, i.e., after November 13, 2013 and October 22, 2014, a soft wet cloth was gently applied to the FCCs to remove any attached biofouling. After November 13, 2013 the FCCs

were stored indoors at room temperature in a dark room until re-immersion on April 1, 2014. Surface roughness measurements were taken for the newly applied and cleaned coating conditions. Figure 6.4 shows the exposure conditions for the FCCs.

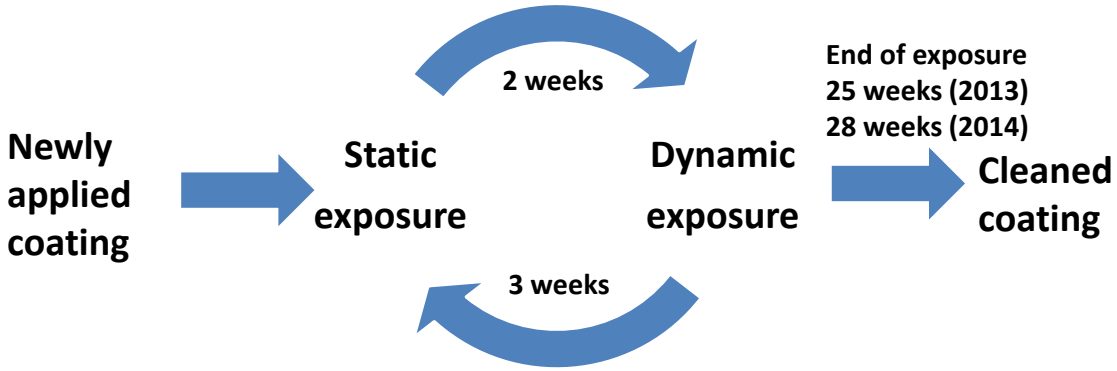

Figure 6.4. Procedure showing the exposure conditions for the FCCs. Drag measurements were carried out at the end of every stage. Prior to immersion, drag measurements for the newly applied FCCs were made. Subsequently, cycles of static and dynamic immersion were carried out and drag measurements were taken prior to changing the exposure conditions. After 25 and 53 weeks, the FCCs were mechanically cleaned, and their drag was measured.

The severity of biofouling was also measured by a visual inspection of the coated cylinder surfaces each week. The coated cylinders were transported to the laboratory rotor (close to the aging setup) and back to the aging setup in buckets with seawater, ensuring that any biofouling would be protected during transportation. The drag measurements carried out in the laboratory rotor began with 100 RPM (i.e., approximately a tangential velocity of 3.2 knots) and then subsequently increased in increments of 100 until reaching 500 RPM (i.e., approximately a tangential velocity 15.8 knots). Each torque measurement lasted 10 minutes, and the average torque value recorded during the last minute was applied to determine the skin friction coefficient. Only the last minute was used in order to ensure minimal and constant contribution from the friction in the bearings, which was found to remain stable after 10 minutes. The torque measurements were carried out in two sequential runs. The first run correlates to the drag performance when weakly adhered biofouling, if present, detaches; the second run correlates to the drag performance of well-attached biofouling.

Materials and sample preparation

The FFC technologies used in the experiment were:

- Silylated acrylate SPC coating
- Fluorinated FRC

- Hydrogel-based FRC (no biocides)
- Hydrogel-based FRC with biocides

The four investigated commercial FCCs were applied according to their specifications from the producer, resulting in a dry film thickness of approximately 100 µm for the SPC coating and 150 µm for the three FRCs. The application was made with an airless spray gun. The same commercial poly(dimethylsiloxane)-based (PDMS) primer was applied below the three FRCs resulting in an approximate dry film thickness of 100 µm. A commercially cured, modified epoxy primer was used as the coating below the SPC coating with an approximate dry film thickness of 100 µm. The top-coats were left to cure at room temperature for one week after application to ensure a high mechanical strength. Table 1.4 provides the basic parameters describing the FCC systems used in the experiments.

The backbone of the three FRCs consist of PDMS. The main differences among the FRCs are the copolymer additives, typically present in a concentration from 1 to 10 wt% (Lejars et al., 2012). The relatively small difference arising from primarily copolymer additives can, however, still be of high importance for the drag performance after exposure to natural seawater (e.g., Lindholdt et al., 2015a). For a more thorough review of FRCs and their working mechanisms, see e.g., Lejars et al. (2012). For information regarding detailed SPC coating working mechanisms, see e.g., Yebra et al. (2004).

Table 1.4. Basic parameters describing the FCCs used in the experiments. All the coatings are solvent-based.

	Fouling control coating systems			
Parameter	Fluorinated FRC	Hydrogel-based FRC (no biocide)	Hydrogel-based FRC with biocide	SPC coating
Top-coat dry film thickness [µm]	150	150	150	100
Application procedure	Airless spray	Airless spray	Airless spray	Airless spray
Primer	Commercial PDMS-based tie-coat used for all FRCs			Commercially cured modified epoxy
Primer dry film thickness [µm]	100	100	100	100
Back-bone structure	Polysiloxane	Polysiloxane	Polysiloxane	Silyl acrylate
Active biocide	None	None	Copper pyrithione	Copper pyrithione
Volume solids [%]	74 ± 2	71 ± 1	70 ± 1	58 ± 1
Color	Red	Red	Red	Brown
Number of components	3 (curing agent, base and, accelerator)	2 (curing agent and base)	2 (curing agent and base)	1
Maximum force when stretched [N]	7.2 ± 2.4	6.4 ± 1.3	6.3 ± 1.8	N/A
Contact angle (after 60 sec.)	79.7° ± 2.1°	28.1° ± 2.9°	92.9° ± 1.9°	88.3° ± 6.4°

Surface roughness measurements

Micro- and macro-roughness were measured on the coated cylinders before immersion and after 25 and 53 weeks of immersion, followed by mechanical cleaning. The micro-roughness consisted of measuring the R_z roughness with a sampling length of 0.8 cm. The mathematical definition of R_z given by Gadelmawla et al. (2002) is

$$\mathrm{R_z} = \frac{1}{n}\left(\sum_{i=1}^{n} \mathrm{p}_i - \sum_{i=1}^{n} l_i\right) \tag{1.4}$$

where n is the number of measurements over the sampling length, p is the vertical distance from the center to the peak, l is the vertical distance from the center to the valley, and i represents individual values from the measurements.

To measure the micro-roughness, a laboratory roughness measuring device, Handysurf E-350, was used. The number of measurements, n, was five when measuring the micro-roughness of the coated cylinders over the sampling length of 0.8 cm. The macro-roughness was measured as the Rt(50) roughness, which is often used when correlating roughness and drag performance of FCCs applied on ships (Lindholdt et al., 2014). Equation 1.3 is also valid when determining Rt(50) values that represent the maximum peak to valley (i.e., $n = 1$)

over a sampling length of 50 mm. The total quality control (TQC) hull roughness gauge of the type DC9000 was used to determine the Rt(50) values. It has a reported accuracy of ±5 μm or < 2%, whichever is greater (TQC, 2012). Sixty individual roughness measurements were made on every coated cylinder for both the micro- and macro-roughness, and they were evenly distributed on the cylinder to obtain an accurate representation of the surface roughness for the entire surface. The Rt(50) roughness measurements for the FRCs, which required special treatment, were performed according to the methods provided by Anderson et al. (1999). If the surface was dry, the stylus hopped over the rubberlike material, and if the surface was too wet, the gauge skidded very easily; both practices would provide erroneous readings (Anderson et al., 1999). To prevent these errors and obtain meaningful measurements, the FRC surfaces were wetted slightly.

Conversion of torque into friction coefficients

This section describes the drag measured for the rotating cylinder wall in the laboratory rotor and the subsequent conversion into friction coefficients. Furthermore, friction coefficients for the rotating cylinder wall were converted into friction coefficients for flat plates, which are assumed to resemble the skin friction of a ship's hull surface. The shear stress applied to the coated cylinder wall while rotating in the aging setup and its conversion to a flat plate are also described. The investigated shear stress range (10–100 Pa) applied to the rotating cylinder wall is similar to that experienced by larger commercial ocean-going ships.

Conversion of laboratory torque values into friction coefficients for cylinders and flat plates

From laboratory rotor torque values to cylinder friction coefficients

The torque measured by the torque sensor (M_T) consists of the contribution from the drag acting on the rotating coated cylinder wall (M_C), on the end surfaces (top and bottom) of the cylinder (M_E), on the outer shaft surface area (M_S), and on the bearings (M_B). In quantitative terms,

$$M_T = M_C + M_E + M_S + M_B \quad (2.4)$$

The relevant drag is that of the FCC surface (M_c), i.e., the rotating coated cylinder wall, excluding all other effects. The contributions from the end surfaces, the shaft, and the bearings are eliminated by a correction factor, which can be expressed as

$$M_{Cor}=M_E + M_B + M_S \quad (3.4)$$

Thus, subtracting the correction factor from the torque values provides the torque contribution from the rotating cylinder wall at the investigated tangential velocities:

$$M_C=M_T-M_{Cor} \quad (4.4)$$

The torque values for the rotating cylinder wall can be converted to skin friction coefficients, C_f, assuming that this value can be directly related to the wall shear stress, τ_w:

$$M_C = \tau_w Ar \quad (5.4)$$

where A is the wetted rotating cylinder wall (excluding the end surfaces) and r is the cylinder radius. The wetted surface area can be expressed as

$$A = 2\pi rh \quad (6.4)$$

where h is the cylinder height.

The wall shear stress can be expressed as a function of the friction coefficient, C_f, the water density, ρ, and the tangential velocity of the cylinder, U (Schlichting, 1968)

$$\tau_w = \tfrac{1}{2} C_f \rho U^2 \quad (7.4)$$

By combining equations 5.4, 6.4 and 7.4, an expression for the skin friction coefficient for the rotating cylinder wall can be derived

$$C_f = \frac{M_C}{\rho U^2 r^2 h \pi} \quad (8.4)$$

Correlation between rotor shear stress and ship speed

The shear stress induced by the rotation of a cylinder is different from the shear stress experienced by the hull surface of a ship, even when the free-stream velocities are identical, because of the different geometries. The free-stream velocity is taken as the moving velocity of the flat plate and in the case of a cylinder as the tangential velocity when rotated. These

differences must be accounted for when converting the laboratory rotor measurements into the full-scale FCC drag performance for a ship (i.e., a large flat plate). The aim of the chosen velocities in this study was to determine the drag performance of FCCs for speeds that are representative of the vast majority of larger commercial ships in the present market.

The skin friction coefficient on the cylinder wall of a smooth surface is described by the following relation for open sea rotors, i.e., with no outer static cylinder present (Theodorsen & Regier, 1944):

$$\frac{1}{\sqrt{C_f}} = 4.07 \cdot \log\left(Re_r \cdot \sqrt{C_f}\right) - 0.6 \tag{9.4}$$

In equation 9.4 Re_r represents the Reynolds number of the cylinder, given as

$$Re_r = \frac{Ur}{\vartheta} \tag{10.4}$$

where r is the radius of the cylinder, U is the tangential velocity of the rotating cylinder, and ϑ is the kinematic viscosity of the fluid.

On the other hand, the theoretical skin friction coefficient on the cylinder wall of a smooth surface in a Coutte type of flow was described by Arpaci and Larsen (1984) as

$$\frac{1}{\sqrt{C_f}} = \frac{1}{k\sqrt{2}} \mathrm{Ln}\left(Re_g \sqrt{\frac{C_f}{2}}\right) + 5.5 \tag{11.4}$$

with k being the von Kármán constant with a value of 0.41. Re_g represents the Reynolds number based on the channel gap between the two cylinders, described as

$$Re_g = \frac{U l_g}{\vartheta} \tag{12.4}$$

where l_g is the gap distance between the outer static and inner rotating coated cylinder, U is the tangential velocity of the rotating cylinder, and ϑ is the kinematic viscosity of the fluid.

In this study, it is assumed that the approximate shear stress on a ship's hull can be determined by that of a smooth, flat plate. According to Schlichting (1968) the average skin friction coefficient representative for an entire smooth, flat plate in the turbulent regime for a Reynolds number up to 10^9 can be found as

$$\bar{C}_f = \frac{0.455}{(log(Re_P))^{2.58}} \quad (13.4)$$

In equation 13.4 Re_P is the Reynolds number based on the length of the plate, given as

$$Re_p = \frac{Ul_p}{\vartheta} \quad (14.4)$$

where U is the velocity of the plate, l_p is the length of the plate, and ϑ is the kinematic viscosity of the fluid.

The average shear stress on a flat, smooth plate can, therefore, be found by combining equations 7.4 and 13.4 as

$$\bar{\tau}_w = \frac{0.2275\rho U^2}{(log(Re_P))^{2.58}} \quad (15.4)$$

Figure 7.4 displays the average shear stress correlations presented above with the dimensions for the applied setup. The open sea rotor used a tangential velocity of 8.1 knots. A kinematic viscosity of $1.37 \cdot 10^{-6}$ m^2/s, i.e., an approximate value of seawater at 10°C (ITTC, 2011), was applied when determining the average shear stress. By using the free-stream velocity and shear stress relationship for the open sea rotor and the laboratory rotor, as shown by equations 9.4 and 11.4, respectively, conversion into the full-scale shear stress of a ship can be determined, as exemplified in Figure 7.4. It is seen that the shear stress is only slightly higher for a flat, smooth plate of 100 m, compared to one of 400 m. However, it must be mentioned that the velocity and shear stress correlation is only valid up to a Reynolds number of 10^9, which is exceeded for the 400 m plate at around 6.6 knots, making the actual shear stress and speed relationship uncertain beyond this velocity. However, for the shorter 100 m plate, the speed and shear stress relation is valid up to a speed of approximately 27 knots. Figure 7.4 shows that a tangential velocity just above 15 knots in the laboratory rotor corresponds to a ship velocity of approximately 19 and 20.5 knots for a ship of 100 and 400 m in length, respectively.

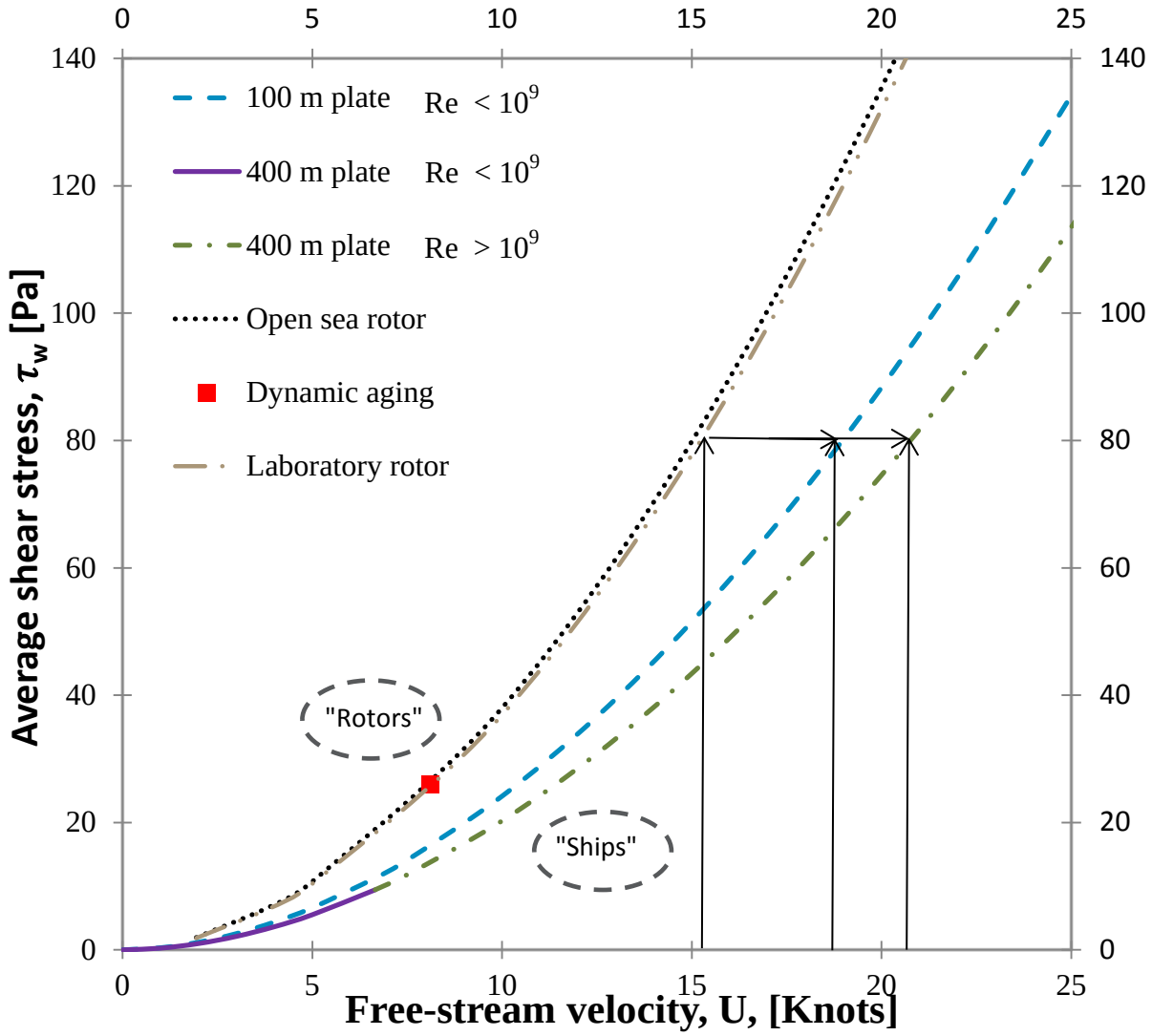

Figure 7.4. Plots of average wall shear stress correlations against free-stream velocity for smooth surfaces for the open sea rotor, including the value for the dynamic aging setup, the laboratory rotor, and a flat plate of 100 m and 400 m at Reynolds numbers below and above 10^9 are included. For the rotors (open and laboratory), the velocity on the x-axis corresponds to the tangential velocity of the cylinder when rotated, and for the flat plates, it corresponds to the moving velocity. The arrows exemplify how to convert tangential rotor velocities to flat plate velocities, i.e., a ship.

Table 2.4 provides the tangential velocities applied during the dynamic aging and the laboratory drag measurements, as well as the corresponding ship velocities for both a 100 m and a 400 m flat, smooth plate, resulting in identical average wall shear stresses. The velocity conversion is based on the assumption that the average shear stress is identical at the converted velocities.

Table 2.4. Tangential velocities of dynamic aging and laboratory rotor setups and the corresponding ship velocity, which results in identical average shear stress experienced by the hull for a smooth surface at 10°C. †Correlation is beyond the valid relationship described in equation 13.4.

		Corresponding ship velocity (i.e., flat smooth plate) [knots]	
Setups	Tangential velocities [knots]	Ship length of 100 m	Ship length of 400 m
Dynamic aging	8.1	10.4	11.4
Laboratory rotor	3.2	3.9	4.7
	6.3	7.9	8.8
	9.5	11.9	13.0†
	12.6	15.8	17.3†
	15.8	19.7	21.5†

Once the average skin friction coefficient has been determined with the laboratory rotor and the tangential rotor velocity has been converted into the corresponding velocity of a ship with a given length, the theoretical effective power (towing power), P_f (in Watt), necessary to overcome the skin friction force of the hull can be determined as

$$P_f = F_f U = \tfrac{1}{2}\rho \bar{C}_f U^3 A_H \quad (16.4)$$

where F_f is the skin friction force, U is the speed of the ship, $\bar{C}_f$ is the average skin friction coefficient, A_H is the wetted hull area, and ρ is the seawater density.

Estimation of the experimental uncertainty

The uncertainty of the measured torque is a combination of the uncertainties of the torque sensor, the reproducibility of the reading, the reproducibility of the sample preparation, and the uncertainty of the correction factor (M_{Cor}). One of the inherent challenges when estimating the uncertainty during the period of FCCs exposure is the fact that biofouling, if attached, is expected to be released during the measurements. This was indeed observed, in particular for the fluorinated FRC, which was the FCC that exhibited the most biofouling. Drag measurements carried out with a biofouled surface, therefore, cannot be repeated; thus, the uncertainty estimations are unknown for biofouled surfaces. However, in the newly applied condition and mechanically cleaned condition after seawater exposure, the measurement uncertainty can be estimated, because it is assumed that the FCC surface will not change significantly during the drag measurements, as there is no biofouling present and the mechanical roughness is not expected to change significantly due to the shear stresses

induced while the cylinder rotates. The drag measurement uncertainty in the newly applied and mechanical cleaned conditions was based on three replicate measurements in each condition at the investigated tangential velocities. In future experiments, the drag uncertainty during the exposure period can be estimated by using replicate cylinders. Table 3.4 provides the standard deviation obtained via measurements in the newly applied condition and mechanically cleaned condition after 25 weeks of seawater exposure, along with the average of the newly applied and mechanically cleaned condition. The average standard deviation obtained from the newly applied condition and from the mechanically cleaned condition after 25 weeks of immersion is assumed to represent the measurement uncertainty for cylinders with and without biofouling. In both the newly applied and mechanically cleaned condition the uncertainty decreased with increasing tangential velocities; this pattern was also observed by Weinell et al. (2003).

Table 3.4. The table provides the uncertainty of the measured torque. Standard deviations from the torque measurements in the newly applied condition, the mechanically cleaned condition after 25 weeks of seawater exposure, and the average of the newly applied and mechanically cleaned conditions are shown. The average standard deviation of the newly applied and mechanically cleaned conditions after 25 weeks of seawater exposure is assumed to represent the measurement uncertainty from the laboratory rotor.

Tangential velocity [Knots]	Newly applied condition [Nm]	Cleaned condition after 25 weeks [Nm]	Average of newly applied and cleaned condition [Nm]
3.2	0.071	0.041	0.056
6.3	0.071	0.037	0.054
9.5	0.064	0.031	0.048
12.6	0.064	0.033	0.049
15.8	0.056	0.035	0.045

Results and discussion

This section presents the skin friction coefficients at the newly applied coating condition and the development of the coefficients over 53 weeks, with mechanical cleaning after 25 and 53 weeks. Measured surface roughness parameters and their correlation to skin friction are discussed. Furthermore, the rating of the biofouling attachment observed on the coated cylinders during the exposure time is presented. The objective of measuring the roughness parameters was to obtain an estimate of the drag of an FCC in clean condition, without biofouling present, which often is the case for a short period after either a new coating has been applied or a soft hull cleaning (i.e., no severe changes in surface roughness). The purpose of determining the biofouling level attached to an FCC from visual measurements

was to determine whether the visual observations could deliver accurate estimations of the actual drag values.

Smooth cylinder

To determine the correction factor, M_{Cor}, the drag of three smooth cylinders made of PVC with heights of 15, 22.5 and 30 cm was measured. Figure 8.4 reveals that a linear relationship between the total torque and the cylinder height exists. Extrapolation of these lines to the interception with the *y*-axis (zero cylinder height) represents the correction factor, M_{Cor}. Note that M_{Cor} is a function of the tangential velocity. It is assumed that the correction factor is independent of the biofouling presence on the sides of the cylinders. This assumed because the flow over the sides of the cylinders with the fairly low biofouling levels encountered during the test period would not significantly alter the flow compared to a clean side. Drag changes in the bearings are not expected, despite increasing shear stress on the sides of the cylinders due to biofouling, because the RPM remained identical and, therefore, the resistance in the bearings would not have been impacted by the presence of biofouling.

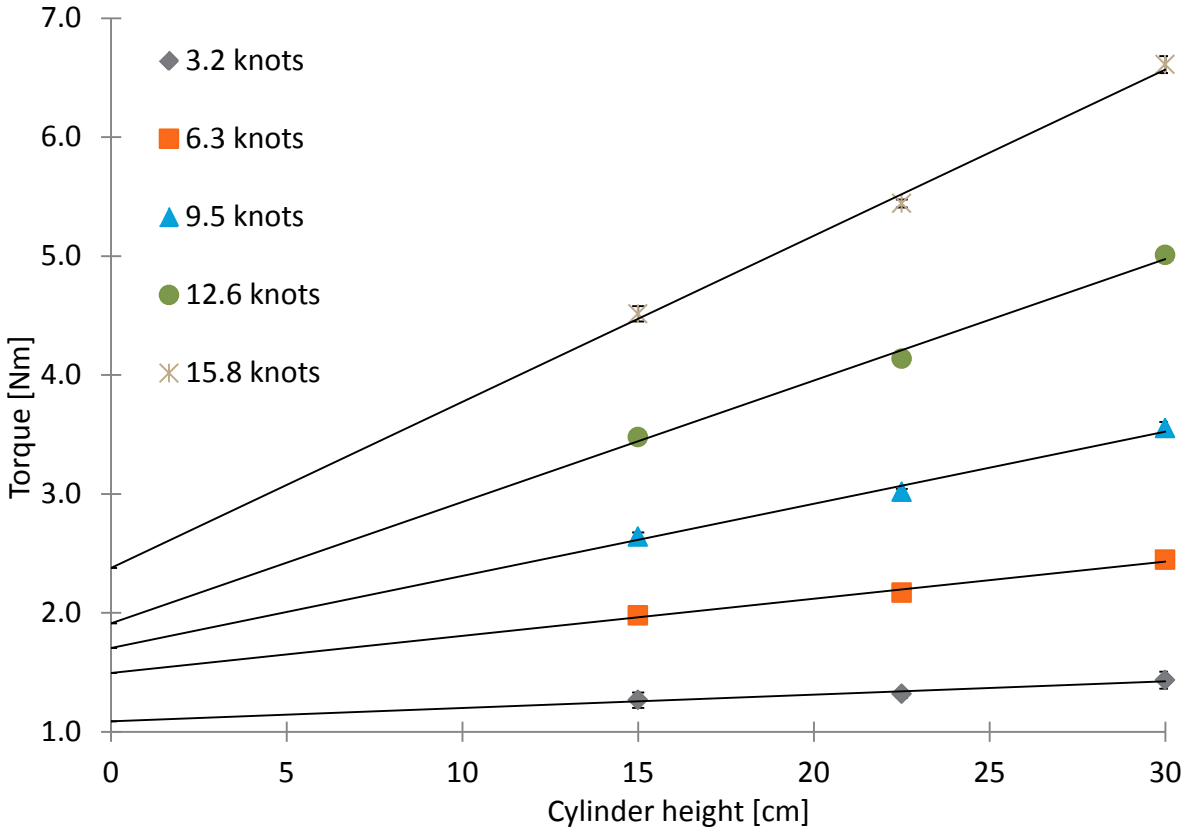

Figure 8.4. Torque values for three smooth PVC cylinders with heights of 15, 22.5 and 30 cm at tangential velocities ranging from 3.2 to 15.8 knots. The correction factor, M_{cor}, is found at the intersection with the y-axis. Symbols represent experimental data.

Material properties

Impact of the coating's surface roughness on drag

The micro- and macro-roughness were measured by R_z and Rt(50), respectively, in the newly applied coating condition and after 25 and 53 weeks of immersion with subsequent mechanical cleaning (see Table 4.4). The surface roughness of the silylated acrylate SPC coating is expected to have been influenced by the mechanical cleaning because brown (reddish) material from the coating remained on the soft cloth during the mechanical cleaning. The surface roughness measured after the mechanical cleaning is, therefore, not potentially a valid indicator of the surface roughness during the last part of the exposure periods for the silylated acrylate SPC coating. However, it could still represent a gentle hull cleaning in which minor impact to the surface is likely to occur. The biofouling attached to the FRCs, if present, was easily released from the surface, and significant changes to the surface roughness are not expected to result from the mechanical cleaning.

Table 4.4. Mean R_z and Rt(50) roughness values with one standard deviation at the newly applied condition, after 25 weeks' immersion with subsequent mechanical cleaning, and after 53 weeks' immersion with subsequent mechanical cleaning.

Coating condition	Roughness parameter	Hydrogel-based FRC (no biocides)	Fluorinated FRC	Hydrogel-based FRC with biocides	Silylated acrylate SPC coating
Newly applied	R_z [µm]	1.0 ± 0.6	0.8 ± 0.3	1.1 ± 0.3	8 ± 1
25 weeks (cleaned)	R_z [µm]	1.0 ± 0.3	0.8 ± 0.4	1.0 ± 0.4	12 ± 5
53 weeks (cleaned)	R_z [µm]	0.9 ± 0.4	1.0 ± 0.6	1.2 ± 0.4	16 ± 4
Newly applied	Rt(50) [µm]	46 ± 23	52 ± 25	39 ± 16	63 ± 21
25 weeks (cleaned)	Rt(50) [µm]	44 ± 20	74 ± 44	62 ± 28	81 ± 39
53 weeks (cleaned)	Rt(50) [µm]	67 ± 43	81 ± 57	59 ± 31	105 ± 79

Table 4.4 shows that the silylated acrylate SPC coating had significantly higher R_z roughness values than the three FRCs. Furthermore, the R_z roughness values remained fairly constant for the FRCs when comparing the measurements before and after exposure. The increase in R_z for the silylated acrylate SPC coating is assumed to be explained primarily by the mechanical cleaning process, as some material from the coating was removed. Compared to the FRCs, the much higher R_z roughness values of the silylated acrylate SPC coating, ranging approximately from a factor 8 to 18 did not translate into a significantly higher drag in the newly applied or mechanically cleaned coating condition. The drag performance of FCCs indicated by their R_z roughness values is, therefore, not an accurate predictor of their drag.

It was found that the average macro-roughness typically increased after the 25- and 53-week immersion period and subsequent mechanical cleaning. However, notice the large standard deviations leaving it doubtful whether the macro-roughness did increase significantly. The silylated acrylate SPC coating was much rougher than all of the FRCs, in the newly applied condition and after 25 and 53 weeks of seawater immersion followed by mechanical cleaning. There were some differences among the measurements of the FRCs. Candries and Atlar (2003a) questioned the validity of using the Rt(50) roughness as a means of estimating the drag performance of FCCs because their rotor and large-plate towing tank experiments did not correlate well with the measured drag and Rt(50) measurements. Candries et al.

(2001) found that a poorly applied FRC exhibited lower drag than an SPC coating, even though the FRC had a higher Rt(50) roughness. Thus, Candries et al. (2001) concluded that Rt(50) may not be a suitable parameter to adequately describe the roughness of FRCs. However, Weinell et al. (2003) found a relationship between drag and the roughness parameters R_z and Rt(50) by using a rotor setup, although only significant at tangential velocities above 25 knots. Flack et al. (2012) stated that drag due to surface roughness depends on many surface parameters, including roughness height, shape, and density. The present study, revealed a strong indication that neither of the two investigated surface height roughness parameters, i.e., Rt(50) and R_z, would be a valid parameter to describe the drag performance of FCCs. Even in the case of the much larger R_z roughness for the silylated acrylate SPC coating, there was no significant impact on the skin friction when compared to the FRCs, which had a much lower R_z roughness and a similar skin friction in the newly applied condition as well as after 25- and 53-week immersion periods followed by mechanical cleaning.

Contact angle

The contact angle was determined for the four FCCs with demineralized water and a plate beneath the coatings, which was heated to 22°C. The static contact angle was measured after 60 seconds, which allowed the single drop (sessile) of 6 µm to settle. Five measurements were carried out on two replicate samples of each FCC. A dry film thickness of approximately 150 µm was obtained on a glass substrate. Table 1.4 shows the average contact angle and the standard deviation. It is clear that the fluorinated FRC, hydrogel-based FRC with biocides, and silylated acrylate SPC coating have similar contact angles, while the hydrogel-based FRC without biocides had a much lower contact angle. The different contact angles reveal the existence of differences in the surface properties. The variations between the FRCs are believed to be due to primarily differences in the copolymer and biocide content. It should, however, be mentioned that the contact angles changed with time and, therefore, also the surface properties of the coating. Ideally, the contact angle should be determined from FCCs that have been exposed to seawater; it is important to classify the surface properties from coatings that have been immersed in water, since seawater exposed coatings are the surfaces biofouling encounters (besides the first short period right after out-

docking). Obviously, this is complicated to measure, as exposed FCCs would dry to some extent while measuring the contact angles, providing uncertainties from this parameter. The hydrogel-based FRC without biocides had a much lower contact angle than the other FCCs which was surprising due to the relatively similar composition. It was in particular surprising that it was much different than the similar hydrogel-based FRC with biocides.

Tensile strength

The tensile strength was measured in a Zwick tensile strength machine of the type Roel. It was only possible to measure the tensile strength of the FRCs due to their flexible nature, whereas the SPC coating did not have sufficient flexibility to be determined. The FRCs were left to cure for two days on a plastic film and afterward cut to fit the grips in the Zwick tensile strength machine. The width was three cm and the distance between the grips, which held the coatings, was 2.5 cm. The stretch velocity was 100 mm/min in a vertical direction. The maximum forces the FRCs exhibited were measured for 10 samples and are seen in Figure 1.4. The forces exhibited by the coatings varied, as they were stretched with the highest force usually obtained just prior to the FRCs breaking. The difference between the coatings was within one standard deviation; thus, distinction of the tensile strength between the FRCs was not possible. However, the FRCs should preferably be tested after exposure to seawater after sufficient time has passed to absorb seawater to saturation. In this way, the tensile strength of the FRCs during realistic exposure conditions can be determined.

Visual biofouling grading

The visual biofouling grading was ranked according to the classification system used by the U.S. Navy, i.e., Navy Ships' Technical Manual (NSTM) (Naval ship's technical manual, 2006) and the American Society for Testing Materials (ASTM) standard D3623 – 78A (ASTM D3623, 2012). The NSTM rating is useful because it provides a rough estimate of the increased shaft power due to biofouling for a larger ship. The impact on the total resistance for an Oliver Hazard Perry class frigate (FFG-7) from the NSTM rating is described by Schultz (2007). The ASTM standard D3623 (ASTM D3623) can be used to describe the biofouling rating of coatings immersed in shallow waters which therefore indirectly provides an FCCs capability of preventing increased surface friction due to biofouling attachment. The biofouling evaluation can be considered subjective, as it is based on individual judgment. Obvious

difficulties exist in estimating the degree of biofouling with the naked eye via thickness, coverage, and type, for example. However, the NSTM rating is considered capable of providing an approximate estimate of the FCCs' drag performance (Schultz, 2007). Table 5.4 shows predictions of the change in total resistance (ΔC_T) for an Oliver Hazard Perry class frigate (FFG-7) with a range of representative coating and biofouling conditions at speeds of 15 and 30 knots, as cited by Schultz (2007). It can be seen that the total resistance increases much when the biofouling rating increases.

Table 5.4. Predictions of the change in total resistance (ΔC_T) for an Oliver Hazard Perry class frigate (FFG-7) with a range of representative coating and biofouling conditions at speeds of 15 and 30 knots (Schultz, 2007).

Description of condition	NSTM rating	% ΔC_T @ U = 15 knots	% ΔC_T @ U = 30 knots
Hydraulically smooth surface	0	-	-
Typical as applied AF coating	0	2%	4%
Deteriorated coating or light slime	10-20	11%	10%
Heavy slime	30	20%	16%
Small calcareous fouling or weed	40-60	34%	25%
Medium calcareous fouling	70-80	52%	36%
Heavy calcareous fouling	90-100	80%	55%

Figure 9.4 provides the NSTM rating during the 53 weeks of seawater exposure. Note, however, that after November 13, 2013, the coatings received a mechanical cleaning with a soft wet cloth leaving the biofouling rating at zero when the FCCs were re-immersed on April 1, 2014. It was found that the fluorinated FRC quickly biofouled and remained higher than the other FCCs during the vast majority of the immersion period. The NSTM rating ranged between 10 and 20 during 2013, and it increased to 50 during 2014 for the fluorinated FRC. The silylated acrylate SPC coating quickly obtained a very thin slime layer, which remained practically constant throughout the remaining exposure period. The hydrogel-based FRC without biocides experienced some or limited biofouling. In 2013, the majority of the observations corresponded to zero, although there were a few observations of 10 and 20 NSTM ratings; in 2014, frequent NSTM ratings of 10 and 20 were detected, as well as a few ratings of zero. The hydrogel-based FRC with biocides experienced little or no visible biofouling until the middle part of the exposure period in 2014, at which time it did experience a minor coverage of thick slime (i.e., 2%-10% coverage), corresponding to an NSTM rating of 10.

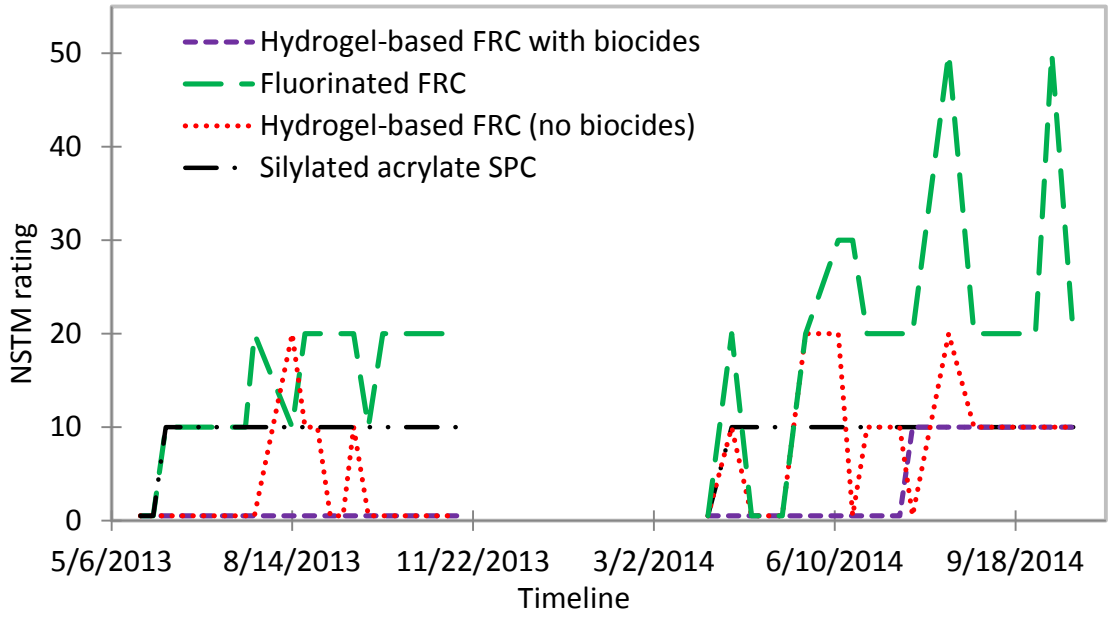

Figure 9.4. NSTM rating over 53 weeks of exposure. Mechanical cleaning occurred after November 13, 2013 leaving the FCCs clean before re-immersion on April 1, 2014.

Figure 10.4 shows the biofouling rating during the 53 weeks of seawater exposure according to the standard ASTM D3623 (ASTM D3623). The biofouling rating from ASTM D3623 (ASTM D3623, 2012) is given a value of 100 if completely free of biofouling, 95 if only incipient biofouling is present and 95 minus the percentage biofouling covering the surface with FCC. The biofouling found on the FCC cylinders was in the vast majority of cases slime and in a few instances some long seaweed (i.e., length of 1 to 10 cm and width of 0.1 to 0.3 mm) and young barnacles were observed on the fluorinated FRC. No mechanical damage was encountered on any of the FRCs which leaves the biofouling resistance identical to the overall performance according to ASTM D3623 (ASTM D3623, 2012).

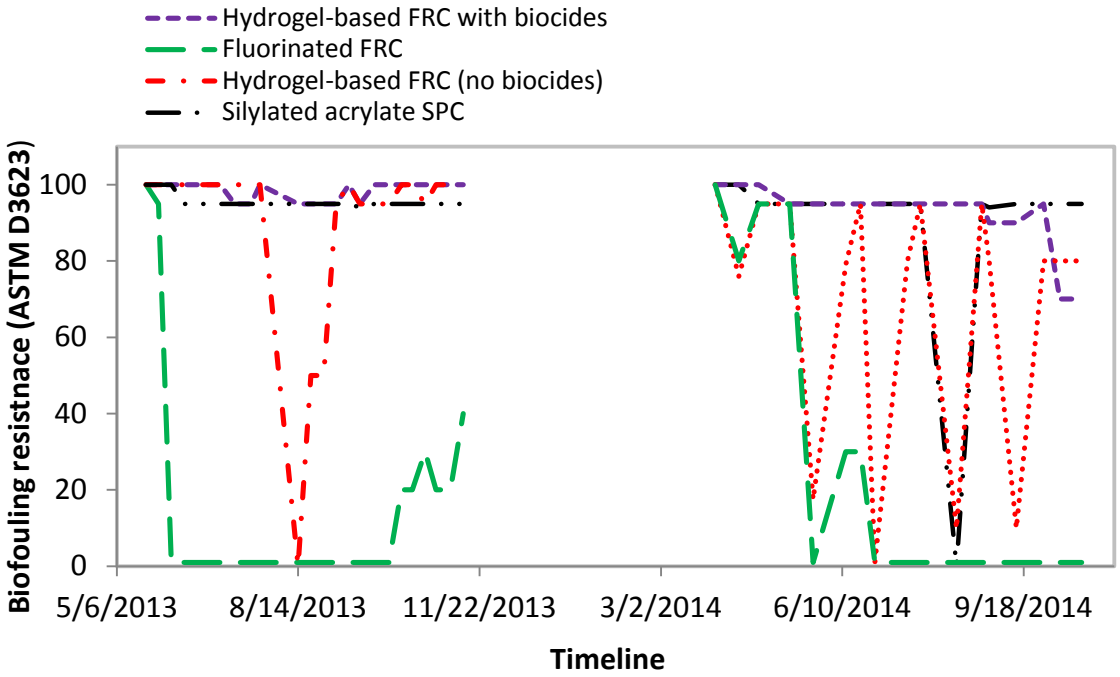

Figure 10.4. Fouling resistance rated via ASTM standard D3623 – 78a (ASTM D3623). Fouling resistance rating (0 to 100) is equivalent to biofouling coverage in percent. "0" indicates complete biofouling coverage and "100" no coverage.

Cushing (1975) stated that the algae activity for temperate waters has a major peak in the spring and a minor peak in the late summer. The trend of fast biofouling attachments primarily observed for the fluorinated FRC could, therefore, be due to a high biofouling upon the initial immersion (May 21, 2013), and a decrease in biofouling attachments by the end of 2013 could be due to the lower biofouling intensity during this period. The biofouling, however, remained more firmly attached at the end of 2014, which could be due to a slightly higher level of biofouling, making it more difficult to self-clean. Another cause may have been the loss of biofouling release properties, due to changes in the surface properties of the FRCs.

Drag performance of fouling control coatings

Newly applied coating condition

The drag performance of newly applied and unexposed FCCs only represents, at best, a very short period immediately after dry-docking. Furthermore, no indication of an FCC's ability to prevent or limit biofouling is provided when measuring the drag of newly applied coatings. It is well-known that biofouling can cause severe drag increase and, therefore, an FCC with low drag in newly applied and unexposed conditions can prove to be a poor choice if the coating

easily biofouls. Nonetheless, the newly applied drag performance serves as a viable tool to establish the expected best possible drag performance because the drag of FCCs typically increases with time, although this is not always the case and minor reductions can occur over time (e.g., Weinell et al., 2003).

The drag performances of the FCCs were measured prior to immersion in order to obtain the newly applied performance. The four FCCs exhibited similar drag performances, particularly at increasing speeds, when the uncertainty decreased. At a tangential velocity of 15.8 knots in the laboratory rotor, which corresponds to a ship speed of approximately 19.7 knots for a 100 m ship (Table 2.4) the skin friction coefficient was 5.7% higher for the fluorinated FRC, 4.4% higher for the silylated acrylate-based SPC coating, and 1.3% higher for the hydrogel-based FRC without biocides, when compared to the hydrogel-based FRC containing biocides. Lindholdt et al. (2015a) measured a smaller and insignificant difference in drag between three of the coatings investigated in this study, i.e., a fluorinated FRC, a hydrogel-based FRC without biocides, and a hydrogel-based FRC with biocides, as opposed to the significant difference found in this study. Figure 11.4 illustrates the skin friction coefficients for tangential velocities ranging from 6.3 to 15.8 knots.

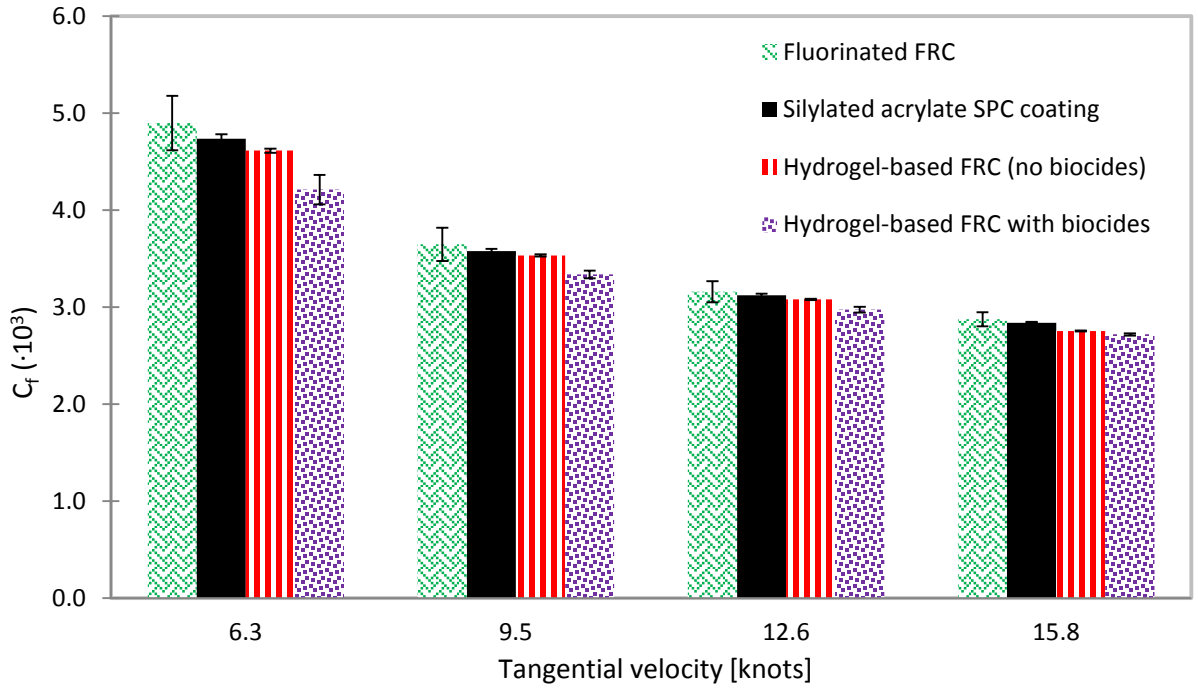

Figure 11.4. Newly applied skin friction coefficients revealing small differences between the FCCs in their newly applied conditions.

Mechanically cleaned coating condition

Figure 12.4 and 13.4 display the skin friction coefficients of the mechanically cleaned coatings after 25 and 53 weeks, respectively. The drag measurements in the mechanically cleaned condition revealed that the differences in drag were smaller than the experimental uncertainty at the higher tangential velocities. It is well-known that, when immersed in seawater, FCCs typically absorb water, which is particularly true for hydrogel-based coatings. Therefore, the mechanically cleaned condition is likely to offer a more accurate representation of the FCC condition relevant for a ship free of biofouling better, as compared to the newly applied condition, where the coating has not been immersed in seawater. The average roughness parameters R_z and Rt(50) were slightly higher for the mechanically cleaned condition compared to the newly applied coating condition, although in most cases within the standard deviation. This increase in roughness would have been expected to result in a slightly higher drag, although a minor decrease was found for the mechanically cleaned coating condition. In short, the differences in the mechanically cleaned conditions were smaller than the experimental uncertainty when the FCCs were tested after 25 weeks; thus, no significant distinction between the FCC drag performances could be made in the clean condition.

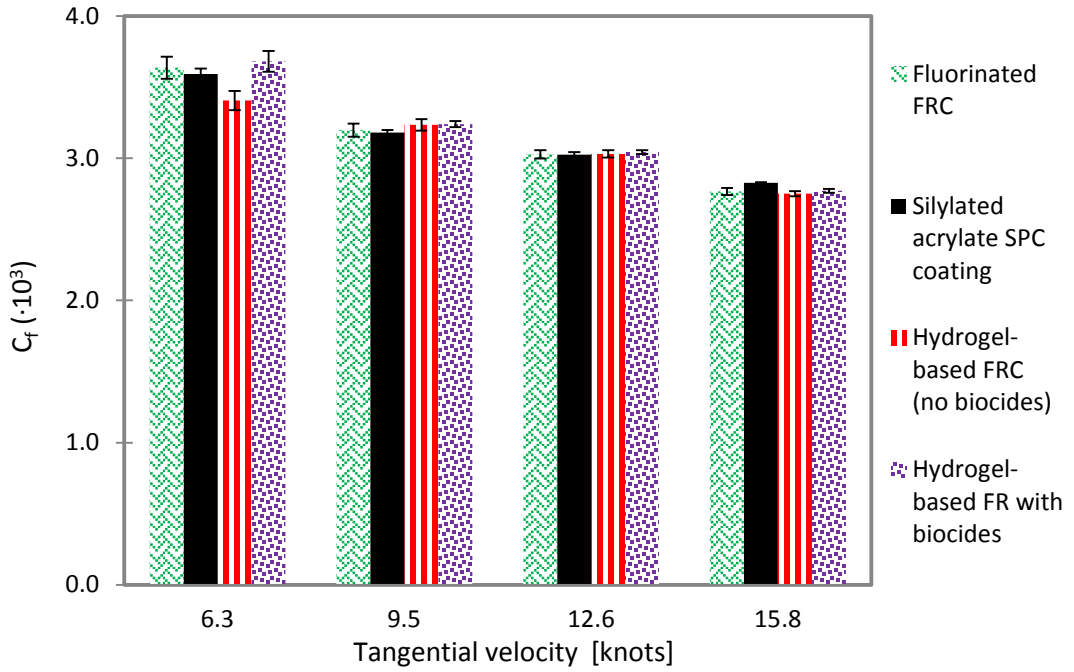

Figure 12.4. Skin friction coefficients for mechanically cleaned FCCs after 25 weeks of seawater exposure.

Figure 13.4 shows the skin friction coefficients after 53 weeks of seawater exposure and mechanical cleaning, confirming the similarity in performance of the FCCs in this condition. Notice that the C_f values are slightly lower in Figure 13.4 compared to the values in Figure 12.4. This could be due to uptake of seawater by the coatings, which apparently causes some levelling of the surfaces over time. This was also partly found by Lindholdt et al. (2015a).

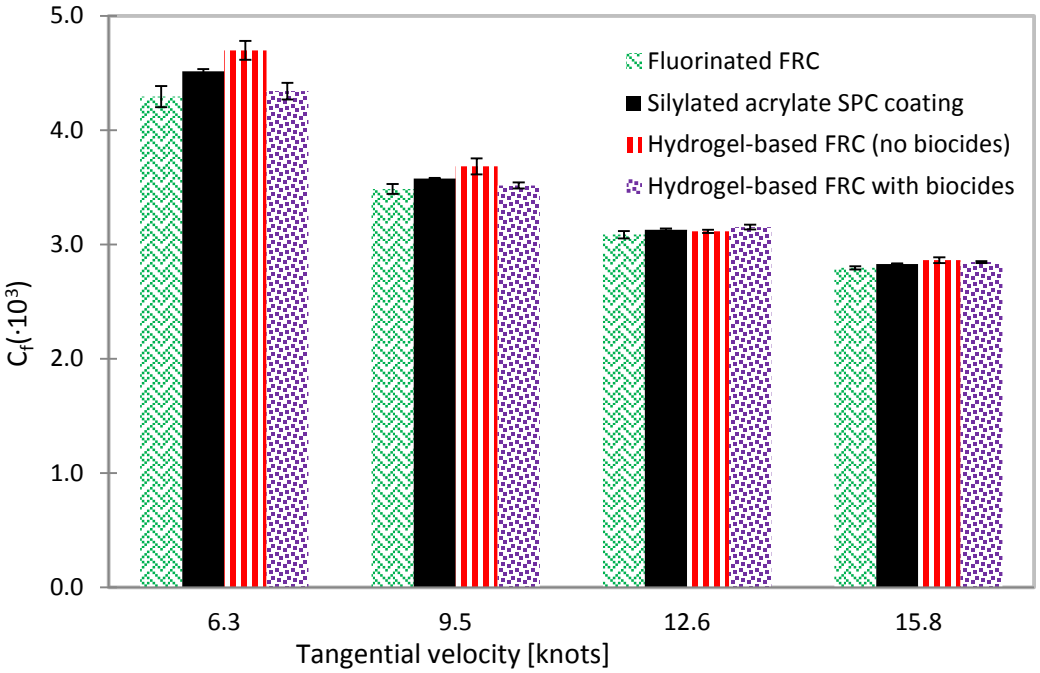

Figure 13.4. Skin friction coefficients for mechanically cleaned FCCs after 53 weeks of seawater exposure.

Long-term drag performance evaluation

One of the major challenges regarding the determination of the drag performance of FCCs is creating a method to predict and accurately measure the long-term performance in conditions that simulate those experienced by ocean-going ships. Figure 14.4 shows the average skin friction coefficients for tangential laboratory rotor velocities of 9.5, 12.6 and 15.8 knots from the second run, i.e., those corresponding to well-attached biofouling, over the course of 53 weeks. The latter mentioned rotor velocities were chosen as they represent a velocity range widely used by a large part of the commercial fleet. The measurements from the second run are shown because they are more applicable to moving ships, since most of the loosely attached biofouling, if present, is assumed to have been released during the first run. The data from May 21, 2013 represent the newly applied condition prior to immersion, while the subsequent measurements were carried out after two weeks of static immersion and then after three weeks of dynamic immersion for the remaining exposure period. The drag was measured after mechanical cleaning after November 13, 2013 and again on October 22, 2014. Below the experimental values in Figure 14.4, a letter indicates the exposure condition which had taken place prior to the drag measurements: N represents the newly applied condition, S represents the static immersion condition, D represents the dynamic exposure condition, and C the mechanically cleaned condition. It is seen that the

hydrogel-based FRC without biocides, the silylated acrylate SPC coating, and the hydrogel-based FRC containing biocides had similar skin friction throughout the entire exposure period, with values often within the experimental uncertainty. The fluorinated FRC, on the other hand, had a much higher skin friction when measured after the static immersion periods in 2013 and after the initial part of the exposure periods in 2014 it was significantly higher, irrespective of the exposure condition being static or dynamic. This reveals that the fluorinated FRC had sufficient biofouling release properties during 2013 to return to a skin friction similar to the newly applied condition, when dynamically exposed. However, it showed inferior biofouling prevention properties, especially pronounced during static immersion, which lead to increased skin friction. When comparing the skin friction of the four FCC systems after dynamic aging had taken place during 2013, the difference was small and often within experimental uncertainty. Evaluation of the four FCCs during 2014 revealed small differences in drag, besides for the fluorinated FRC. The results reveal the performance of the coatings applied to a ship traveling 3 out of 5 weeks and being idle for the remaining two weeks in waters similar to those at Roskilde Fjord. Furthermore, the results show that the immersion condition impacted the resulting skin friction significantly, revealing the need for immersion conditions representative of traveling ship patterns, rather than the typical approach of static immersion followed by drag measurements. The biofouling rating of the four FCCs provided in Figure 10.4 revealed varying ratings throughout the season with values ranging from zero to 100. The biofouling rating and increased total resistance noted in Table 5.4 reports an increased total resistance due to biofouling ranging from 2% to 34% in the case of an Oliver Hazard Perry class frigate moving at 15 knots. When comparing the skin friction coefficients and the biofouling rating, a qualitative correlation was found, although minor changes in the skin friction were not consistently reported along with a higher biofouling rating. The visual biofouling rating is, therefore, useful when aiming at an evaluation of an approximate increase in resistance, but providing an accurate estimate of the drag based solely on visual inspection is, indeed, complicated.

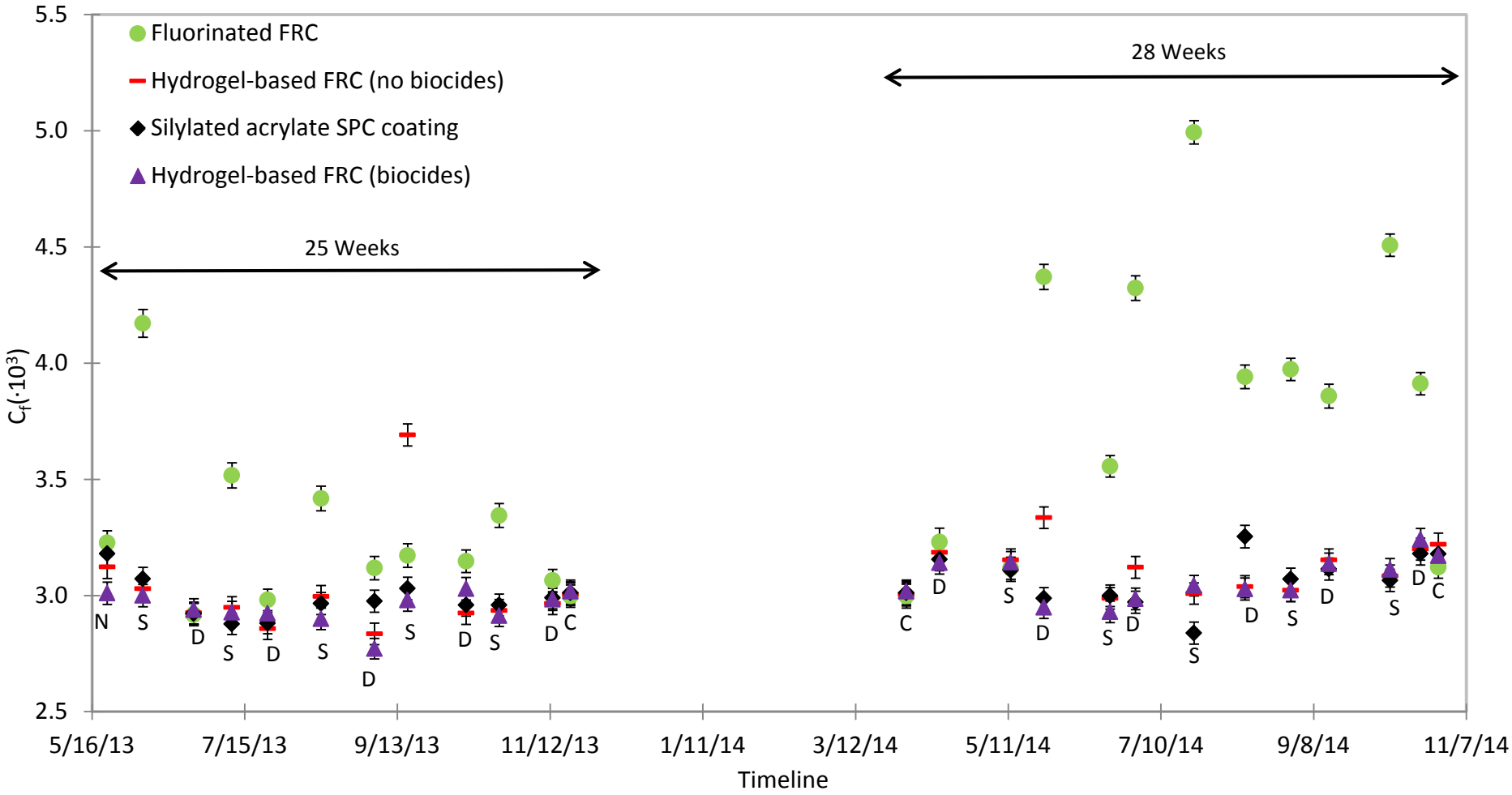

Figure 14.4. Skin friction coefficients in the newly applied condition (May 21, 2013), long-term condition (from May 22, 2013 to November 13, 2013 and from April 1, 2014 to October 22, 2014) and mechanically cleaned condition (shown as values at November 20, 2013 and October 30, 2014). The long-term average skin friction coefficients are based on tangential rotor velocities of 9.5 to 15.8 knots from the second runs. The measurement points with an N below them represent the newly applied condition, those with an S represent the static immersion condition, those with a D represent the dynamic exposure condition, and those with a C represent the mechanically cleaned condition.

Figure 15.4 shows the average skin friction coefficients for the entire 53-weeks exposure (i.e., 25 data points for each FCC), whereas Figure 14.4 showed the skin friction coefficients at the various investigated dates. Clearly, the difference between the best performing FCCs is small. The average difference, relative to the best performing FCC (i.e., the hydrogel-based FRC with biocides) based on the three highest tangential velocities, where the measurement uncertainty is lowest, was 17.7% for the fluorinated FRC, 1.2% for the hydrogel-based FRC, and 0.6% for the silylated acrylate SPC coating. The two hydrogel-based FRCs and silylated acrylate SPC coating performed within the experimental uncertainty.

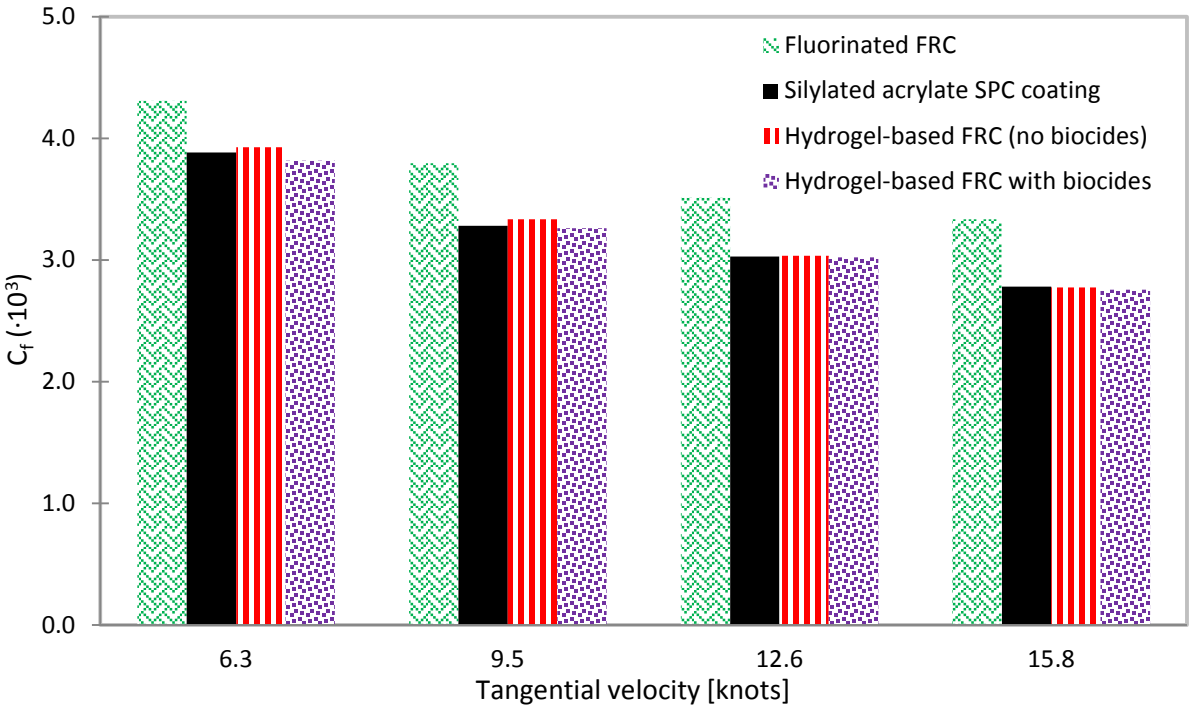

Figure 15.4. The average skin friction coefficients based on the entire 53-weeks exposure period (i.e., 25 data points for each FCC) at the investigated tangential rotor velocities.

The fluorinated FRC was by far the coating most prone to biofouling attachment. The impact of skin friction (i.e., biofouling on the FCC), exposure conditions (i.e., static or dynamic) and measurement conditions (i.e., 1. or 2. run) are, therefore, more relevant to study for this coating, as opposed to the other fairly clean FCCs. Figure 16.4 provides the average skin friction coefficients of the fluorinated FRC for the tangential velocity range of 9.5 to 15.8 knots for the first and second runs. The skin friction coefficients were often lower for the second run, which is explained by the release of biofouling. In most cases, the difference was significant when static immersion occurred prior to the drag measurements, while mainly insignificant when dynamic immersion occurred prior to the drag measurements. This

reveals that even though the dynamic aging was operated at 8.1 knots and the laboratory rotor operated up to 15.8 knots, a significant release of biofouling did not occur at the higher tangential velocities if dynamic aging had occurred beforehand.

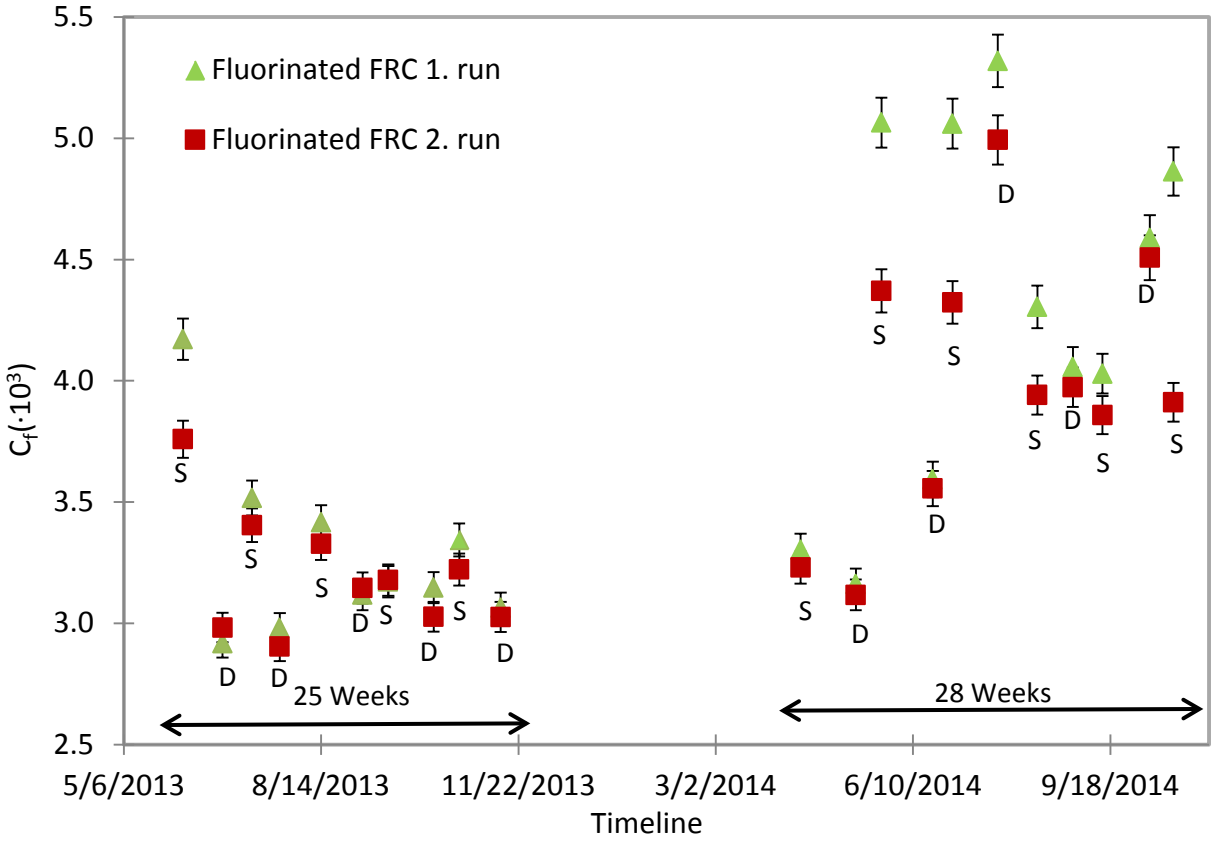

Figure 16.4. Average skin friction coefficients for tangential rotor velocities of 9.5 to 15.8 knots during the 53-week immersion period from the first and second runs for the fluorinated FRC. S and D represent the static and dynamic immersion periods, respectively, prior to the drag measurements.

Table 6.4 shows the differences in the average skin friction coefficients at tangential laboratory rotor velocities of 9.5, 12.6, and 15.8 knots for the four investigated FCCs during the entire exposure period, including the values for the mechanically cleaned conditions. The average differences in the skin friction coefficients between the first and second runs of drag measurement are also shown; this data indicate that some biofouling was released, as the skin friction coefficients decreased between the first and second run. The results from the first run indicate the capability of an FCC to resist and release biofouling, while results of the second run primarily provide the drag of well-attached biofouling, which could be expected on a moving ship. The small difference in the skin friction coefficient for the hydrogel-based

FRC containing biocides is explained by the fact that almost no biofouling attached during the 53 weeks of exposure.

Table 6.4. Average skin frictions coefficients for tangential rotor velocities of 9.5, 12.6 and 15.8 knots during the 53-week immersion period, and the differences between measurements of the first and second run.

	Average skin friction coefficient for 9.5 to 15.8 knots during the 53-weeks immersion period		
FCC system	C_f ($\cdot 10^3$) 1. run	C_f ($\cdot 10^3$) 2. run	ΔC_f between 1. and 2. run (%)
Fluorinated FRC	3.73	3.55	4.95%
Hydrogel-based FRC	3.12	3.05	2.32%
Silylated acrylate SPC	3.08	3.03	1.74%
Hydrogel-based FRC with biocide	3.02	3.01	0.13%

As a potential way to improve the long-term setup it was considered to install a torque sensor on the aging setup to avoid the regular detachment of cylinders and obtain in situ measurements. In this case the main gain would be continuous measurements and, therefore, potentially a more detailed knowledge of the development of the FCCs' drag over time. However, extra effects from changes in bearing resistance and biofouling attachment on the top and bottom of the cylinder and shaft would be difficult to extract from the measurements, causing uncertainties that are minimized with the land-based rotor setup. The change in friction of the bearings is expected to vary significantly over time due to wear from a continuous use and the presence in a highly corrosive seawater environment (including seawater splashes), compared to the well-protected and less used land-based laboratory rotor setup. Furthermore, although the aging setup was located in a fairly well-protected location, waves and currents are expected to impact the measurements. The much higher economic cost of installing four torque sensors, which can be expected to have a limited life-time in the highly corrosive marine environment, should also be mentioned.

Fuel and power predictions for a tanker

In this section, an illustrative example of fuel and power predictions for a medium sized tanker, i.e., Tarantella (Shipyard Trogir, 2014), is presented. Based on the skin friction coefficients estimated from the laboratory rotor, the power consumption from Tarantella at various velocities and the fuel consumption based on its normal operating speed are estimated. Tarantella has a length between each perpendicular of 176 m, a draught design of 11 m, and a breadth of 32 m, i.e., a wetted surface area of approximately 9540 m^2.

Tarantella has a typical operating speed of 14 knots, which results in a fuel consumption of 30 tons per day when the hull is free of biofouling (Shipyard Trogir, 2014). Figure 17.4 displays the power consumption due to skin friction in the mechanically cleaned condition after 25 weeks (i.e., average of the four FCCs in the mechanically cleaned condition) and for the four investigated FCCs based the average values during the 53 weeks of exposure (see Figure 15.4). Equation 16.4 was used to determine the power consumption due to skin friction based on a seawater density of 1025 kg/m^3 and the laboratory rotor skin friction coefficients. Tangential rotor velocities of 6.3, 9.5, 12.8 and 15.8 knots correspond to ship velocities for the investigated ship of 8.30, 12.35, 16.38 and 20.25 knots, with a kinematic seawater viscosity at 10°C (i.e., 1.37 m^2/s).

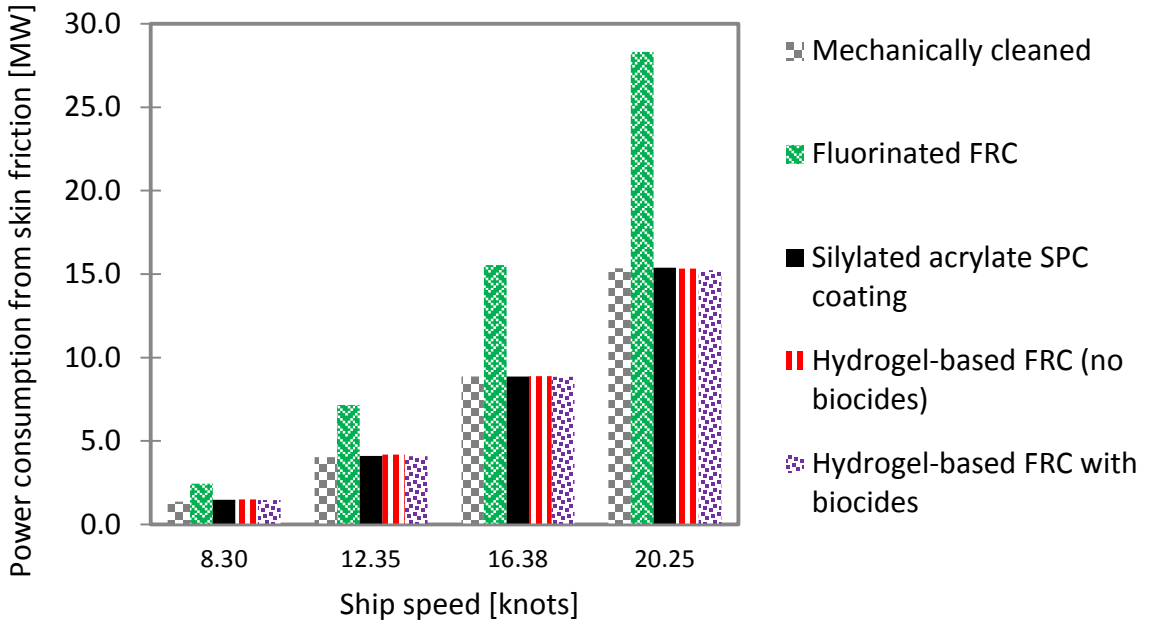

Figure 17.4. Power consumption due to skin friction in the mechanically cleaned condition after 25 weeks of exposure, and the average skin friction from 53 weeks of seawater exposure for the investigated FCCs.

Figure 17.4 reveals that there are very small differences in power consumption for the investigated FCCs, besides the fluorinated FRC. The increase in fuel consumption for the fluorinated FRC resulted in an increase of 5.1 tons per day compared to the clean condition when operated at 14 knots. This is based on the assumption that the skin friction is responsible for 70% of the total resistance (e.g., MAN Diesel & Turbo (2011)) and, therefore, also fuel consumption. With an assumed operating activity of 80% at typical speed (14 knots) and an oil price of $500 USD per ton of bunker oil, an additional yearly fuel expense for Tarantella would be $0.75 million USD.

The visual biofouling rating for the fluorinated FRC during the 53-weeks exposure period ranged between 0 and 50; the majority of the ratings being either 10 or 20, which according to Schultz (2007) would result in increase of 11% and 20% in total resistance for an Oliver Hazard Perry class frigate. The increase in skin friction of the fluorinated FCC compared to newly applied condition when evaluated over the entire 53-weeks exposure period was approximately 18%. Assuming that the frictional contribution to the total resistance of the investigated ship is 70%, a total increase in resistance will then be approximately 26%. With an increase of this order for the frigate, the predictions by Schultz (2007) would be a biofouling rating of 20 to 30, which matches well with biofouling observations on the fluorinated FRC cylinder. This shows that the biofouling rating can be used to obtain a first approximate estimate of the biofuling impact on the total resistance and, therefore, also on the fuel consumption. However, the laboratory drag measurements provided a much higher accuracy and less uncertainty than the visual biofouling evaluation.

Conclusions

This study employed a setup to systematically study the drag performance of FCCs over time in the presence of biofouling species (i.e., natural seawater) at typical speeds and activity conditions for larger commercial ships. Only small and often insignificant differences in the drag performance between a hydrogel-based FRC containing biocides, a hydrogel-based FRC without biocides, and a silylated acrylate SPC coating were found over a period of 53 weeks with seawater exposure. The fluorinated FRC showed a drag performance similar to the other FCCs when evaluated in the newly applied condition and in the mechanically cleaned condition. However, it became biofouled after approximately two weeks, and remained so with varying degrees throughout the entire exposure periods, which resulted in a significantly higher drag during the majority of the exposure period. The three other FCCs only had limited biofouling attachment, and the newly applied drag performance was, therefore, similar to that found during the 53-weeks exposure period. As the three best performing FCCs hardly changed over the period of one year it is suggested that future drag measurements can be carried out with less frequent intervals, e.g., every two or three months. If, however, significant changes in the level of biofouling are observed via regular

inspection, e.g., every two or three weeks, then drag measurements are recommended. For a coating with substantial changes in drag over shorter time, which was the case for the fluorinated FRC, frequent drag measurements (e.g., every two or three weeks) are recommended. The best performing coating was the FRC with biocides incorporated. It is believed that it primarily was the biocide release of this hydrogel-based FRC which outperformed the other hydrogel-based FRC without biocides as their copolymer content and type were similar. The fluorinated FRC primarily differed in copolymer additives, which is believed to be the primary reason for the much worse performance compared to the hydrogel-based FRCs without biocides. The SPC coating operates with a very different biofouling prevention method to the FRCs making a direct comparison between the biofouling prevention methods complicated, but the SPC coating was found to perform at a similar level of the two hydrogel-based FRCs.

Since biofouling will likely occur at some time during the service life of an FCC, the newly applied drag performance and any related roughness parameters are poor indicators of the long-term drag performance. However, if an FCC remains free of biofouling, the drag in the newly applied condition can be a valid indicator of the drag performance, even long after coating application. The need for simulating exposure conditions similar to those of ocean-going ships was shown. Static immersion, which often does not represent larger commercial ships, but is widely used to characterize the performance of FCCs, often resulted in a significantly higher drag, compared to the dynamic immersion periods.

Chapter 5 – Comparison of studies from the friction disk machine and the rotor setups

Four different FCCs were used in the experiments conducted with the FDM and the rotor setups: a hydrogel-based FCC with biocides incorporated, a hydrogel-based FRC without biocides, a fluorinated FRC, and a silylated acrylate SPC coating. Even though the top-coats were identical, a number of differences existed between each of the FCCs used in the experiments with the FDM and the rotor setups. These are outlined in Table 1.5. The FDM was used for the static exposure study due to the ease of cleaning the backside, which was touching the raft during exposure. Furthermore, due to the flat geometry, a more even biofouling attachment was believed to occur during static immersion for a disk, as opposed to the cylindrical shape of a cylinder. In addition, it was of interest to investigate the roughness profile in detail, as it was believed that a flat geometry (disk) would replicate a hull's shape better than a cylinder. The rotor setup was chosen for the exposure condition, consisting of cycles with dynamic and static exposure. The cylindrical shape was believed to create a more random flow than that over a rotating disk surface, thereby preventing biofouling patterns unrepresentative for a hull during a voyage. In Figure 1.5, a distinct biofouling pattern from the bottom of the cylinder (disk shape) is seen. A more random biofouling pattern was observed on the sides of the cylinders, with no apparent pattern, which therefore, is believed to replicate the biofouling conditions on a voyaging hull better than a disk would. The biofouling pattern on a disk after dynamic immersion could be a poor representative of a hull with biofouling for a voyaging ship and could potentially lower the surface friction, due to the biofouling patterns in comparison to a disk with more random biofouling.

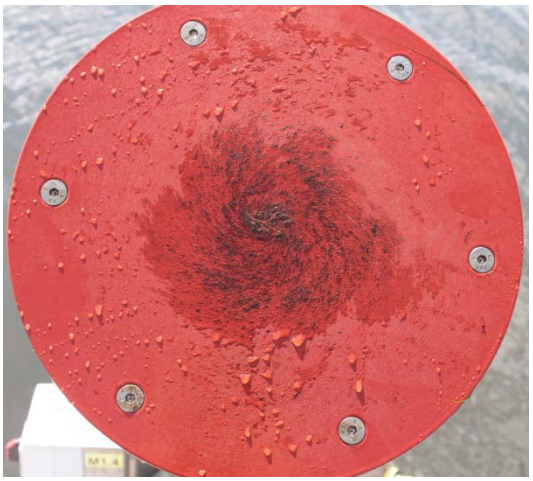

Figure 1.5. Biofouling pattern observed at bottom of cylinder.

Table 1.5. Comparison of the FDM and rotor setup experiments, including measurement setup, coating systems, immersion conditions, surface characterization, and experimental uncertainty.

Experiment	FDM	Rotor setup
Geometry of coated object	Disk	Cylinder
Dry film thickness of top-coat	Identical for both experiments	
Top-coat	Backside and edge were all coated with the hydrogel-based FRC with biocides. The coating that was investigated was applied on the top.	The two lids attached to the cylinders during immersion had the hydrogel-based FRC without biocides applied. The coating that was investigated was applied to the side of the cylinder.
Coating below the top-coat	Commercial epoxy primer in two layers, with a final DFT of approximately 200 µm. Commercial tie-coat products with a DFT of approximately 100 µm.	The tie-coat applied to the disks was used as a primer on the cylinders, i.e., no tie-coat and only primer below top-coat.
Substrate	Aluminum	PVC
Immersion periods	Period 1: June 6, 2013 to July 8, 2013 (i.e., 31 days). Period 2: July 16, 2013 to October 6, 2013 (i.e., 82 days). A total of 113 days' immersion (≈16 weeks).	Period 1: May 21, 2013 to November 13, 2013 (25 weeks) Period 2: April 1, 2014 to October 22, 2014 (28 weeks) A total immersion of 53 weeks.
Mechanical cleaning	Prior to immersion of the 2. Period (July 16, 2013)	Prior to immersion of the 2. Period (31 March, 2014)
Immersion method	Static	Alternating static and dynamic immersion consisting of 2 weeks' static immersion followed by 3 weeks' dynamic immersion.
Geographical location of immersion site	Harbor of Den Helder, the Netherlands	Roskilde Fjord, Denmark
Approximate temperature at immersion site during immersion	15°C to 21°C (Klijnstra, 2014)	5°C to 25°C
Salinity at immersion site during exposure period	2.65 wt% to 2.94 wt% (Klijnstra, 2014)	1.2 wt% (Pedersen, 2010)
Immersion depth below water level	Approximately 30 cm to 50 cm	10 cm to 40 cm (from top to bottom of cylinder
Surface characterization method	Laser profilometry was used to measure the surface roughness and waviness parameters of the newly applied FCC. An area of 50 mm x 45 mm (i.e., 22.5 cm^2) was evaluated on every disk. The applied cut-off length was 0.8 mm.	R_z roughness with a sampling length of 0.8 cm and Rt(50) roughness.
Size	Radius of 11.45 cm and a height ranging from 0.6 to 0.7 cm (depending on the thickness of the substrate and the paint system).	Diameter and height of 30 cm

Estimated experimental uncertainty	0.42% at 1500 RPM (see Table 1.3 for the remaining RPMs)	1.08% at 500 RPM

It is imperative to compare the results obtained from the two studies, in order to identify similarities and differences due to the different exposure conditions and measurement setups. Table 2.5 shows the ranking based on the measurements made with the FDM and rotor setup, with respect to drag performance in the newly applied coating condition and after exposure. It is seen that the drag ranking is generally in agreement between the methods, which could justify that static performance could be used to rank the drag performance of top-coats for voyaging ships to a fair degree. However, the difference in absolute performance is not seen from the ranking. For instance, the fluorinated FRC was, by far, the worst coating, with respect to drag performance after static immersion (measured with FDM) and also after static and dynamic immersion cycles (measured with rotor setup). However, the absolute change in drag when compared to the newly applied condition was much larger after static immersion as opposed to cycles of static and dynamic immersion.

Table 2.5. Ranking of drag performance of FCCs from the second run, based on the average torque coefficient values measured at the three highest Reynolds numbers. The ranking is based on "1" representing the *best performance* (lowest drag) and, with decreasing performance, "4" representing the *worst performance* (highest drag).

Top-coat	Hydrogel-based FRC with biocides	Hydrogel-based FRC without biocides	Silylated acrylate SPC	Fluorinated FRC
Newly applied condition based on the FDM measurements	1-4	1-4	1-4	1-4
Newly applied condition based on the rotor setup measurements	1	2-4	2-4	2-4
1. exposure period (i.e., July 8, 2013) period, based on the FDM measurements	1-2	1-2	3	4
Average ranking during 1. exposure period (i.e., May 21, 2014 to October 22, 2014) period, based on the rotor setup measurements	1	2	3	4
2. Exposure period (i.e., October 6, 2013), based on the FDM measurements	1-2	1-2	3	-
Average ranking during 2. exposure period (i.e., April 1, 2014 to October 22, 2014), based on the rotor setup measurements	1	3	2	4

Table 3.5 provides the biofouling rating, according to ASTM D3623 (ASTM D3623, 2012), for the static immersion study and the study with cycles of dynamic and static immersion, as well as a description of the type of biofouling. It was found that one month of static immersion resulted in a much more severe biofouling rating, compared to the average biofouling rating for exposure to dynamic and static immersion. It is believed that the static immersion is significantly worse with respect to biofouling attachment and, therefore, primarily responsible for the differences in the biofouling rating of the experiments. However, differences in the geometry of coated objects, temperature, salinity, and other local seawater conditions could also be important factors responsible for differences observed in the biofouling development.

Table 3.5. Biofouling rating, according to ASTM D3623 (ASTM D3623, 2012), for the static immersion study and the study with cycles of dynamic and static immersion, with a description of the type of biofouling.

Type of study	Static immersion	Dynamic and static immersion
Geometry	Disk	Cylinder
Exposure condition	Static immersion	Cycles of dynamic and static immersion
Location	Harbor of Den Helder, the Netherlands	Roskilde Fjord, Denmark
Top-coat/biofouling rating	Biofouling rating according to ASTM D3623 after one month of immersion	Average biofouling rating according to ASTM D3623 during the entire immersion period
Silylated acrylate SPC coating	0 (80% medium thick slime and 20% diatoms)	93 (mainly very limited slime)
Fluorinated FRC	0 (60% medium thick slime, 10% barnacles and 30% young barnacles)	21 (mainly thin and thick slime, with shorter periods of long seaweed and young barnacles)
Hydrogel-based FRC without biocides	67 (30% very thin slime and 3% barnacles)	82 (mainly clean and in some shorter periods thin slime)
Hydrogel-based FRC with biocides	45 (50% very thin slime 5% diatoms)	96 (mainly clean and in some shorter periods minor thin and/or thick slime)

Chapter 6 – Conclusions and further work

Conclusions

A systematic overview of the literature and description of the experimental methods used to quantify the drag of FCCs has been made, revealing the need for drag performance test methods that more closely resemble the exposure conditions that larger commercial ships typically encounter during actual voyages. It was determined that the drag performance of FCCs varies depending on whether the FCC coating is newly applied, has received dynamic exposure, or has received static seawater exposure. Most commonly, drag measurements are performed for newly applied coatings and after static exposure. This approach is limited because only the drag performance during idle periods can be feasibly predicted, leaving the drag performance uncertain for ships that are primarily moving. However, the static exposure test method does have an advantage in its severity, as more biofouling is expected to attach during static immersion than during dynamic immersion. Thus, drag measurements based on the static immersion can realistically be viewed as the worst exposure conditions. Significant differences in the drag performances of FCCs will typically occur faster when the coatings are statically immersed as opposed to dynamically exposed, but the biofouling release properties, which are crucial for some FCCs, are, to a large extent, neglected during static immersion.

In an experimental study, five FCCs in a newly applied coating condition was applied on completely smooth substrates, which revealed a small difference in drag and, in most cases, one that was less than the experimental uncertainty. After one month of static immersion, a significant difference was detected for some of the FCCs. The hydrogel-based FRC with biocides had the lowest friction, while the fluorinated FRC had the highest friction. The hydrogel-based FRC without biocides and the two SPC coatings showed intermediate performances. After 3.5 months of static immersion, the hydrogel-based FRCs showed superior drag performance, compared to the SPC coatings. Static immersion after 3.5 months was sufficient to distinguish the superior drag performance of the FCCs, although performances in realistic (i.e., primarily dynamic exposure) conditions are still uncertain. Two FCC systems, i.e., a hydrogel-based FRC with biocides and a silylated acrylate SPC

coating, were tested in their newly applied condition with various substrate roughness (i.e., roughness below coatings) values. Increased substrate roughness led to increased drag for both FCC systems, but the FRC was impacted less by the higher substrate roughness than the SPC coating. The substrate roughness is therefore of importance in drag performance and must be accounted for when evaluating drag performance of FCCs. The FRC with biocides incorporated showed in the static exposure study to be of similar drag performance in the newly applied condition, but was capable of limiting the biofouling more than the other FCCs when exposed statically. The biocides incorporated in the FRC is believed to provide an extra defense mechanism against biofouling which is particularly useful during idle periods for FCCs due the lack of self-cleaning from water flowing over the surface.

A setup capable of exposing coatings to realistic exposure conditions, as opposed to only static immersion, was applied to four commercial FCCs, which were exposed via ocean-placed rotor setups for 53 weeks in Roskilde Fjord, Denmark, i.e., in relatively cold seawater (salinity 1.2 wt%), from the spring of 2013 to the autumn of 2014. It was found that the skin friction generally increased more during the static periods, compared to the dynamic ones. Furthermore, with regard to the entire exposure period, it was found that the skin friction of the investigated FCCs decreased in the following order: fluorinated FRC (highest skin friction), hydrogel-based FRC without biocides, silylated acrylate SPC coating, and hydrogel-based FRC with biocides (lowest skin friction). However, the differences in skin friction between the latter three coatings were found to be small and often within the experimental uncertainty. After 25 weeks of immersion and mechanical cleaning, the differences in skin friction were, on average, less than 1%, i.e., within the experimental uncertainty, for velocities relevant for larger commercial ships. The hull roughness parameters, determined as the Rt(50) and R_z parameters, were found to be poor predictors of the drag. From the cycles of dynamic and static immersion there was a clear tendency throughout the periods with highest biofouling pressure (i.e., late spring and summer period) that both the biofouling level and drag increased more during static immersion compared to dynamic immersion. Despite the drag performance ranking typically did not change when comparing dynamic and static immersion the absolute difference in drag performance became much less after dynamic immersion. It is therefore important to assess FCCs under realistic

exposure conditions if a fair estimate of the absolute drag difference between FCCs shall be credible. Furthermore, the long exposure period did for three out of four quality top-coat products not yield a substantial increase in drag, i.e., typically less than 2% compared to the newly applied condition. The importance of determining the drag performance in realistic exposure condition over a long period and ideally until a full dry-dock period is completed was found to be recommendable because the drag performance could not be revealed exactly by either the initial performance or from a short-term study for the fluorinated FRC which received the most biofouling. The varying performance over time of the season and exposure conditions were found to influence the drag performance, although only to a minor degree for the hydrogel-based coatings and SPC coating, leaving it necessary to investigate the FCC drag performance in the time period which it would be used until recoated. A long-term exposure would provide an accurate estimate of the absolute difference in drag performance.

The measurements from the rotor setup and FDM showed that, to a large extent, there was accordance with the drag performance ranking. However, there was a large difference in the absolute drag performance, which is believed to be due to the different exposure conditions, in the form of static immersion and cycles of dynamic and static immersion, and to the differing substrate material, salinity, and temperature of seawater. By comparing the studies, it was found that the static immersion study, in this case, could be used to obtain a fairly accurate drag performance ranking, but the absolute difference in drag performance was uncertain for voyaging ships and more accurately provided by the rotor setup.

Further work

The literature review and long-term rotary drag performance study revealed the need for FCCs to be aged in conditions similar to those experienced by the commercial fleet. Although such a method was developed and proved capable of determining the long-term drag performance of FCCs, improvements in the developed rotary setup could further strengthen the long-term drag performance determination. The developed setup has four cylinders and is therefore only capable of resembling one traveling pattern, if four different FCCs are to be compared under the same conditions. Ideally, it would be useful to simulate more traveling

patterns in order to determine the optimal FCC with respect to drag performance for different traveling patterns that might be applicable to various generic ship classes. This could, for instance, be accomplished by employing a total of 12 cylinders. 8 static cylinders setups could be installed on the present raft, without increasing the cost of the raft much. Four FCC cylinders could be statically immersed. The other 8 cylinders would switch from static to dynamic immersion on the raft. In this way, the four rotating cylinder setups could be utilized all the time, instead of only 60% of the time, as they were for the experiments described in Lindholdt et al. (2015b). The following test series of activities for four different FCCs is suggested, using four rotating cylinder setups and 8 static immersion setups:

- 4 FCCs with 100% static immersion,
- 4 FCCs with 70% static immersion and 30% dynamic immersion, and
- 4 FCCs with 70% dynamic immersion and 30% static immersion.

The static immersion would likely represent the worst exposure conditions (Lindholdt et al., 2015b). It would, however, also represent a minor part of the industrial fleet, such as floating petroleum storage off-loading (FPSO) units and pleasure boats. The traveling pattern, with 70% static immersion and 30% dynamic immersion, would represent naval ships, for instance, as they have a fairly low activity. The high activity, consisting of 70% dynamic immersion and 30% static immersion, would adequately represent the majority of the larger industrial fleet, such as container ships, bulk carriers, roll on–roll off (ro-ro) ships, cruise ships, tankers, and passenger ships. However, there is some variation in both the activity and operating speed of these ships. In addition to the previously noted advantages, combining these three suggested immersion patterns would reveal the effect of dynamic and static immersion.

One of the drawbacks with the current ocean-placed rotor setup is the lack of replicate samples. Therefore, the uncertainty of important parameters, such as paint application and biofouling intensity, remain unknown, since only the measurement uncertainty from the laboratory rotor can be determined. These earlier parameters could be determined by using the same FCC system and exposing several FCC cylinders in the same conditions. The difference in biofouling intensity experienced by FCC cylinders in the ocean-placed rotor setup and the quality of the paint application and their impact on drag is left unknown

without replicates. Replicates would provide the uncertainty of these latter parameters mentioned. However, if the rotor positions of the coated cylinders on the raft are frequently changed, one can assume that the influence of varying biofouling intensity at the exposure site will be minimized.

The ocean-placed rotary setup was located in Roskilde Fjord, Denmark, which contains brackish and relatively cold water; thus, the biofouling intensity is significantly lower than that in many locations with warmer waters (i.e., typically higher biofouling intensity). Furthermore, ships typically do not spend much time in brackish waters, but almost only time in waters with the salt content found in the ocean, which is approximately twice as large as in Roskilde Fjord, i.e., 3.3 wt% to 3.8 wt% salt (Yebra et al., 2004). An improvement for this setup would, therefore, be to relocate it to a site where the salt content is similar to that which ocean-going ships primarily encounter. Furthermore, the site should ideally be in warm waters, where there is high biofouling intensity. This would have the advantage of revealing differences in drag performance faster than in waters with low biofouling intensity. One of the major challenges in the field of FCC drag performance is striving to obtain results quickly, in order to reveal the best performing FCC. Today there are no accelerated tests that reliably and expediently determine the best performing FCC. Locations with high biofouling intensity are, therefore, presently used as the fastest way to reveal the FCCs with the best performance.

Another improvement would be to extend the exposure period to that of a typical dry-dock period, rather than only one year, as the vast majority of commercial ships have dry-docking intervals much longer than this, i.e., typically three to five years, and at times, up to 7.5 years. FCCs in a newly applied condition typically have little or no significant difference in drag. The difference in drag performance does typically increase with time, when the coating is exposed to an environment with natural biofouling present. The importance of long-term measurements is obvious when determining the average drag resistance over a dry-dock period and, subsequently, its impact on the fuel consumption and harmful exhaust gas emissions. Additionally, more than one test site should be used to determine the drag performance of FCCs, because larger commercial ships often spend time in waters with

varying biofouling intensities. By exposing FCCs in various locations with different biofouling intensities, the performance of the investigated FCC systems could reveal differences in drag performance in these environments and would determine if the performance ranking depends on the biofouling intensity (location). For instance, one type of FCC may be preferable in warmer waters, while another FCC may be preferable in colder waters. There are several options to improve the aging setup and exposure conditions:

- expose more cylinders with different activity patterns;
- age FCCs in a location with high biofouling intensity;
- age FCCs in locations with varying biofouling intensity, i.e., low, medium and high;
- use replicate samples; and
- increase the exposure period.

There are also many possibilities to improve the laboratory rotor setup so that more accurate measurements can be obtained. In the current design, there are two bearings below the torque sensor, which both contribute to the measured torque and, therefore, the uncertainty, because the friction in the bearings is subject to changes due to wear, room temperature, lubrication, and rotational speed. Several options could minimize or remove the contribution from the bearings. Ideally, the contribution could be completely removed if the torque sensor was placed below them. However, the torque sensor must have sufficient mechanical strength to resist the vibrations in this position when the cylinder is rotated at high RPMs. Otherwise, the torque sensor could be placed between the two bearings, which would remove the frictional contribution from one of them and thereby reduce their uncertainty. Another option could be to construct a system to heat the lubrication in the bearings and keep them at a constant temperature, thereby maintaining a constant drag contribution from the bearings. The viscosity of water does have some influence on the torque measurements, and placing the laboratory rotor setup in a room with a constant temperature would ensure a constant and identical temperature in the bearings and in the water in the tank prior to drag measurements being taken; this would ensure an identical impact on the viscosity of water and friction in the bearings over time. The temperature of the water in the water tank could be kept constant by using a heat exchanger to either add or remove energy from the water in order to keep the water temperature constant during rotation. In effect, the recommended improvements for the laboratory rotor setup are to

minimize or remove the friction from the bearings and to install a heat exchanger to keep the temperature fairly constant in the water tank.

It was found that the friction of the three best performing FCCs hardly changed over the period of one year. It is, therefore, suggested that drag measurements be carried out every two or three months. If, however, significant changes in the level of biofouling are observed via regular inspection, e.g., every two or three weeks, then a drag measurement is recommended. By carrying out fewer drag measurements, time-consuming measurements will be avoided, the risk of damaging the cylinders due to transport will be reduced, the biofouling release during drag measurement in the laboratory scale rotors will be reduced, and the potential damage to biofouling due to exposure out of its natural habitat (i.e., water tank) will be minimized.

All of the suggestions given in this chapter would yield more effective estimates of the drag performance of FCCs. Finally, once the performance is known with accuracy, it will be much easier to determine the most important properties responsible for quality drag performance of FCCs in realistic exposure conditions. This would, hopefully, quicken the process of developing even better FCCs than those presently available and, ultimately, ensure excellent drag performance of FCCs for an extensive period of time. Many challenges still exist, but with the methods and findings presented in this thesis, combined with the recommendations offered, significant improvements are very likely.

Nomenclature

A	Surface area	m^2
A_{air}	Cross-sectional area of the ship above water	m^2
A_H	Wetted hull area	m^2
AHR	Average hull roughness	m
ASTM	American Society for Testing Materials	-
C	Mechanically cleaned	-
C_A	Air resistance coefficient	-
C_D	Drag coefficient	-
C_f	Increase in skin friction coefficient	-
ΔC_f	Difference in skin friction coefficient	-
$\bar{C}_f$	Average skin friction coefficient	-
C_H	Total drag coefficient for a hull	-
C_m	Non-dimensional disk torque coefficient	-
$\bar{C}_{m,H}$	Average non-dimensional disk torque coefficients based on the three highest Reynolds numbers (Re = $1.18 \cdot 10^6$, Re = $1.39 \cdot 10^6$ and Re = $1.60 \cdot 10^6$)	-
$C_{m,ref}$	Average C_m of the disks in the newly applied coating condition applied to smooth substrates	-
C_T	Total drag coefficient	-
ΔC_m	Difference in non-dimensional disk torque coefficients compared to the reference value	-
CDP	Control depletion polymers	-
C_R	Form drag resistance coefficient	-
C_T	Total resistance coefficient	-
ΔC_T	Change in total resistance coefficient (ΔC_T)	-
D	Dynamic	-
DFT	Dry film thickness	m
ΔC_T	Change in total resistance	-
ΔC_f	Difference in skin friction coefficient	-
F_A	Air resistance force	N
FCC	Fouling control coating	-
FDM	Friction disk machine	-
Fr	Froude number	-
FRC	Fouling release coating	-
F_f	Skin friction force	N
FPSO	Floating petroleum off-loading	-
F_R	Form drag force	N
F_T	Total resistance	N
g	Gravitational acceleration	$m \cdot s^{-2}$
h	Height of cylinder	m
ISO	International standards organization	-
ITTC	International towing tank conference	-
k	Von Karmen constant (0.41)	-
l_g	Gap distance between inner (rotating) cylinder and outer (static) cylinder	m
l_p	Length of plate	m
l	Vertical distance from center line to peak	m
L	Length	m
M	Recorded torque	N·m

M_B	Torque from the bearings	N·m
M_C	Torque on the side of the rotating cylinder	N·m
M_{Cor}	Correction factor	N·m
M_E	Torque from the top and bottom of the cylinder	N·m
M_S	Torque from the shaft	N·m
M_T	Torque measured by torque sensor	N·m
n	Number of measurements	-
N	Newly applied	-
NSTM	Navy Ships' Technical Manual	-
$\emptyset$	Swirl factor	-
p	Vertical distance from center line to peak	m
ρ	Density	$kg \cdot m^{-3}$
Pa	Pascal	$N \cdot m^{-2}$
P_E	Theoretical effective power (towing power)	$J \cdot s^{-1}$
PVC	Polyvinylchloride	-
r	Radius	m
R_a	Average roughness	m
Re	Reynolds number	-
Re_g	Reynolds number for laboratory rotor setup based on its gap distance between the (inner) rotating and outer (static) cylinder	-
Re_r	Reynolds number for a cylinder based on its radius	-
Re_p	Reynolds number for a flat plate based on its length	-
Re_s	Reynolds number for a ship	-
RPM	Rounds per minute	min^{-1}
Rt(50)	Roughness parameter	µm
R_z	Roughness parameter	µm
S	Static	-
SP	Shaft power	$J \cdot s^{-1}$
ΔSP	Difference in shaft power	$J \cdot s^{-1}$
SPC	Self-polishing copolymer	-
TBT	Tributyltin	-
TNO	Toegepast Natuurwetenschappelijk Onderzoek's	-
TQC	Total quality control	-
R_t	Total roughness	
τ_w	Wall shear stress	Pa
$\bar{\tau}_w$	Average wall shear stress	Pa
U	Velocity	$m \cdot s^{-1}$
ϑ	Kinematic viscosity	$m^2 \cdot s^{-1}$
W_a	Average waviness	m
W_t	Total waviness	m
ω	Angular velocity	$radians \cdot s^{-1}$

References

Aldred, N, Scardino, A, Cavaco, A, de Nys R, Clare, AS “Attachment strength is a key factor in the selection of surfaces by barnacle cyprids (Balanus amphitrite) during settlement.” Biofouling, 26 287–299 (2010)

Anderson, CD, Townsin, RL, Candries, M, “Idiosyncracies of low surface energy (foul-release) antifoulings: drag, roughness and maintenance.” Presented by Anderson, CD, at the 10th International Congress on Marine Corrosion and Fouling, Melbourne, (AUS) (1999).

Amfilokhiev, W, Conn, J, “Note on the Interaction between the viscous and wavemaking component resistances.” Royal Institution of Naval Architects Transactions, 113 43–57 (1971)

Andrewartha, J, Perkins, K, Sargison, J, Osborn, J, Walker, G, Henderson, A, Hallegraeff, G, “Drag force and surface roughness measurements on freshwater biofouled surfaces.” Biofouling, 26 487–496 (2010)

Almeida, E, Diamantino, TC, de Sousa, O. “Marine paints: the particular case of antifouling paints.” Prog. Org. Coat., 59 2–20 (2007)

Arpaci, VS, Larsen, PS, “Convection Heat Transfer.” Prentice-Hall, Englewood Cliffs, NJ, (USA), ISBN: 9780131723467, (1984)

ASTM D3623 – 78a, “Standard Test Method for Testing Antifouling Panels in Shallow Submergence”, (Reapproved 2012)

Berglin, M, Larsson, A, Jonsson, PR, Gatenholm, P. “The adhesion of the barnacle, Balanus improvisus, to poly (dimethylsiloxane) fouling-release coatings and poly (methyl methacrylate) panels: the effect of barnacle size on strength and failure mode.” J. Adhes. Sci. Technol., 15 1485–1502 (2001)

Barrett, M, “HMS Illustrious – effects of no anti-fouling.” Naval Architect., E128–E129 (1985)

Barton, A, Sargison, J, Brandner, P, Walker, G “A force balance to measure the total drag of biofilms on test plates.” Aus. Fluid Mech. Conf., 16 819–824 (2011)

Blunt, L, Jiang, X. “Advanced techniques for assessment surface topography: development of a basis for 3D surface texture standards "SURFSTAND"”. London (UK). Elsevier. (2003)

Bohlander, J, Zealand, MBN, “Review of options for in-water cleaning of ships.” New Zealand: MAF. Biosecurity 42 1–34 (2009)

Brett, TM, “Head-loss measurements on hydroelectric conduits.” J. Hydraulics Division, 106 173–190 (1980)

Candries, M, “Drag, boundary-layer and roughness characteristics of marine surfaces coated with antifoulings.” [PhD Thesis]. Department of Marine Technology UK: University of Newcastle-Upon-Tyne. (2001)

Candries, M, Atlar, M, “Estimating the impact of new-generation antifoulings on ship performance: the presence of slime.” Proceedings of IMarEST-Part A, J. Marine Engineering and Technology, 13-22 (2003a)

Candries, M, Atlar, M, “Experimental investigation of the turbulent boundary layer of surfaces coated with marine antifoulings.” J. Fluids Eng., 127 219–232 (2005)

Candries, M, Atlar, M, Mesbahi, E, Pazouki, K. “The measurement of the drag characteristics of tin-free self-polishing co-polymers and fouling release coatings using a rotor apparatus”. Biofouling, 19 27–36 (2003b)

Capurro, LRA, “Oceanography for practicing engineers”. In: Griffith, DE, editor. New York: Barnes & Noble, Inc., ISBN: 9780389005032, (1970)

Chambers, LD, Stokes, KR, Walsh, FC, Wood, RJ, “Modern approaches to marine antifouling coatings” Surface and Coatings Technology, 201 3642–3652 (2006)

Chang, W, Hirvonen, M, Grönqvist, R. “The effects of cut-off length on surface roughness parameters and their correlation with transition friction”. Saf. Sci., 42 755–769 (2004)

Childs, PRN, Rotating flows. Butterworth-Heinemann, Oxford (UK), ISBN: 978-0-12-382098-3, (2010)

Christensen, BE, Characklis, WG, “Physical and chemical properties of biofilms.” In: Biofilms, pp. 93–130, New York, NY. Wiley, ISBN: 978-0471826637, (1990)

Conn, JFC, Lackenby, H, Walker, WP, “Resistance experiments on the Lucy Ashton.” Trans INA., 95 350–436 (1953)

Corbett, JJ, Winebrake, PJJ, Green, E, Comer, B, “Energy and GHG emissions savings analysis of fluoropolymer foul release hull coating”. Energy and Environmental Research Associates, LLC., (2011)

Cushing, DH, “Marine ecology and fisheries.” Cambridge University Press, Oxford (UK), ISBN: 9780521205016, (1975)

Det Norske Veritas (DNV). [Accessed on June 3, 2014]. Available from: http://www.dnv.com/industry/maritime/publicationsanddownloads/publications/dnvcontainershipupdate/2010/2-2010/75yearsthecoatingchallenge.asp. (2010)

De Jong, P, Te, GM, Kiezebrink, E, “Prediction of the adherence, growth and release of microorganisms in production chains.” Int. J. Food Microbiol., 74 13–25 (2002)

Dick, JD, Nowacki, LJ, “Accelerated, Simulated-Service Exposures of Antifouling Coating Systems for Ships and Navigational Buoys.” Organic Coatings and Plastic Chemistry, 39 (1978)

Dobretsov, S, Abed, RMM, Voolstra, CR, “The effect of surface colour on the formation of marine micro and macrofouling communities.” Biofouling, 29 617–627 (2013)

Fathom Focus. “Hull Coatings for Vessel Performance.” [Accessed May 14, 2014]. Available from: http://fathomshipping.com/userfiles/files/b85b16066a682bcef16114f6b63c65b2.pdf. (2013)

Fitzsimmons, P, Ellis, J, “A two-parameter roughness analyser and performance software.” International Workshop on Marine Roughness and Drag.” London: RINA., 4 1–13 (1990)

Flack, KA, Schultz, MP, Rose, WB, “The onset of roughness effects in the transitionally rough regime.” Int. J. Heat Fluid Flow, 35 160-167 (2012)

Froude, W, “Experiments on Surface Friction.” British Association Reports, (1872)

Gadelmawla, E, Koura, M, Maksoud, T, Elewa I, Soliman, H, “Roughness parameters.” J. Material Processing Technology, 123 133–145 (2002)

Germanischer Lloyd SE. “Rules for Classification and Construction. VI Additional Rules and Guidelines. Guidelines for Extended Dry-Dock Interval.” [Accessed May 14, 2014]. Available from: http://www.gl-group.com/infoServices/rules/pdfs/gl_vi-11-5_e.pdf. 1-12 (2013 edition)

Ghani, MPA, Karim, K, Milani, K, “Experimental investigation of the drag characteristics of different ship hull coating with using rotor apparatus.” Jurnal Mekanikal, 31 92–102 (2010)

Grigson, C, “Drag losses of new ships caused by hull finish.” J. Ship Res., 36 182–196 (1992) Granville, P, “Drag-characterization method for arbitrarily rough surfaces by means of rotating disks.” J. Fluids Eng., 104 373–377 (1982)

Hama, FR, “Boundary-layer characteristics for smooth and rough surfaces.” SNAME., 333–356 (1954)

Haslbeck, EG, Bohlander, GS, “Microbial biofilm effects on drag-lab and field.” SNAME., 3A:1-7 (1992)

Havelock, TH, “The pressure of water waves upon a fixed obstacle.” Proc. R. Soc. Lond., 175 409–421 (1940)

Hellio, C, Yebra, D, “Advances in marine antifouling coatings and technologies.” Woodhead Pub. Cambridge (UK), ISBN: 978-1-84569-386-2, (2009)

Hochkirch, K, Brandt, H, “Fullscale hydrodynamic force measurement on the Berlin Sail–Force–Dynamometer.” 14th Chesapeake Sailing Yacht Symposium, 1–13 (1999)

Holm, E, Schultz, M, Haslbeck, E, Talbott, W, Field, A, “Evaluation of hydrodynamic drag on experimental fouling-release surfaces, using rotating disks.” Biofouling, 20 219–226 (2004)

Howell, D, Behrends, B, “A review of surface roughness in antifouling coatings illustrating the importance of cutoff length.” Biofouling, 22 401–410 (2006)

ISO (International Organization of Standardization), Geometrical Product Specifications (GPS) – Surface texture: Profile method – Rules and procedures for the assessment of surface texture, ISO 4288: 1996 (Switzerland: International Organization of Standardization) (1996)

ITTC (International Towing Tank Conference), "ITTC – Recommended Procedures Fresh Water and Seawater Properties." Revision 02, 1-45 (2011) [Accessed on February 12, 2014]. Available from: http://ittc.sname.org/CD%202011/pdf%20Procedures%202011/7.5-02-01-03.pdf. (2011)

Karunanidhi, SV, Kumar, R, Dokos, L, "Strategic analysis of the global market for marine coatings." [Accessed on June 13, 2013]. Available from: http://www.frost.com/sublib/display-report.do?intraQuery=Strategic+analysis+of+the+global+market+for+marine+coatings.+&id=M861-01-00-00-00&bdata=&x=0&y=0. Frost & Sullivan, 1–191 (2012)

Kawaguchi, Y, Ashida, T, Ando, H, Senda, T, "Development of drag reducing antifouling paint and experimental investigation on mass transfer phenomenon near the painted wall." 1–10

Khor, YS, Xiao, Q, "CFD simulations of the effects of fouling and antifouling." Ocean Eng., 38 1065–1079 (2011)

Kiil, S, Weinell, CE, Pedersen, MS, Dam-Johansen, K. "Analysis of self-polishing antifouling paints using rotary experiments and mathematical modelling." Ind. Eng. Chem. Res., 40 3906–3920 (2001)

Kiil, S, Dam-Johansen, K, Weinell, CE, Pedersen, MS, Codolar, SA, "Dynamic simulations of a self-polishing antifouling paint exposed to seawater." J. Coatings Technol., 74 45–54 (2002)

Kim, W, Van, S, Kim, D, "Measurement of flows around modern commercial ship models." Exp. Fluids., 31 567–578 (2001)

King, M, "The measurement of ship hull roughness." Wear., 83 385–397 (1982)

Kinsman, B, Wind waves: their generation and propagation on the ocean surface. Courier Dover Publications, Mineola, NY, ISBN: 9780486646527, (1965)

Klijnstra, JW, Measured at TNO/Endures BV facilities, Personal e-mail correspondence, 8 December, 2014 (2014)

Kovach, BS, Swain, G, "A boat-mounted foil to measure the drag properties of antifouling coatings applied to static immersion panels." Proc. Int. Symp. Seawater Drag Reduction., Newport, RI, 1998

Lackenby, H, "Resistance of ships, with special reference to skin friction and hull surface condition." Archive: Proc. Inst. Mech. Eng. 176 981–1014 (1962)

Leer-Andersen, M, Larsson, L, "An experimental/numerical approach for evaluating skin friction on full-scale ships with surface roughness." J. Mar. Sci. Technol., 8 26–36 (2003)

Lejars, M, Margaillan, A, Bressy, C, "Fouling release coatings: a nontoxic alternative to biocidal antifouling coatings." Chem. Rev., 112 4347–4390 (2012)

Lewthwaite, J, Molland, A, Thomas, K, “An investigation into the variation of ship skin frictional resistance with fouling.” Trans. RINA., 127 269–284 (1985)

Lindholdt, A, Dam-Johansen, K, Olsen, SM, Yebra, DM, Kiil, S, “Effects of biofouling development on drag forces of hull coatings for ocean-going ships: a review.” Accepted for publication in J. Coatings Technology and Research, December 2014 (2014)

Lindholdt, A, Dam-Johansen, K, Olsen, SM, Yebra, DM, Klijnstra, JW, Kiil, S,”Measurements of drag performance of statically exposed fouling control coatings using a spinning disk.” The article is intended for publication in a scientific and relevant journal in early 2015 (2015a)

Lindholdt, A, Dam-Johansen, K, Olsen, SM, Yebra, DM, Kiil, S,” Estimation of long-term drag performance of fouling control coatings using an ocean-placed raft with multiple rotors.” The article is intended for publication in a scientific and relevant journal in early 2015 (2015b)

Loeb, G, Laster, D, Gracik, T, “The influence of microbial fouling films on hydrodynamic drag of rotating discs.” In: Costlow JD, Tipper RC, editors. Marine Biodeterioration: an interdisciplinary study. Annapolis, MD: Naval Institute Press. pp. 88–94 (1984)

Malone, JA, Little, DE, “Effects of hull foulants and cleaning/coating practices on ship performance and economics.” Soc Nav Arch Mar Eng., 88 75–101 (1980)

MAN Diesel & Turbo, “Basic principles of ship propulsion.” [Accessed on February 12, 2014]. Available from: http://www mandieselturbo com/files/news/filesof5405/5510_004_02%20low pdf. (2011)

Mei, CC, Stiassnie, M, Yue, DKP, “Theory and applications of ocean surface waves: nonlinear aspects.” World Scientific publishing, Singapore, (2005)

Millett, J, Anderson, C, “1997, Fighting fast ferry fouling.” Fast'97, Conference Papers, 1 493–495 (1997)

Mirabedini, S, Pazoki, S, Esfandeh, M, Mohseni, M, Akbari Z. “Comparison of drag characteristics of self-polishing co-polymers and silicone foul release coatings: a study of wettability and surface roughness.” Prog. Org. coat. 57 421–429 (2006)

Moody, LF, “Friction factors for pipe flow.” Trans ASME., 66 671–684 (1944)

Molland, AF, “The maritime engineering reference book: a guide to ship design, construction and operation”. Butterworth-Heinemann, Oxford (UK), ISBN: 9780750689878, (2008)

Monfared, H, Sharif, F, “Design guidelines for development of tin-free antifouling self-polishing coatings using simulation.” Prog. Org. coat., 63 79–86 (2008)

Munk, T, Kane, D, Yebra, D, “The effects of corrosion and fouling on the performance of ocean-going vessels: a naval architectural perspective”. In: Advances in marine antifouling coatings and technologies, pp. 148-176 Woodhead Pub., Cambridge (UK), ISBN: 978-1-84569-386-2 (2009)

Musker, AJ, “Universal roughness functions for naturally-occurring surfaces.” Trans. Can. Soc. Mech. Eng., 1 1–6 (1980-1981)

Naval ship’s technical manual “Waterborne underwater hull cleaning of navy” [Accessed on December 2, 2014]. Available from: http://www.hnsa.org/wp-content/uploads/2014/07/ch081.pdf (2006)

Newman, J, Marine hydrodynamics, MIT press., ISBN: 9780262140263, (1977)

Olsen, SM, Yebra, DM, “On the use of the term ‘self-polishing’ for antifouling paints.” Prog. Org. Coat., 76 1699–1700 (2013)

Padhy, CP, Sen, D, Bhaskaran, PK, “Application of wave model for weather routing of ships in the North Indian Ocean.” Nat. Hazards., 44 373–385 (2008)

Paik, JK, Frieze, PA, “Ship structural safety and reliability.” Prog. Struc. Eng. Mater. 3:198–210 (2001)

Parnell, KE, Kofoed-Hansen, H, “Wakes from large high-speed ferries in confined coastal waters: management approaches with examples from New Zealand and Denmark.” Coastal Manag., 29 217–237 (2001)

Pedersen, MI, ”Effektvurdering af åleudsætninger i Roskilde Fjord.” DTU Aqua-report 230 (2010)

Picologlou, BF, Characklis, WG, Zelver, N, “Biofilm growth and hydraulic performance” J. Hydraulics Division, 106 733–746 (1980)

Salta, M, Wharton, JA, Stoodley, P, Dennington, SP, Goodes, LR, Werwinski, S, Mart, U, Wood, RJK, Stokes, KR, “Designing biomimetic antifouling surfaces.” Philosophical Transactions of the Royal Society A: Mathematical, Physical and Engineering Sciences, 368 4729–4754 (2010)

Scardino, AJ, Guenther, J, De Nys, R, “Attachment point theory revisited: the fouling response to a microtextured matrix.” Biofouling, 24 45–53 (2008)

Scardino, AJ, De Nys, R, “Mini review: Biomimetic models and bioinspired surfaces for fouling control.” Biofouling, 27 73–86 (2011)

Schlichting, H, Boundary layer theory. McGraw-Hill, New York, ISBN: 978-3540662709, (1968)

Schultz, MP, “Turbulent boundary layers on surfaces covered with filamentous algae” Transactions-American Soc. Mech. Eng., J. Fluids Eng., 122 357-363 (2000)

Schultz, MP, “The relationship between frictional resistance and roughness for surfaces smoothed by sanding.” J. Fluids Eng., 124 492–499 (2002)

Schultz, MP, “Frictional resistance of antifouling coating systems.” J. Fluids Eng., 126 1039–1047 (2004)

Schultz, MP, “Effects of coating roughness and biofouling on ship resistance and powering.” Biofouling, 23 331–341 (2007)

Schultz, M, Bendick, J, Holm, E, Hertel, W, “Economic impact of biofouling on a naval surface ship.” Biofouling, 27 87-98 (2010)

Schultz, M, Myers, A, “Comparison of three roughness function determination methods.” Exp. Fluids, 35 372-379 (2003)

Schultz, M, Swain, G, “The effect of biofilms on turbulent boundary layers.” J. Fluids Eng., 121 44-51 (1999)

Schultz, MP, Swain, GW, “The influence of biofilms on skin friction drag.” Biofouling, 15 129–139 (2000)

Shipyard Trogir, [Accessed on November 25, 2014]. Available from: http://www.hb.hr/LinkClick.aspx?fileticket=RetQFnntemc=(2014)

Swain, GW, Kovach, B, Touzot, A, Casse, F, Kavanagh, CJ, “Measuring the Performance of Today’s Antifouling Coatings.” J. Ship Production, 23 164-170 (2007)

Theodorsen, T, Regier, A, “Experiments on drag of revolving disks, cylinders, and streamline rods at high speeds.” National Advisory Committee for Aeronautics, 793 367-384 (1944)

Thomas, J, Choi, S, Fjeldheim, R, Boudjouk, P, “Silicones containing pendant biocides for antifouling coatings.” Biofouling, 20 227-236 (2004)

Thouvenin, M, Peron, J, Charreteur, C, Guerin, P, Langlois, J, Vallee-Rehel, K, “A study of the biocide release from antifouling paints.” Prog. Org. Coat., 44 75-83 (2002)

Klijnstra, J, E-mail correspondence from Job Klijnstra at TNO/Endures BV, 4 July 2014 (2014)

Townsin, R, “The ship hull fouling penalty.” Biofouling, 19 9-15 (2003)

Townsin, R, Anderson, C, “Fouling control using low surface energy, foul release technology.” In: Advances in marine antifouling coatings and technologies, pp. 693-708. Woodhead Publishers, Cambridge (UK), ISBN: 978-1-84569-386-2, (2009)

Townsin, R, Byrne, D, “Speed, power and roughness: the economics of outer bottom maintenance, Speed, power and roughness.” Royal Institution of Naval Architects, 6 459-483 (1980)

TQC (Total Quality Control) [Accessed on November 25, 2014]. Available from: http://www.hull-roughness.com/product/hull-roughness-analyser-dc9000 (2012)

Ünal, UO, Ünal, B, Atlar, M, “Turbulent boundary layer measurements over flat surfaces coated by nanostructured marine antifoulings.” Exp. Fluids, 52 1431-1448 (2012)

U.S. Naval Institute. “Marine fouling and its prevention.” Woods Hole Oceanographic Institute. ISBN: 9780870213625, (1952)

Visscher, J. Paul. “Nature and extent of fouling of ships' bottoms.” No. 1031. US Government Printing Office (1928)

Watanabe, S, Nagamatsu, N, Yokoo, K, Kawakami, Y, “The augmentation in frictional resistance due to slime.” J. Kansai Soc. Naval Architects, 131 45-51 (1969)

Weinell, CE, Olsen, KN, Christoffersen, MW, Kiil, S, “Experimental study of drag resistance using a laboratory scale rotary set-up.” Biofouling, 19 45-51 (2003)

Yebra, DM, Kiil, S, Dam-Johansen, K, “Antifouling technology-past, present and future steps towards efficient and environmentally friendly antifouling coatings.” Prog. Org. Coat., 50 75-104 (2004)

Zargiel, KA, Swain, GW, “Static vs dynamic settlement and adhesion of diatoms to ship hull coatings.” Biofouling, 1-15 (2013)

Appendices

Appendix I – User manual for laboratory rotor setup and aging setup

This section a detailed manual for both the laboratory rotor setup where drag performance of the coated cylinders have been carried out and the aging site where the coated cylinders were exposed are presented. In Figure 1A, the methodology applied to estimate the drag performance of the coatings is seen. The coatings shall first be applied with FCC desired to tested and subsequently be immersed either statically or dynamically followed by laboratory rotor measurements. The laboratory scale rotor measurements are used to determine the drag performance of the FCCs.

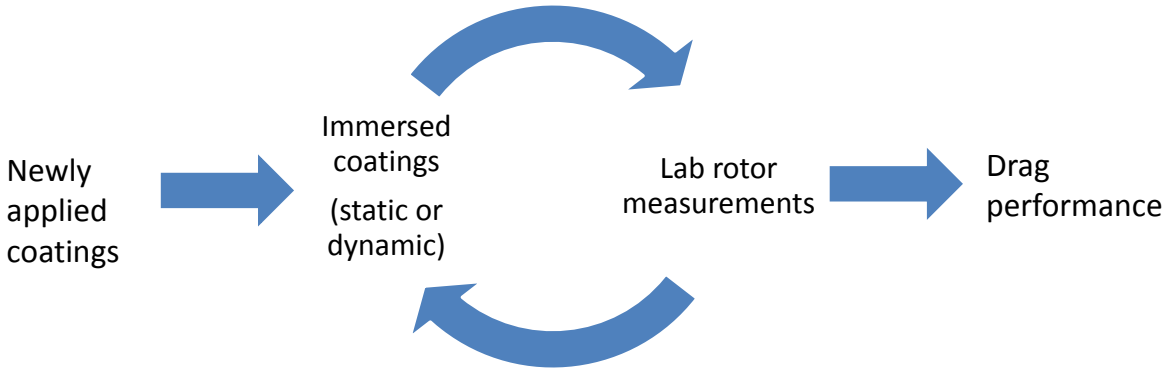

Figure 1A. Methodology used to determine the drag performance of coatings.

Appendix Ia – Laboratory rotor setup

Table 1A shows the main components of the laboratory setup and their primary purpose.

Table 1A. Laboratory scale rotor components and their primary purpose.

Component	Primary purpose
Cooling system on engine	The cooling system is placed on top of the engine to ensure sufficient cooling. Without a cooling system overheating of the engine could occur, in particular at low RPMs.
Engine	Provide sufficient power to rotate the cylinder, shaft and overcome other resistances. The capacity of the engine is 7.5 kW which is sufficient to run up to 1500 RPM with the current cylinder design.
Shaft and cylinder mounting system	The shaft shall keep the cylinder in place and minimize vibrations. At the tip of the shaft threads can be attached and dismantled in order to comply with the attachment system of the cylinder being tested.
Bearings	Stabilize shaft while being rotated. The two bearings are placed below the torque sensor which, therefore, unfortunately impacts the torque measurements.
Torque sensor	Measure torque when the shaft and cylinder is rotating. The torque sensor used was a 50 Nm strain gauge transducer from Nordisk Transducer Teknik (NTT).
Taco meter	The taco meter measures the rotations per minute (RPM) the shaft (cylinder) rotates.
Outer static cylinder	The outer static cylinder should ideally provide a Couette flow, i.e., constant shear stress along the height of the cylinder which is due to laminar flow and only viscous drag force.
Rotor cylinder (coated)	The rotor cylinder is the substrate for the coating being tested.
Water tank	Contain water with stable temperature. The water tank can contain 500 l which ensures large temperature increases due to friction from a rotating cylinder would take substantially longer than a normal test period of 3.5 hours with intermittent stops does not occur. Furthermore, if the room temperature should change, for instance, 5°C during normal test period of 3.5 hours this does not lead to substantial temperature change of the water in the tank.
Pulley system	Move cylinder, motor, shaft, engine etc. up and out of the water tank and back again when desired. The pulley system is pneumatic which is why pressurized air must be available.
Frame setup	Keep every part together both during idle and operating condition.
Control box	Set RPMs of rotating cylinder and restart system if shut-down safety systems starts, e.g., excessive vibration.
Torque monitoring program	The program WinTA2USB version 1.3 was used to record the torque measured by the torque sensor. The program must be installed on the computer record the data.

Shaft

The shaft is stainless steel of the type 316 with a diameter of 5.5 cm and a length of 1.2 m. It is covered with a rubber layer to prevent corrosion of the parts that are in contact with water.

Figure 2A. Shaft with rubber protection.

Engine and cooling system

The engine is a 7.5 kW, 400V, 1500 RPM, AC (type K21R 132 M4 from Frimodt Pedersen A/S) including frequency converter (type 12.F4.S1E-3440). The frequency converter makes it possible to adjust the rotational speed from 0 to 1500 RPM. The capacity of the engine is larger than necessary for the specific purpose (3-30 knots). However, if desired a larger cylinder or higher speed can be obtained. The engine is equipped with additional ventilation to improve the cooling of the motor, which can be necessary when running at low RPM values in order to avoid overheating of the engine.

Figure 3A. The 7.5 kW engine used to rotate the cylinder in the tank and the additional cooling on top of the engine.

Bearings

The two bearings used is of the type SKF Pop Release SYT 50 F, see Figure 4A. The two bearings are both placed below the torque sensor, which means that the resistance by them is also picked up by the torque sensor. The bearings must be lubricated frequently which, however, depends on how often they are used. A significant decrease in resistance, i.e., 0.3 Nm, was measured by the torque sensor when there was a lack of lubrication. A lack of lubrication can be detected due to severe noise increase from the bearings. Frequent lubrication is, therefore, recommended, although only major change in resistance occurs when there is a lack of lubrication. Lubrication can be added at the orange tips seen Figure 4A. It is recommended to use the same type of lubrication at all times to avoid changes in resistance from the bearings. If a change in lubrication takes place it is recommended to determine the resistance from the bearings with this lubrication.

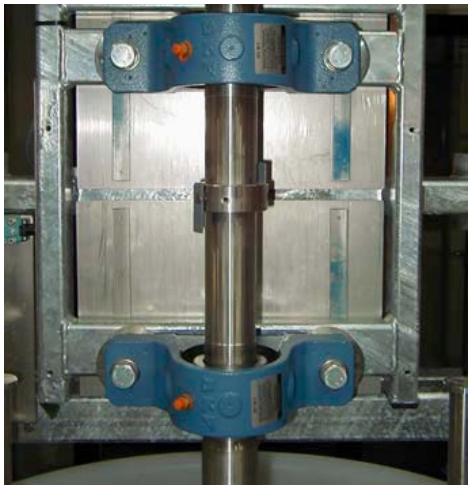

Figure 4A. The bearings at the shaft.

Torque sensor

The torque sensor, which is placed on the shaft above the two bearings, is a transducer that picks up the torque while the cylinder rotates. The wire from the torque sensor is connected to the computer, which records the torque picked up by the torque sensor. The uncertainty on the reading of the torque sensor as provided by the supplier (Nordisk Transducer Teknik - NTT) is 0.1 Nm.

Figure 5A. Torque sensor and mounting system to the shaft. The wire is connected to the computer, which records the torque picked up by the torque sensor.

Calibration of torque sensor

The torque sensor needs to be calibrated in order to convert the reading picked up by the torque sensor into a torque value. Two different types of calibration setups were used to determine the reading and the conversion into a torque value. One setup determined the

reading corresponding to a torque value while the torque sensor was placed on the shaft. The torque sensor was retrieved from the shaft and placed in a setup fixing it to a well-known distance and mass in another calibration setup. Figure 6A shows the setup where the torque sensor is placed on the shaft, i.e., at the same position as when carrying out drag measurements. A two meter straight metal stick was mounted on the shaft just below the torque sensor. It was mounted in the center in a manner that balanced the torque (weight) so that no net torque toke place at either tip of the metal stick. A wheel, which could rotate around its center point with a low friction, was placed in a 90° angle with respect to the metal stick. A string ran from the beginning part of the metal stick to its end and then to the wheel in 90° angle. At the end of the string a light bucket hung in the thread. The downward force at a given length (i.e., torque) could then be changed by adding a well-known mass to the bucket. By having the wheel in a 90° angle and a known distance from the center of the torque sensor the torque values experienced by the torque sensor could be determined, see e.g., Equation (1A).

$$T = L \cdot M \tag{1A}$$

where T is the torque, L is distance from the centre of the metal stick and M is the mass attached to the end of the string.

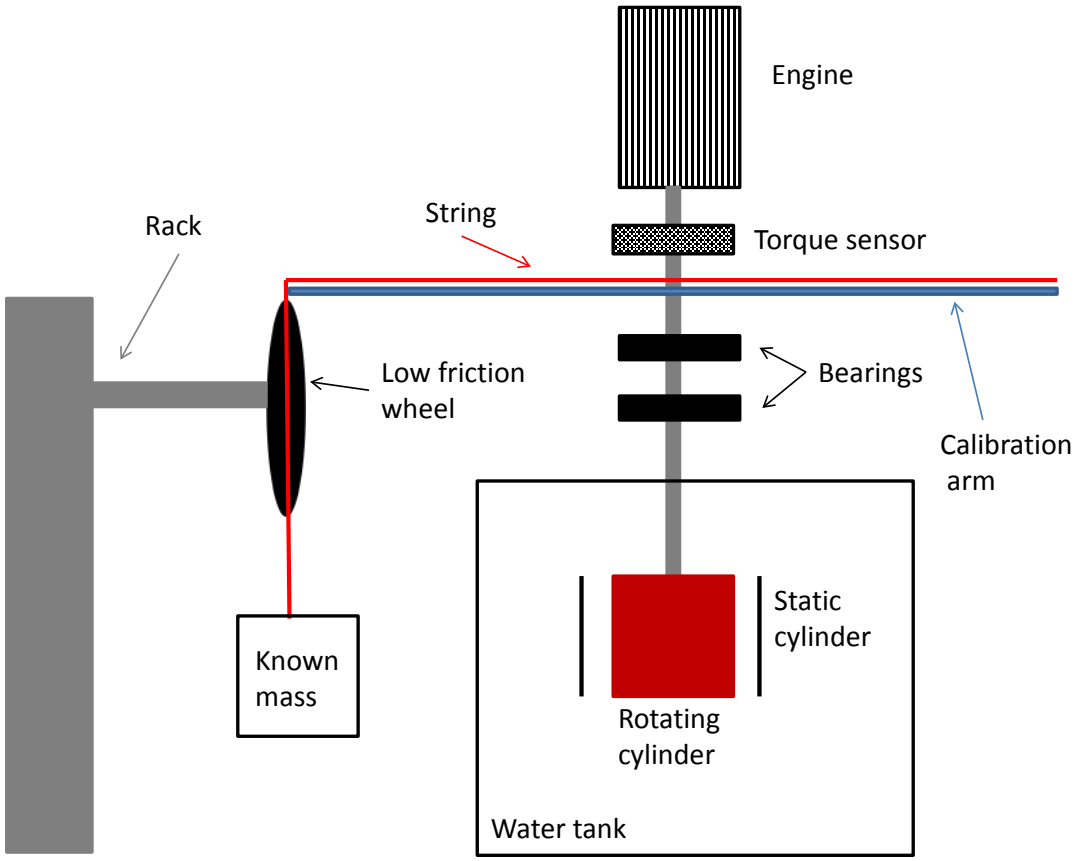

Figure 6A. Calibration setup with torque sensor mounted at the shaft.

Figure 7A shows another calibration setup, which works on the same principle as the setup shown in Figure 6A. In this setup, the torque sensor was retrieved from the setup and fixed. A wooden stick of well-known length was attached to the centre of the torque sensor. At the tip of the wooden stick a well-known mass was attached. Equation 1A was applied to convert the reading displayed into a torque value.

Figure 7A. Calibration setup where the torque sensor was retrieved from the shaft and mounted in a setup.

Figure 8A shows the calibration curve of both setups. The linear trendline of the calibration curves for the two setups are very close to unity, see Table 2A. The torque values from the well-known distance and mass and the reading from torque sensor displayed a conversion of one, as the slopes for both calibration setups were within 1% accuracy with a slope value of one. The slope value applied for the C_f determination was therefore set to 1.0.

Table 2A. Linear trend line and R-squared value for the two setups used to calibrate the torque sensor. For the linear trend line equation y is the moment attached and x is the display reading.

Parameter	Torque sensor placed at shaft	Torque sensor retrieved from shaft
Linear trend line equation	y = 1.0136x + 0.0241	y = 1.0073x - 0.068
R^2	0.9999	0.9999

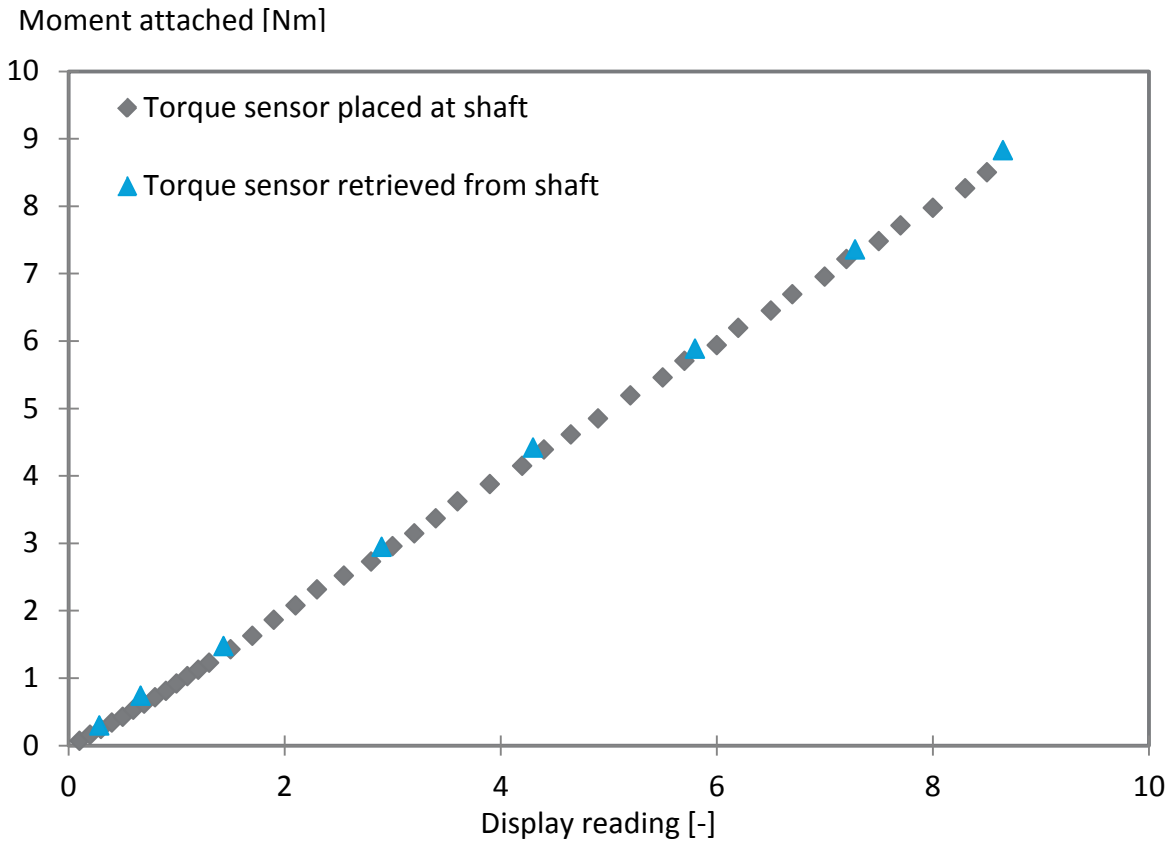

Figure 8A. Display reading and the moment attached to the torque sensor from the two applied calibration setups.

Inductive sensor

An inductive sensor of the type NAMUR IM12-04N-N-ZW0 is placed at the shaft. The distance between the magnet and sensor must be less than 3 mm in order to measure with high accuracy.

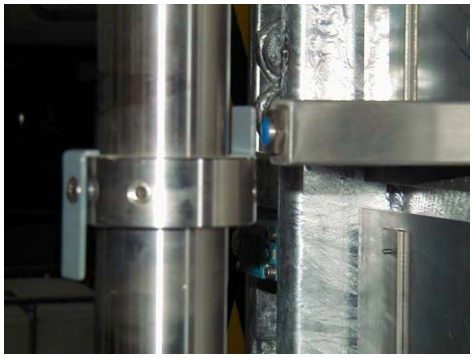

Figure 9A. Inductive sensor.

Outer static cylinder

It was the intention to create a constant and well-defined shear stress on the rotating cylinder. This is approached by using a "Couette" setup. The setup consisted of two concentric cylinders with the innermost (the rotor cylinder) in rotation and the outer

cylinder being static. The outer static cylinder has a diameter of 38 cm. The inner rotating cylinder was 30 cm leaving a gap of 4 cm between the inner rotating and outer static cylinder. The outer static cylinder is made of PVC and had a height of 31 cm, see Figure 10A. The gap was, however, too large to obtain a Coutte flow.

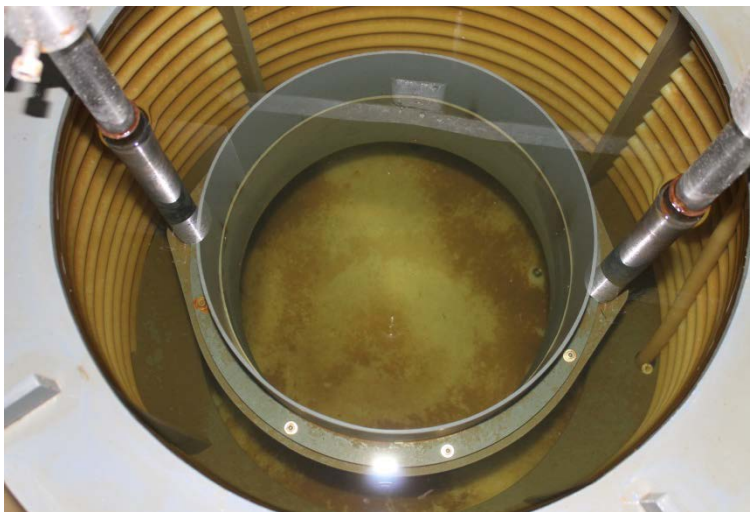

Figure 10A. Outer static cylinder with 31 cm in height and 38 cm in diameter.

Rotor cylinders

Coated rotor cylinder

Figure 11A displays a coated rotor cylinder with a height of 30 cm and a diameter of 30 cm. Disks must be placed on the top and bottom of the cylinder before measuring the drag. The smooth PVC disks had a height of 0.5 cm. The total height of the cylinder during drag measurements was, therefore, 31 cm.

Figure 11A. Coated cylinder. The grips used to attach and dismantle cylinders from the laboratory rotor and aging setup are seen at the bottom of the cylinder.

Figure 12A shows the mounting system. The cylinder was attached or detached by turning the coated cylinder directly on to the shaft where a thread was attached. The inner thread used to attach to the coated cylinder had a thread that matched the one on the shaft.

Figure 12A. Thread mounted to shaft. The thread was used to attach the coated cylinders.

Figure 13A shows a coated cylinder with a handle attached. The grips were used to move the cylinder without touching the side of the cylinder, which is extremely important, as it can otherwise impact the surface of the coating on the cylinder, both when clean and especially when there is biofouling present.

Figure 13A. Cylinder with grips attached to one end which was used to move the coated cylinder.

Figure 14A shows the setup just prior to attachment of a coated cylinder. The wooden board was used to ease the attachment process.

Figure 14A. A coated cylinder detached from shaft and a wooden board used to support the cylinder and ease the attachment process is seen. A smooth PVC disk is seen on the top part of the cylinder. The grips are seen in the bottom part of the cylinder.

Figure 15A shows the smooth PVC top and bottom disks, which were attached to the coated cylinder during drag measurements. The same smooth PVC disks were used on all four cylinders, because the drag differences would then presumably be identical on the top and bottom. Six screws were used to mount each disk on the rotor cylinder.

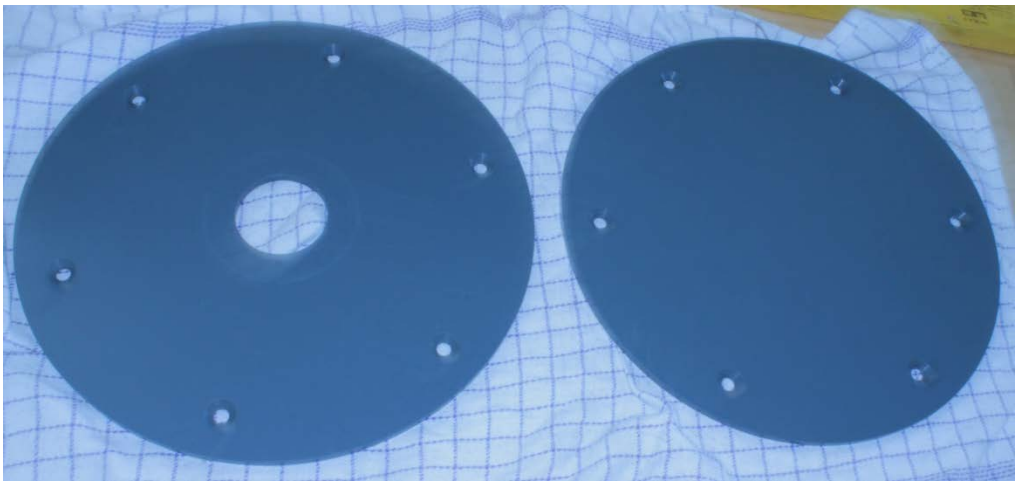

Figure 15A. Top disk (left) and bottom disk (right) attached to cylinder during drag measurements.

Smooth cylinders

Three smooth cylinders with a height of 15 cm, 22.5 cm and 30 cm, which all had a diameter of 30 cm, were used to determine the correction factor, i.e., all other factors besides the one from the side of the cylinder. Figure 16A shows the three smooth cylinders.

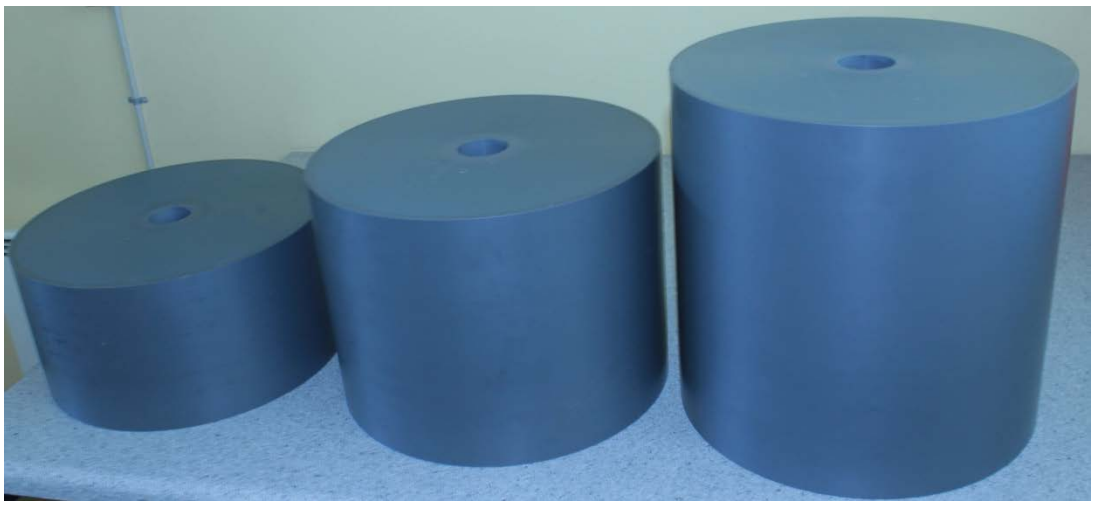

Figure 16A. The three smooth cylinders of 15.0 cm, 22.5 cm and 30.0 cm.

The mounting system of the smooth cylinders works by turning the cylinder directly on to the shaft (no screw at the tip of the shaft) and the inner thread on the shaft matches the screw inside the smooth cylinder, see Figure 17A.

Figure 17A. Picture of the top and the inside of the smooth cylinder. The mounting system of the smooth cylinder works by turning the cylinder directly on to the shaft (no screw) and into the inner thread of the shaft.

Cylinder with strips

The cylinder with strips was only used in the initial stage of the project to verify that the laboratory rotor system could detect differences in drag between smooth and rough surfaces. It has the advantage compared to the cylinders which were exposed that it is easy to attach a coating system. However, it also has the disadvantage that the strips must be placed carefully in order to prevent impact on the form drag which can take place if the strips are not tightly attached. Furthermore, the strips only covers part of the cylinder area making the effective coated area less than the total area of the side of the cylinder. The cylinder with strips was used by Weinell et al. (2003) when studying the drag of coating. Figure 18A displays the mounting system of the cylinder with strips. The cylinder with strips is attached to the shaft by tightening a screw after the cylinder has passed through the shaft, see lower part of Figure 18A. Furthermore, attachment of rough plastic strips attached to the cylinder is seen.

Figure 18A. Rotor cylinder with plastic strips attached. Mounting of the cylinder with strips is done by tightening the screw after the cylinder has passed through the shaft.

Water tank

The water tank is a circular polypropylene tank (0.90 m in diameter and 1.12 m in height) and can contain 580 l. The tank consists of polypropylene preventing corrosion. The tank was provided with eight ¾" pipe stubs 100 mm from the bottom which could be connected to a cooling system, instrumentation or other equipment. Furthermore, a 1" tap was mounted at the bottom to empty the tank. Along the periphery inside the water tank a heat exchanger was placed, which, however, was not used. A lid, which was divided in two parts, could be placed on top of the water tank to minimize water evaporation.

Figure 19A. The 580 l polypropylene tank.

Pulley system

To lift the rotor cylinder from the water tank a pulley system is used. The total weight of the motor, shaft, cylinder and guide amounts to about 90 kg. To lift the total weight a pneumatic

piston system is used, which means that compressed air supply must be connected to the pulley system, see Figure 20A. The control of the pulley takes place from the control box by turning the “up/down” key either left or right.

Figure 20A. The pneumatic piston.

Figure 21A. Compressed air pressure reading equipment which is located on the left part of the frame setup.

Frame setup

The frame consisted of sectional iron welded together. The whole frame was hot galvanized. The lower part (910 mm × 1200 mm) of the frame surrounded the water tank and the upper part (height 2900 mm) above the tank supported the guide for the engine, including the pulley system, see Figure 22A.

Figure 22A. The frame setup.

Control box

The rotor setup was operated from the control box, see Figure 23A. The rotations per minute (RPM) was adjusted manually from the control box by turning the “speed adjustment” button. The RPM was measured by an inductive sensor pointing at the shaft and the RPM value was seen at the “display”. The signal was converted by a frequency counter and the value was monitored on the display at the control box. The RPM value could often be difficult to set exactly at the desired value and the RPM value would often vary around a mean value with ± 1 RPM and at times with ± 2. For instance, if 300 RPM was the desired value the display might vary from 298 to 302 in severe cases, while more often it would vary from 299 to 301. If the mean display value could not be matched exactly to the desired RPM it was then possible to normalize the torque by assuming a linear change in torque around small deviations from the display value to the desired value, see Equation 2A.

$$\mathrm{Torque}_{\mathrm{Normalized}} = \mathrm{Torque}_{\mathrm{measured}} \frac{\mathrm{RPM}_{\mathrm{display}}}{\mathrm{RPM}_{\mathrm{desired}}} \quad (2A)$$

The RPM of the cylinder could be started and stopped by pressing the “start/stop” bottoms. One emergency button was located on the box and one on each side of the metal frame. Before an inspection, the rotation was stopped by the “stop” button. Then the cylinder was elevated by switching the “up” bottom, which activated the pressurized air to enter the elevation piston. A safety contact blocked the “start” bottom in case the rotor was lifted to the upper position. The steel frame was also equipped with a safety vibration sensor. In case of abnormal vibrations or bumps rotation would. To activate the system again the “reset” bottom had to be pressed. In case of activation of one of the emergency bottoms the “main reset” bottom had to be pressed. After an inspection the “down” button was activated and the rotation would start with the “start” button. During operation the engine/rotor unit was fixed to the frame by two bolts on each side of the frame.

Figure 23A. Control box and buttons.

Torque monitoring program

The program used to record the torque picked up the torque sensor was WinTA2USB. Prior to recording the torque the following settings were set:

- Capacity set for 50 Nm
- Conversions per second 5, which gives 5 data points per second.
- Resolution 5 giving 5 decimals on the recorded data.
- Channel 1 enabled
- Acquisition time of 800 min. The recording was stopped prior to 800 min, but this would ensure sufficient time when recording.
- Acquisition interval Max
- File name: As desired.
- Samples for moving average of 16
- Find Peak Threshold of 2

The button “Start Test” was pressed when it was desired to start recording. “Stop Test” was pressed when the data recording had finished. The “Stop Test” was not seen in Figure 24A, but appeared after “Start Test” had been pressed. “Export Excel as xls file” was pressed to transfer the data to Excel. It could then be saved and manipulated in Excel.

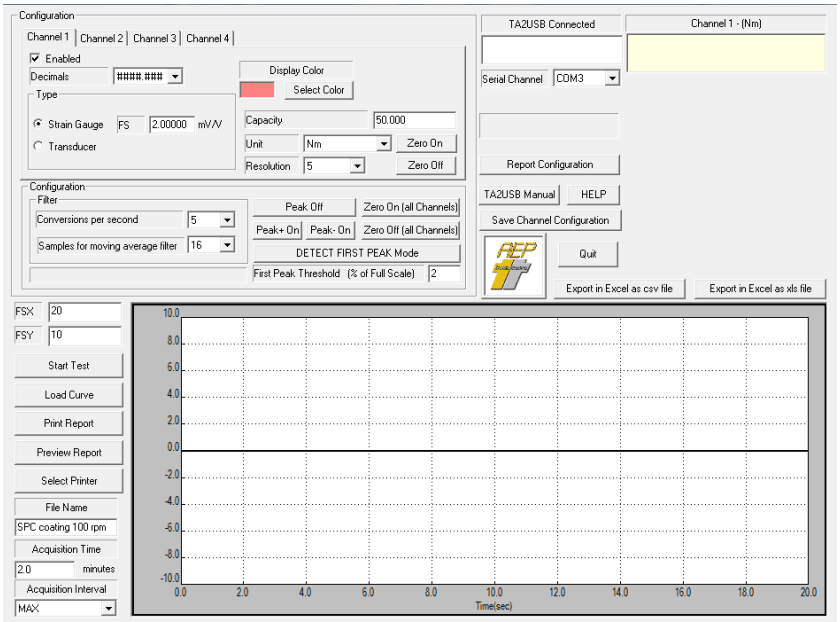

Figure 24A. Screen dump when the program was ready to record the torque due to rotation.

Safety

It was deemed that the main risks to personal could arise from cloths or body parts being caught in the setup while rotating, which potentially could lead to severe injury. Prevention of this occurred by shielding the rotating shaft and careful use of the setup. The other hazards deemed possible to cause personal injury was from the upper part hitting a person working on the system, e.g., when mounting or detaching a cylinder. This could occur if sudden pressure drop occurred due to lack of compressed air supply. Prevention of this occurred by working in positions not directly under the upper part, which would prevent personal injury in case of the upper part dropping down due to, for instance, sudden lack of compressed air.

Drag measurement protocol

This section describes the procedure to carry out the drag measurements. The objective of using this procedure was to minimize the measurement uncertainty, which was judged to primarily arise from the resistance in the bearings. Figure 25A displays the measurement protocol when measuring the drag performance of the coated cylinders. Prior to attaching a cylinder the system was run at 350 rpm (no cylinder) in order to stabilize the drag impact from the bearings by heating the lubrication in the bearings via rotation. Subsequently, the cylinder is attached. Next step was to run the system at first 100 RPM for 10 minutes and then increments of 100 RPM toke place followed by 10 minutes of measurements until

reaching 500 RPM. Afterwards, a second run toke place in the same manner as the first run. The torque values of the last minute was used because the reading was fairly stable due to constant drag impact from the bearings.

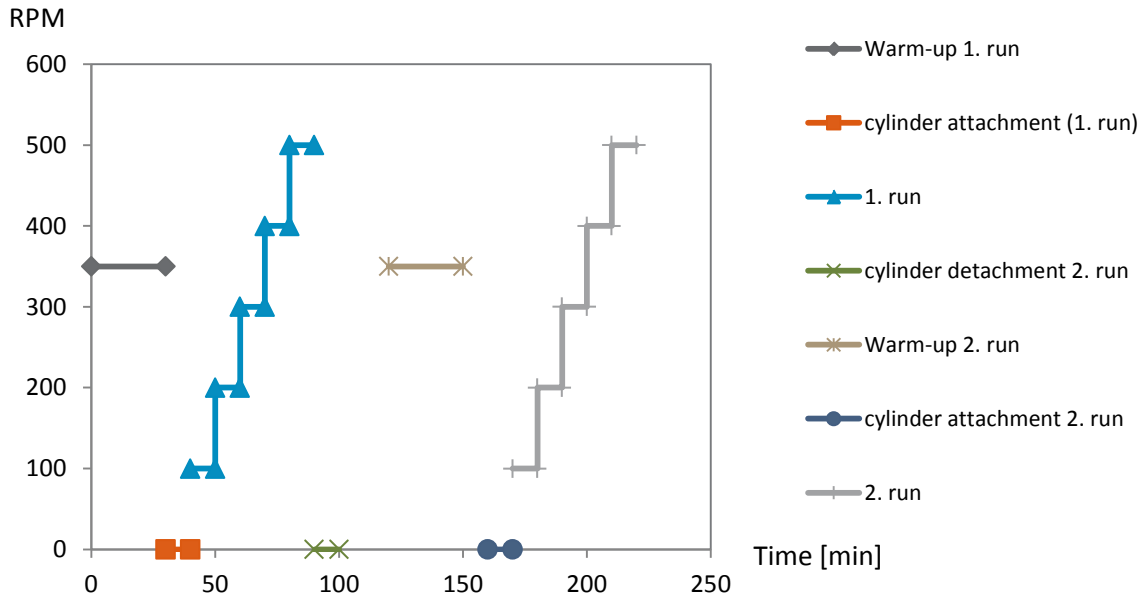

Figure 25A. Drag measurement protocol used when measuring drag of coated cylinders.

Appendix Ib – Aging setup

The aging setup could expose four cylinders dynamically and two cylinders statically. Figure 26A shows a picture of the raft with both static and dynamic setups.

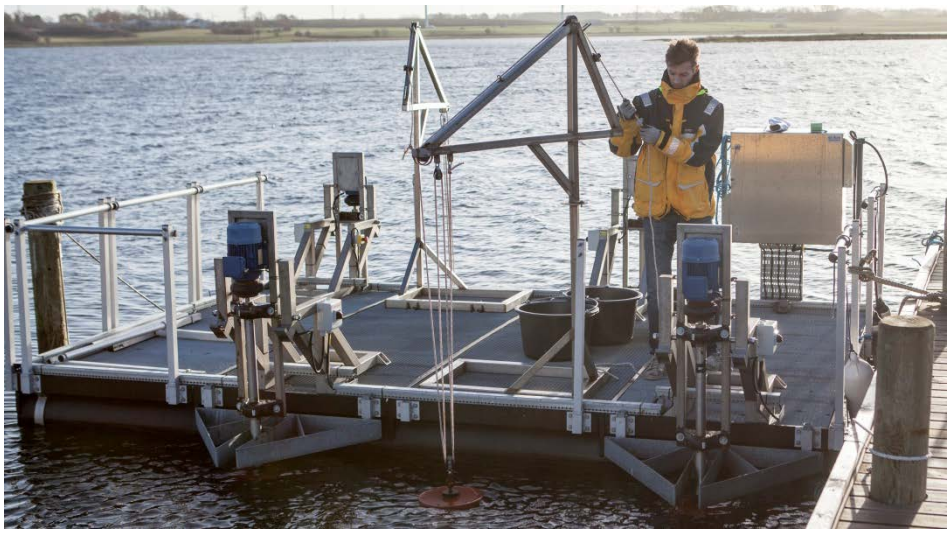

Figure 26A. Four cylinders exposed dynamically and two statically.

Dynamic rotor immersion setup

Figure 27A shows the front view of the dynamic rotor setup.

Figure 27A. Front view of the dynamic rotor setup.

Table 3A shows the main components and their primary purpose for the aging setup.

Table 3A. Aging rotor components and their primary purpose.

Component	**Primary purpose**
Engine	Rotate cylinder
Frame	Keep all the parts together
Frequency converter	Ensure correct tangential speed (RPM)
Shaft	Ensure rigid structure
Bearings	Ensure vibrations are minimized and keep shaft aligned
Emergency stop	Stop rotation of all cylinders immediately when pressed
Manual stop	Stops a single rotor setup
Cylinder attachment/detachment system	Ensure coated cylinders can be attached and detached so they can be tested with respect to drag in the laboratory rotor setup
Protection system	Ensure floating objects do not touch coated cylinders
RPM measurement	Ensure correct tangential speed (RPM)

Engine

The engine powered the system in order to rotate the cylinder. It was an asynkronmotor IE2 Type MS2 90L6. It had a capacity of 1.1 KW and a maximum rotational speed of 900 RPM. The maximum frequency was 50 HZ. The ingress protection (IP) code was IP55. This means that it could resist ingress of small objects, almost entirely dust, water jets at a distance of 6 mm at any location for 3 minutes with a water volume of 100 litres per minute, and a pressure of 100 kPa at a distance of 3 m. IP 55 was judged and proven through two summer seasons, i.e., approximately one year, to provide sufficient protection for the engines, even in the highly corrosive marine environment. The engine was operated at 15 Hz (270 RPM)

which was judged to be the lowest frequency it could be operated at in order to still provide sufficient cooling to the engine. It happened twice that an engine had stopped, but it could be restarted again. One time it failed completely, presumably due to overheating as the fan providing cooling had melted and the failure occurred in the warmest period of the summer 2014. The broken engine was replaced with a new one and the dynamic aging process could continue after the replacement. The temperature and wind conditions must be taken into account when determining the lowest RPM the engine can run at. If desired to run at lower than 270 RPM (15 Hz) or at warmer locations with less wind to cool the engine then additional cooling must be installed. 16 A og 400 V were specified requirements for the engines.

Figure 28A. Engine with an effect up to 1.1 Kw.

Frame

The frame setup keept the entire setup together. It was bolted to the raft in four places. The stick, which the rotor system could be rotated around, must be tightened with two bolts to prevent it from detachment of the frame when the cylinder is rotating, as the vibrations otherwise could loosen the stick, if only attached with one bolt.

Figure 29A. Frame bolted to the raft. Two screws are seen on the ends of the stick going horizontally through the frame which ensured that the cylinder could flipped out of the water.

Frequency converter

Four frequency converters were placed in the electrical cabinet, see Figure 30A.

Figure 30A. Frequency converters M.1.1, M1.2, M1.3, M1.4 and electrical cabinet.

Each of the frequency converters were connected to one engine. The RPM was controlled by changing the frequency at the converter. There were 6 buttons “RUN”, “STOP”, “ESC”, “ENT” and “arrow up” and “arrow down”, see Figure 31A.

Figure 31A. Frequency converters of the type Bonfiglioli Vectron Agile.

The arrows were used to lower or increase the frequency. “RUN” started the engine and “STOP” stopped the engine. The buttons “ESC” and “ENT” were used when there was an error, which had to be handled to make engines run. These latter buttons were not necessary during normal operation, but only if there was an error. If there was an error it would be shown on the display and the meaning of the error could be found in the user manual, which can be downloaded on the internet from the supplier’s homepage. The frequency converter was the type Bonfiglioli Vectron Agile.

Shaft

The shaft was connected to the engine and went through the two bearings and was then attached to the cylinder. The shaft provided sufficient mechanical strength to keep the structure in position together with the two bearings.

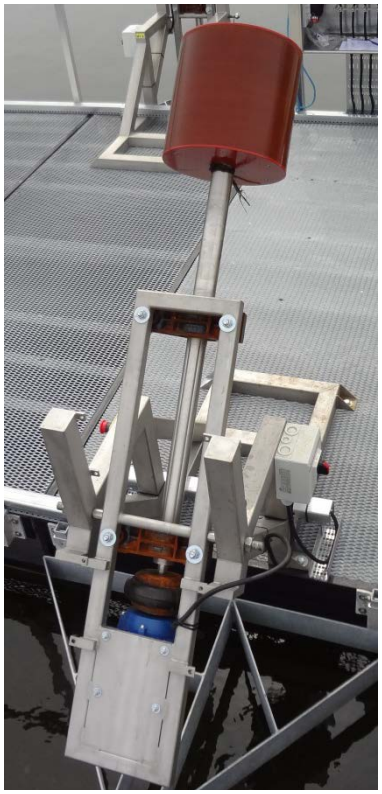

Figure 32A. Shaft, which was attached to the engine, going through two bearings and connected to a cylinder.

Bearings

The two bearings were supposed to keep the shaft aligned and dampen the vibrations due to rotation of the shaft and cylinder. The bearings had to be lubricated frequently to prevent corrosion by ingress of air and water. Lubrication was carried out by pumping oil lubrication into the small hole on the right side of the bearing. When adding lubrication to the bearings it had to be added until it came out on either the lower or upper part of the bearing because it then meant that the inner part was full. If increase occurred in noise it was a sign that there was likely not sufficient lubrication.

Figure 33A. One of two bearings at the dynamic rotor setup.

Emergency stop

There was one emergency stop on the lower right part of the frame. All four rotors stopped when the emergency stop button was pressed and they could not be started until the button was released.

Figure 34A. Emergency stop button. Located on the lower right part of the frame.

Manual stop

There was a manual stop button on the lower left part of the frame. It was not intended to be used to stop the cylinders. It only worked on the rotor system to which it was connected to, and did not work as the emergency stop button, that works on all four engines.

Figure 35A. Manual start and stop button. Located on the lower left part of the frame.

Cylinder attachment and detachment system

When attaching or detaching the coated cylinder it was essential that the sides, i.e., excluding the top and bottom, were not touched in any way. To avoid touching the sides of the cylinders a system was developed to deal with this. The first step when detaching the cylinder in order to subsequently measure the drag at the laboratory scale rotor was to flip the cylinder around the axis that went through the frame setup. It did not require much force as the system was well-balanced and lightly pressing down on the upper part of the frame by using one's bodyweight was sufficient to flip it around. However, care had to be taken to not push too hard, which prevented the cylinder from flipping around very fast. Furthermore, care to counteract the motion of the rotating setup once the cylinder had passed the tipping point and would move towards the inner part of the raft was needed. The frame setup was designed so that the cylinder and other parts could rest on the frame when flipped, making it easy to detach the cylinder subsequently, see Figure 36A.

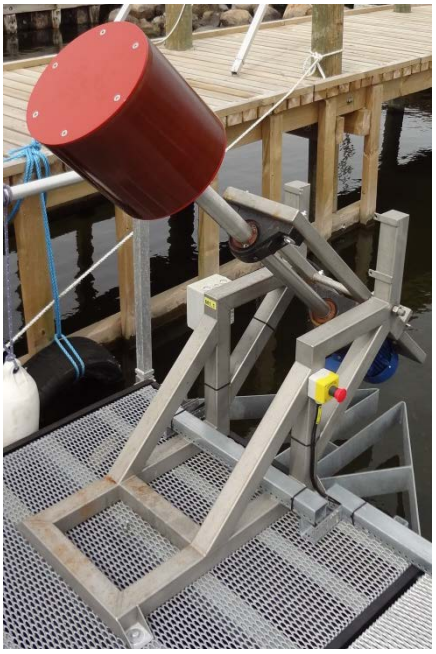

Figure 36A. Rotor system flipped around.

After flipping the rotor system around the next step was to remove the upper lid. The six screws were unscrewed and the disk was removed with the hands, see Figure 37A.

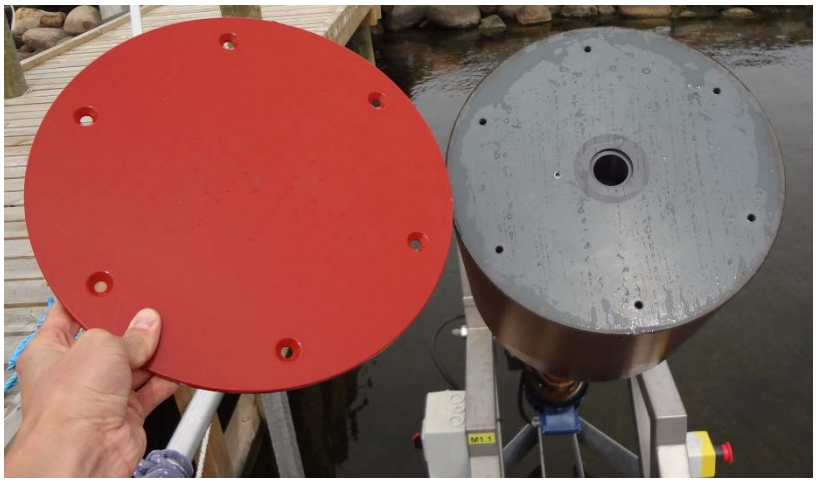

Figure 37A. Bottom disk removed after unscrewing the six screws, which kept it in place.

After removing the disk the grip was placed on the top part of the cylinder. When the grip was placed it could be used to turn the cylinder free from the shaft and afterwards hold it, see Figure 38A.

Figure 38A. Grip used to move and turn the cylinder free from the shaft.

After the cylinder was detached from the shaft it was placed in a bucket with a bottom part, which had a stick to keep the cylinder in place and prevent the sides of the cylinder from touching the bucket during transport, see Figure 39A and 40A.

Figure 39A. System used to transport cylinder and prevent the sides from being touched. The upper left part was placed at the bottom of the bucket.

Figure 40A. Bucket to transport cylinder that could be filled with seawater to preserve biofouling.

Protection system

The protection system consisted of a triangular shaped metal (galvanized) where the shaft fit into. The protection frame was easily attached to the raft by using the specifically built system seen on the left and right part of Figure 41A. It was deemed unlikely that objects would hit the coated cylinders, as they were protected from floating objects by the triangular frame.

Figure 41A. Triangular frame protecting the coated cylinders from floating objects.

Measurement of rotational speed

Figure 42A shows a handheld digital tachometer from Diesella A/S which was used to measure the RPM. It measured the RPM by pointing the laser beam at the shaft where a 1 x 1 cm paper of grey color was placed on the shaft. The tachometer was set for RPM and the RPM was shown when pressing the "on" button on the left side. The tachometer was tested against the inductive sensor on the laboratory scale rotor and found to give RPM values that agreed with more than 99% of what the inductive sensor RPM value showed.

Figure 42A. Handheld digital tachometer used to measure the RPM at the aging site.

Safety

The largest risk when operating the equipment was judged to arise from a persons' cloth being caught in while cylinder rotated. It was, therefore, advised to always turn off the engines when being on the raft. The risk of the platform sinking was very low because the PVC tubes, which ensured sufficient buoyancy, were filled with polystyrene, so in the case that a fracture occurred to the tubes water would be prevented from filling the tubes.

Static immersion

Two static immersion setups were constructed and placed at the aging test site in October, 2013. The purpose of the static immersion was two-fold. Primarily it was desired to investigate the same coating systems and their impact on friction by comparing the cyclic static/dynamic cycles and only static exposure. Furthermore, it gave the possibility of testing more cylinders in a cycle of static/dynamic exposure by interchanging the cylinders at the static setup in combination with the rotor setup. In this way the rotor setup could be running constantly, while cycles of static/dynamic immersion could take place. The mechanism used to raise and lift the cylinder from the static setup worked by a lift and lock mechanism at the test setup. Figure 43A shows the static setup with a cylinder lifted above the seawater.

Figure 43A. Static immersion test setup at the raft with a cylinder lifted up from the seawater.

Appendix II - Roughness measurements

This section describes the methods used to measure the roughness parameters of the coatings in the newly applied condition and after mechanical cleaning.

TQC hull gauge analyzer

The TQC hull gauge analyser (TQC, 2012) was used to measure the macro-roughness on the coated cylinders in the form of Rt(50), see Figure 44A. Water was sprayed onto the FRCs in order to wet the surface as the TQC equipment otherwise could not be moved over the surface, because the stylus needle got stuck in the coating when dry. This obviously could

have impacted the roughness measurements. For the SPC coating it was not necessary to wet the surface. 60 measurements were made on each cylinder at locations evenly spread out on the cylinders when determining the average Rt(50) roughness.

Figure 44A. Macro roughness measured by TQC hull gauge analyser on coated cylinders (TQC, 2012).

Micro roughness by Handy surf equipment

A laboratory roughness measuring device, i.e., Handsurf E-350 was used to measure the micro-roughness. 60 measurements were made of the R_z value with an evaluation length of 0.8 cm to measure the micro-roughness of the coated cylinder surfaces. After 60 measurements the Handsurf E-350 was calibrated on two surfaces with a well-defined roughness. Figure 45A shows the two calibration surfaces (left side) and the Handysurf E-350 equipment (right side).

Figure 45A. The surfaces used to calibrate the equipment (left side) and the Handy-surf E350 (right side).

Appendix III - Visual biofouling of exposed marine coatings

The NSTM rating provides an estimate of the biofouling condition and increased total resistance of naval ship. However, the NSTM rating consist of broad categories so in order to present minor changes in biofouling the following rating was used, which shows in more

detail the biofouling level. However, no correlation to the increase in total resistance for ships exist with the present biofouling rating , but in this particular case where less severe biofouling was found on the coatings, except for the fluorinated FRC, a biofouling grading system was developed to grade the low biofouling condition in more details. The developed biofouling rating system with focus on low level biofouling conditions, which, however, does not provide an impact on fuel consumption, is presented in Table 4A.

Table 4A. Biofouling grading system with focus on low biofouling intensity.

Description in words and biofouling coverage in percent	Value given
Completely clean	1
Very limited thin slime, i.e., ca 1% coverage	2
Limited thin slime, i.e., ca 2% coverage	3
Minor thin slime, i.e., ca. 5% coverage	4
Intermediate thin slime coverage, i.e., 5-49% coverage	5
Major thin slime coverage, i.e., 50-80% coverage	6
Full thin slime coverage, i.e., 90-100% coverage	7
Thin slime coverage of 50-100% and 0-19% thick coverage	8
Thin slime coverage of 50-100% and 20-49% thick coverage	9
Thin slime coverage of 50-100% and 50-100% thick coverage	10
Barnacles present	11
Long slime, i.e., 0-1 cm	11
Very long slime, i.e., above 1 cm	12

Figure 46A shows the biofouling rating with focus on low biofouling intensity and its development over time based on Table 4A. It is seen that the coatings biofouling rating varies over time, but that it generally increases. The hydrogel-based FRC with biocides had the lowest biofouling rating at almost any time. The hydrogel-based FRC without biocides had a lower biofouling rating than the SPC coating most of the time with a few weeks where the rating was higher. The fluorinated FRC had the highest biofouling rating during the majority of the weeks.

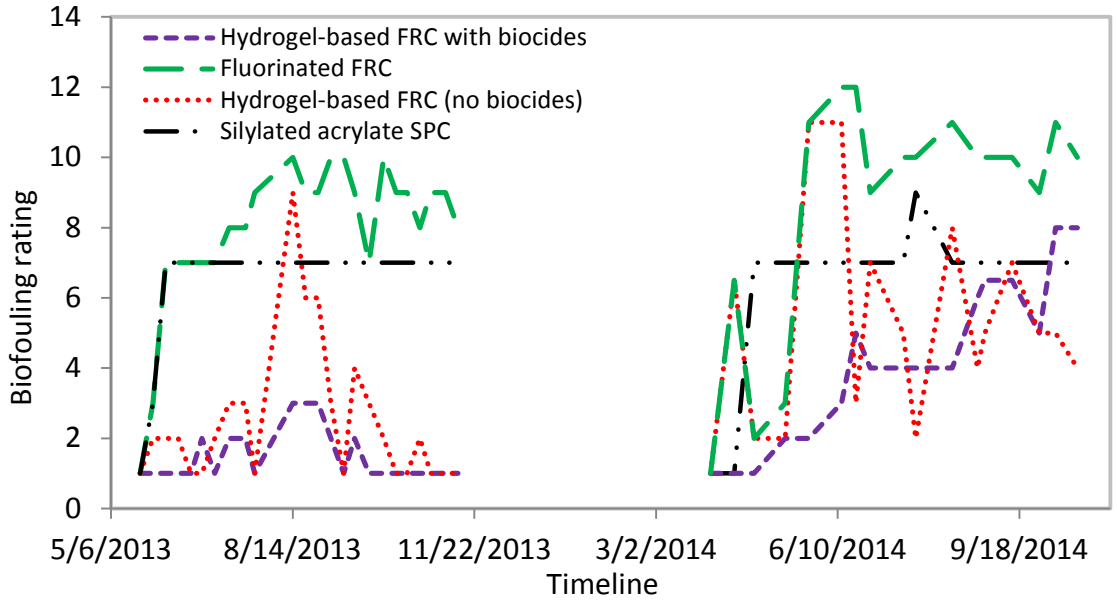

Figure 46A. Biofouling rating over time based on ratings from Table 4A. At the end of 2013 season the coatings were cleaned and on April 1, 2014 resulting in a biofouling rating of 1.

Appendix IV – Continuous measurement setup

The setup described in this PhD dissertation, i.e., particularly in appendix I, has the advantage that it has proven capable of measuring skin friction and changes of skin friction over time in conditions mimicking those of moving ships. However, it has the obvious drawback that changes in skin friction in the time between the measurement points are not known. It could, therefore, be an improvement of the current setup if continuous measurements could take place directly at the aging setup rather than obtaining only a drag performance value every two or three weeks. It was considered to develop such a system, but unfortunately there was insufficient time. However, in this section the pros and cons considered are described by such a setup. The fundamental idea is to place a torque sensor on the shaft as seen in Figure 47A.

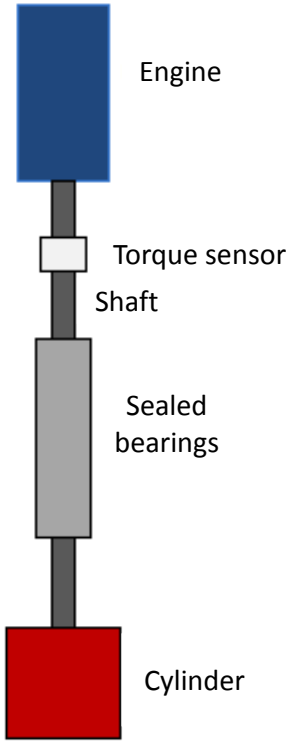

Figure 47A. Position of engine, torque sensor, shaft and closed house for bearings for the continuous measurement setup.

The advantages of installing a torque sensor on the shaft providing continuous torque (drag) measurements are many, with the most important being; (a) measurement of small drag changes over time should provide a more accurate estimation of the skin friction's development over time, (b) vast amount of data which could be used to accurately evaluate the statistical uncertainty of the drag measurements, (c) avoid transportation and detachment and attachment of cylinders, which removes the risk of possible damage of coatings and biofouling and (d) less manual work. There are, however, also some drawbacks connected to the idea of placing a torque sensor on the shaft where the main reason considered is that the torque measurement uncertainty can potentially be very large. Furthermore, a high cost due to equipment and also increased data treatment due to larger and likely more scattered data collected are expected. The increased measurement uncertainty compared to the laboratory scale was determined to be primarily due to; (a) current impacting shear stress, although the degree depends on the current at the test site. It is likely to be a small impact if the tangential velocity of the rotor is much higher than the current. (b) Wear in bearings, i.e., increase in the bearing's friction. However, if a torque sensor could be installed below the bearings an increase in the friction from the bearings

would have no impact on the torque measurements. The torque sensor must, however, be able to withstand the potentially increased corrosion rate due to shorter distance to the surface. It must, furthermore, be mechanically sufficiently strong to withstand the forces in horizontal and vertical directions arising from waves, current and cylinder. (c) Fouling on the shaft and the top and bottom parts of the cylinder would cause increased torque and complicate the evaluation of the skin friction of the tested coatings. (d) Large seawater temperature differences could take place at the test site during a substantial test period. However, this obviously depends on the location, whereas the temperature could be controlled with a heat exchanger in the water tank of laboratory rotor or constant room temperature in the location of the laboratory rotor. (e) Side-by-side comparison of the coated cylinders' drag becomes more uncertain because different setups will be used to measure the drag of each coated cylinder instead of using one setup with the same systematic errors, if any. Furthermore, the coated cylinders might experience different current, seawater temperature, wave impact and other natural forces, even if placed relatively close to each other, which could make the drag comparison more uncertain than if measured with the same setup. However, this uncertainty could be minimized if the coated cylinders frequently changed position. (f) The conversion of in situ torque measurement of relevance for larger industrial ships, i.e., typically larger than 100 m, is more uncertain due to the larger measurement uncertainty.

In order to compensate for some of the issues related to the measurement uncertainty a blank cylinder could at times be used to evaluate the forces impacting the system over time. Furthermore, the top and bottom part of the cylinder could be painted with the same coating system in order to give the top and bottom drag contribution. It could then be argued that the relative drag changes compared to other coatings would be caused by the coating system on the side of the cylinder. Longer cylinders could potentially also be used to minimize the contribution of the top and bottom. The need for a smaller size cylinder, which could be easily handled by one person, might be less as regular detachment, transportation and attachment might be avoided because the measurement take place in situ. If the bearings were placed above the torque sensor measurements with a smooth blank cylinder or measurements without a cylinder could be a way to measure the changes of friction in

the bearings over time and also estimate any other changes in the system. However, the measurements will then only be calibrated at the times when a blank cylinder is attached leaving the friction in the bearings developed over time unknown in between the smooth blank cylinder measurements. The changes in friction in the bearings could be minimized by continuously changing the lubrication, which should come from a reservoir of oil lubrication which could keep it at a fairly high and constant temperature (above 60°C). This would minimize the change in friction from the bearings, because the lubrication would be at a constant temperature. Furthermore, the outside temperature would have little impact on the viscosity because of the high temperature of the oil lubrication, because the viscosity would only change slightly with small temperature changes (e.g., 5°C) when the lubrication is at a high temperature, for instance, above 50°C. If the continuous measurement setup should be constructed one or two blank cylinders could be used to investigate the system over the first short time in operation (e.g., days or weeks) and subsequently over longer time (months and years) in order to measure the torque development of the system over time (i.e., wear in bearings, fouling contribution on shaft, changes in current and wave impact). The initial measurements will include: (a) 24 hours torque measurements in calm weather, which should provide torque values for calm weather conditions and impact of temperature changes in the seawater (day and night temperature); (b) 24 hours torque measurements in rough sea state, which together with the calm weather measurements could be used to evaluate the impact of waves and rough sea state on the drag measurements and thereby the reliability and reproducibility of the torque measurements.

If the continuous measurement setup should be constructed the following design properties are deemed necessary: (a) the torque measurement range shall at least be 0 – 15 Nm; the torque measurements shall have an accuracy of 0 – 2 %; (c) the temperature shall be measured; and the friction from the bearings, if placed below torque sensor, shall be low and constant.

Appendix V - Coating application

The coatings were applied according to their product data sheet. The application was carried out with an airless spray for all the coatings, i.e., both primers and top-coats. Figure 48A and 49A shows the top-coat application on a disk and a cylinder by airless spray, respectively.

Figure 48A. Top-coat application on disk with airless spray.

Figure 49A. Top-coat application on cylinder with airless spray. Primer is seen as the grey coating.